STUDIES ON THE EFFECT OF NANOSIZED CERAMIC FILLER IN POLY (VINYL ALCOHOL)-LITHIUM PERCHLORATE BASED POLYMER ELECTROLYTES

LIM CHIN SHEN

DISSERTATION SUBMITTED IN FULFILMENT OF THE REQUIREMENT FOR THE DEGREE OF MASTER OF SCIENCE

DEPARTMENT OF PHYSICS
FACULTY OF SCIENCE
UNIVERSITY OF MALAYA
KUALA LUMPUR

2012

UNIVERSITI MALAYA

ORIGINAL LITERARY WORK DECLARATION

Name of Candidate: **LIM CHIN SHEN** (I.C/Passport No: 870926-10-5375)

Registration/Matrix No: **SGR100080**

Title of Project Paper/Research Report/ Dissertation/Thesis ("this Work"):

STUDIES ON THE EFFECT OF NANOSIZED CERAMIC FILLER IN POLY (VINYL ALCOHOL)-LITHIUM PERCHLORATE BASED POLYMER ELECTROLYTES.

Field of Study: **ADVANCED MATERIALS**

I do solemnly and sincerely declare that:

(1) I am the sole author/writer of this Work;
(2) This Work is original;
(3) Any use of any work in which copyright exists was done by way of fair dealing and for permitted purposes and any extract from, or reference to or reproduction of any copyright work has been disclosed expressly and sufficiently and the title of the Work and its authorship have been acknowledged in this Work;
(4) I do not have any actual knowledge nor do I ought reasonably to know that the making of this work constitutes an infringement of any copyright work;
(5) I hereby assign all and every rights in the copyright to this Work to the University of Malaya ("UM"), who henceforth shall be owner of the copyright in this Work and that any reproduction or use in any form or by any means whatsoever is prohibited without the written consent of UM having been first had and obtained;
(6) I am fully aware that if in the course of making this Work I have infringed any copyright whether intentionally or otherwise, I may be subject to legal action or other action as may determined by UM.

Candidate's Signature Date

Subscribed and solemnly declared before,

Witness's Signature Date

Name:
Designation:

ABSTRACT

In this study, three polymer electrolyte systems are prepared by means of solution casting technique. These polymer electrolytes consist of poly (vinyl alcohol) (PVA) (host polymer), lithium perchlorate ($LiClO_4$) (dopant salt) and different types of ceramic fillers [antimony trioxide (Sb_2O_3) and titanium oxide (TiO_2)]. The prepared polymer electrolyte samples with various wt. % of filler content were subjected to X-ray diffraction (XRD), impedance spectroscopy, morphological, and thermal studies. 60 wt. % of PVA and 40 wt. % of $LiClO_4$ shows the highest ionic conductivity of 2.61×10^{-5} S cm^{-1} at room temperature. The highest ionic conductivity increased to 9.51×10^{-5} S cm^{-1} and 1.30×10^{-4} S cm^{-1} with the addition of Sb_2O_3 and TiO_2, respectively. The prepared polymer electrolyte systems obey the Arrhenius rule. XRD analyses reveal the suppression in crystallinity of PVA upon the addition of $LiClO_4$ and inorganic fillers. Incorporation of Sb_2O_3 and TiO_2 shifts the glass transition temperature, T_g to a lower temperature at which the flexibility of polymer backbone was enhanced. SEM images reveal the modification of surface morphology upon the addition of $LiClO_4$ and inorganic fillers. TGA studies indicate that the thermal stability of polymer electrolyte increases significantly when Sb_2O_3 and TiO_2 were introduced to polymer electrolyte which results in the second onset decomposition temperature being shifted to higher temperature. Electric double layer capacitors (EDLCs) were prepared by sandwiching the polymer thin films with two carbon electrodes. Results reveal that the polymer electrolyte with fillers attains higher specific capacitance compared to polymer electrolyte without filler. The prepared

EDLCs have the capacitance retention over 90% which demonstrates the EDLC cells have excellent electrochemical stability.

ABSTRAK

Dalam kajian ini, tiga sistem polimer elektrolit disediakan melalui kaedah "solution casting". Polimer electrolit terdiri daripada poli (vinil alkohol) (PVA), litium perklorat ($LiClO_4$) (pendopan garam) dan dua jenis filler [antimoni trioksida (Sb_2O_3) dan titanium oksida (TiO_2)] telah disediakan.Polimer electrolit yang disediakan dengan pelbagai kandungan fillerdan kemudian dikaji dengan pembelauan sinar-X (XRD), impedansi, morfologi, dan kajian terma.Bagi sistem pertama, PVA (60 wt.%) dan $LiClO_4$ (40 wt%) adalah nisbah yang paling serasi yang mencapai kekonduksi ionik yang tertinggi $2.61 \cdot 10^{-5}$ S cm^{-1} di suhu bilik.Selain itu, kekonduksi ionik yang tertinggi dicapai dalam sistem kedua dan ketiga adalah $9.51 \cdot 10^{-5}$S cm^{-1} dan $1.30 \cdot 10^{-4}$ S cm^{-1}, masing-masing. Tiga sistem polimer elektrolit mentaati peraturan Arrhennius.Analisis XRD mendedahkan penindasankristalinitas dalam polimer matriks dan in berlaku apabila penambahan $LiClO_4$ dan pengisi. Penambahan Sb_2O_3 dan TiO_2 telah megalih suhu peralihan kaca, T_g kepada suhu yang lebih rendah di mana fleksibiliti polimer telah dipertingkatkan. SEM imej mendedahkan pengubahsuaian morfologi permukaan atas tambahan pengisi $LiClO_4$ dan bukan organik. Kajian TGA menunjukkan kestabilan terma polimer elektrolit meningkatkan apabila Sb_2O_3 dan TiO_2 telah diperkenalkan kepada polimer elektrolit dan mengalihkan shuhu penguraian permulaan kedua kepada suhu yang lebih tinggi. Dari kajian permohonan, elektrik kapasitor lapisan berganda (EDLC) telah disediakan dengan mengepit dua elektrod karbon di antara filem polimer nipis.Keputusan mendedahkan polimer elektrolit dengan pengisi mencapai kemuatan tertentu yang lebih tinggi berbanding dengan polimer elektrolit tanpa

pengisi. EDLC yang telah disediakan mempunyai pengekalan kapasitan lebih 90% menunjukkan sel EDLC mempunyai kestabilan cemerlang elektrokimia yang agak tinggi.

Acknowledgement

First of all, I would like to take this opportunity to express my special appreciation to Dr Ramesh T. Subramaniam (supervisor) and Dr Siti Rohana Majid (co-supervisor) for their supervision and constant support. During my study, both of them are helping me to complete the thesis writing. In addition, I appreciate their enthusiasm, inspiration, and their great efforts to explain things concise and precise concerning to my research.

Sincere thanks to all my lab members (Liew Qian Wen, Teoh Kok Hau, Sim Lina, Teo Li Peng, Din and etc.) from Center of Ionics, University of Malaya as they assist me to improve the understanding on my research field and useful information. Gratitude also goes to University of Malaya as this work was supported by Fundamental Research Grant Scheme (FRGS) from Ministry of Higher Education, Malaysia and Universiti Malaya Research Grant. They provide me an advance laboratory with apparatus, various types of instrument and good working environment.

Last but not least, my deepest gratitude goes to my beloved parent and my loves one for their cooperation, encouragement, constructive suggestion and full of support for the thesis completion, from the beginning till the end.

TABLE CONTENTS

		Page
ORIGINAL LITERARY WORK DECLARATION		ii
ABSTRACT		iii
ACKNOWLEDGEMENT		vii
LIST OF PUBLICATIONS		xii
LIST OF TABLES		xiii
LIST OF FIGURES		xiv
LIST OF ABBREVIATIONS		xvii
CHAPTERS		
1	**INTRODUCTION**	1
	1.1 Overview of polymer electrolyte	1
	1.2 Application of polymer electrolytes	2
	1.3 Advantages and drawbacks of polymer electrolytes	3
	1.4 Objectives of study	4
2	**LITERATURE REVIEW**	6
	2.1 Solid state ionics	6
	2.1.1 Crystalline electrolytes	7
	2.1.2 Glass electrolytes	7
	2.1.3 Molten electrolytes	7
	2.1.4 Polymer electrolytes	8
	2.2 Classification of polymer electrolyte	9
	2.2.1 Solid polymer electrolyte	9
	2.2.2 Gel polymer electrolyte	11
	2.2.3 Composite polymer electrolyte	12
	2.3 Ionic conductivity in polymer electrolyte	14
	2.3.1 Degree of crystallinity	16
	2.3.2 Salt concentration in polymer electrolyte	17
	2.4 Basic requirement for lithium salt	18
	2.4.1 Thermodynamics of salt dissolution in polymer matrix	19
	2.4.2 Hard/Soft Acid Base (HASB Principle)	20
	2.5 Characteristic of poly (vinyl alcohol) (PVA)	22
	2.5.1 Properties of PVA	23
	2.6 Lithium perchlorate ($LiClO_4$)	25
	2.7 Antimony trioxide (Sb_2O_3)	26
	2.8 Titanium oxide (TiO_2)	27
	2.9 Electric double layer capacitor (EDLC)	28
	2.9.1 Electrode material	30

3 Experimental procedure 32
3.1 Materials 32
3.2 Preparation of polymer electrolyte 32
3.2.1 First system (PVA-$LiClO_4$ based polymer electrolyte) 33
3.2.2 Second system (PVA-$LiClO_4$-Sb_2O_3 based polymer electrolyte) 33
3.3.3 Third system (PVA-$LiClO_4$-TiO_2 based polymer electrolyte) 34
3.3 Impedance spectroscopy 35
3.4 X-ray Diffraction (XRD) 37
3.5 Scanning electron microscope (SEM) 38
3.6 Differential scanning calorimetry (DSC) 39
3.7 Thermogravimetric analysis (TGA) 40
3.8 Linear sweep voltammetry (LSV) 41
3.9 Fabrication of EDLC 42
3.10 Characterization of EDLC 43
3.10.1 Cyclic voltammetry test (CV) 43
3.10.2 Galvanostatic charge discharge technique 43
3.10.3 Low frequency impedance spectroscopy 44
3.11 Summary 44

4 Results and Discussion I 46
4.1 Electrical properties 46
4.1.1 Impedance studies 46
4.1.1.1 First system (PVA-$LiClO_4$ based polymer electrolyte) 46
4.1.1.2 Second system (PVA-$LiClO_4$-Sb_2O_3 based polymer electrolyte) 49
4.1.1.3 Third system (PVA-$LiClO_4$-TiO_2 based polymer electrolyte) 51
4.1.2 Temperature dependence ionic conductivity studies 53
4.1.2.1 First system (PVA-$LiClO_4$ based polymer electrolyte) 53
4.1.2.2 Second system (PVA-$LiClO_4$-Sb_2O_3 based polymer electrolyte) 55
4.1.2.3 Third system (PVA-$LiClO_4$-TiO_2 based polymer electrolyte) 57
4.1.3 Dielectric behaviour studies 58
4.1.3.1 First system (PVA-$LiClO_4$ based polymer electrolyte) 58
4.1.3.1.1 Dielectric relaxation studies 58
4.1.3.1.2 Frequency-dependence ionic conductivity studies 60
4.1.3.1.3 Frequency dependence of loss tangent 62
4.1.3.2 Second system (PVA-$LiClO_4$-Sb_2O_3 based polymer electrolyte) 64

4.1.3.2.1 Dielectric relaxation studies 64
4.1.3.2.2 Frequency-dependence ionic conductivity studies 66
4.1.3.1.3 Frequency dependence of loss tangent 68
4.1.3.3 Third system (PVA-$LiClO_4$-TiO_2 based polymer electrolyte) 71
4.1.3.3.1 Dielectric relaxation studies 71
4.1.3.3.2 Frequency-dependence ionic conductivity studies 72
4.1.3.3.3 Frequency dependence of loss tangent 74
4.2 XRD studies 77
4.2.1 First system (PVA-$LiClO_4$ based polymer electrolyte) 77
4.2.2 Second system (PVA-$LiClO_4$-Sb_2O_3 based polymer electrolyte) 81
4.2.3 Third system (PVA-$LiClO_4$-TiO_2 based polymer electrolyte) 84
4.3 Morphological studies 87
4.3.1 First system (PVA-$LiClO_4$ based polymer electrolyte) 87
4.3.2 Second system (PVA-$LiClO_4$-Sb_2O_3 based polymer electrolyte) 91
4.3.3 Third system (PVA-$LiClO_4$-TiO_2 based polymer electrolyte) 93
4.4 DSC studies 95
4.4.1 First system (PVA-$LiClO_4$ based polymer electrolyte) 96
4.4.2 Second system (PVA-$LiClO_4$-Sb_2O_3 based polymer electrolyte) 98
4.4.3 Third system (PVA-$LiClO_4$-TiO_2 based polymer electrolyte) 100
4.5 TGA studies 102
4.5.1 First system (PVA-$LiClO_4$ based polymer electrolyte) 102
4.5.2 Second system (PVA-$LiClO_4$-Sb_2O_3 based polymer electrolyte) 104
4.5.3 Third system (PVA-$LiClO_4$-TiO_2 based polymer electrolyte) 105
4.6 Summary 107
4.6.1 First system (PVA-$LiClO_4$ based polymer electrolyte) 107
4.6.2 Second system (PVA-$LiClO_4$-Sb_2O_3 based polymer electrolyte) 108
4.6.3 Third system (PVA-$LiClO_4$-TiO_2 based polymer electrolyte) 109

5 Results and Discussion II 111

5.1 Comparison of PL-4 with PLS-6 on the performance of EDLC 111
5.1.1 LSV test 111
5.1.2 CV test 113
5.1.3 Galvanostatic charge-discharge technique 116
5.1.4 Impedance studies 120
5.2 Comparison of PL-4 with PLT-8 on the performance of EDLC 123
5.2.1 LSV test 123
5.2.2 CV test 124
5.2.3 Galvanostatic charge-discharge technique 128
5.2.4 Impedance studies 130
5.3 Summary 133

6 Conclusion 135
LIST OF REFERENCES 138

LIST OF PUBLICATION

International Journal

Chin-Shen Lim, S. Ramesh, S. R. Majid, (2012). The effect of antimony trioxide on poly (vinyl alcohol)-lithium perchlorate based polymer electrolytes. *Ceramic International*, in press. DOI: 10.1016/j.bbr.2011.03.031. (*ISI/SCOPUS Cited Publication*)-Tier 1

International Conference

Chin-Shen Lim, S.Ramesh, S. R. Majid, The Effect of Nanosized Sb_2O_3 Addition on Poly (vinyl alcohol)- Lithium Perchlorate Based Polymer Electrolytes, International Conference on Materials for Advanced Technologies, Suntec, Singapore, 26th June-1st July 2011. (Poster)

Chin-Shen Lim, S.Ramesh, S. R. Majid, Ionic Conductivity Enhancement Studies of Nanocomposite Polymer Electrolyte based on PVA-$LiClO_4$-TiO_2, International Conference on Materials for Advanced Technologies, Suntec, Singapore, 26th June-1st July 2011. (Poster)

National Conference

Lim Chin Shen, S.Ramesh, The Effect of Antimony Trioxide on Poly(vinyl alcohol) Lithium Perchlorate Based Polymer Electrolytes , Physics Research Colloquium 2012, University of Malaya, 28-29th May 2012.

List of Tables

Table		Page
2.1	Specific capacitance of EDLC using different lithium based polymer electrolytes.	29
3.1	Designation and composition of first polymer electrolyte system.	33
3.2	Designation and composition of second polymer electrolyte system.	34
3.3	Designation and composition of third polymer electrolyte system	35
3.4	The function of instrument for characterisation of polymer electrolyte	44
3.5	The function of instrument for characterisation of EDLC device	45
4.1	Crystallite size of PL-1, PL-3, PL-4 and PL-5 for diffraction peak at $2\theta=19.8^{o}$	80
4.2	Crystallite size of PLS-2, PLS-6 and PLS-8 for diffraction peak at $2\theta=19.8^{o}$	83
4.3	Crystallite size of PLS-2, PLS-6 and PLS-8 for diffraction peak at $2\theta=19.8^{o}$	87
4.4	Glass transition temperature (T_g) in DSC analyses for pure PVA, PL-1, PL-3, PL-4 and PL-5	97
4.5	Glass transition temperature (T_g) in DSC analyses for PLS-2, PLS-6 and PLS-8.	99
4.6	Glass transition temperature (T_g) in DSC analyses for PLT-4, PLT-8 and PLT-10	101
4.7	Total weight loss (%) at temperature range of 210 ℃-280 ℃ in TGA analyses for PL-1, PL-3, PL-4 and PL-5	103
4.8	Total weight loss (%) at temperature range of 210 ℃-280 ℃ in TGA analyses for PLS-2, PLS-6 and PLS-8	105
4.9	Total weight loss (%) at temperature range of 210 ℃-280 ℃ in TGA analyses for PLT-4, PLT-8 and PLT-10	107

LIST OF FIGURES

Figure		Page
2.1	Schematic diagram of mixed amorphous and crystalline regions in semi-crystalline polymer structure.	16
2.2	Chemical structure of PVA	22
2.3	Chemical structure of $LiClO_4$	25
2.4	Schematic diagram of an EDLC cell	28
3.1	Impedance spectroscopy	35
3.2	A typical complex impedance plot of polymer electrolyte	35
3.3	X-ray Diffractometer	38
3.4	Scanning electron microscope	39
3.5	Differential scanning calorimetry	40
3.6	Thermogravimetric analyzer	41
3.7	Autolab PGSTAT 12 potentiostat/galvanostat	42
3.8	Neware battery cycler	43
4.1	Complex impedance plot for PL-1	47
4.2	Complex impedance plot for PL-4	48
4.3	The variation of ionic conductivity values as a function of $LiClO_4$ concentration.	48
4.4	The variation of ionic conductivity values as a function of Sb_2O_3 concentration.	51
4.5	The variation of ionic conductivity values as a function of TiO_2 concentration.	52
4.6	Arrhenius plots of ionic conductivity of PL-1, PL-3, PL-4 and PL-5.	55
4.7	Arrhenius plots of ionic conductivity of PL-4, PLS-2, PLS-6 and PLS-8	57
4.8	Arrhenius plots of ionic conductivity of PL-4, PLT-4, PLT-8 and PLT-10	58
4.9	Variation of real part of dielectric constant (ε') with frequency at ambient temperature for PL-1, PL-3, PL-4 and PL-5.	60
4.10	Variation of logarithm conductivity as a function of frequency for PL-1, PL-3, PL-4 and PL-5.	62
4.11	Variation of tan δ with frequency for PL-1, PL-3, PL-4 and PL-5 at room temperature.	64
4.12	Variation of real part of dielectric constant (ε') with frequency at ambient temperature for PL-4, PLS-2, PLS-6 and PLS-8.	66
4.13	Variation of logarithm conductivity as a function of frequency for PL-4, PLS-2, PLS-6 and PLS-8.	67
4.14(a)	Variation of tan δ with frequency for PL-4, PLS-2 and PLS-8 at room temperature.	70
4.14(b)	Variation of tan δ with frequency for PLS-6 at room temperature.	70

4.15	Variation of real part of dielectric constant (ε') with frequency at ambient temperature for PL-4, PLT-4, PLT-8 and PLT-10.	72
4.16	Variation of logarithm conductivity as a function of frequency for PL-4, PLT-4, PLT-8 and PLT-10.	73
4.17(a)	Variation of tan d with frequency for PL-4, PLT-4 and PLT-10 at room temperature.	76
4.17(b)	Variation of tan d with frequency for PLT-8 at room temperature.	76
4.18	XRD pattern for (a) pure PVA and (b) $LiClO_4$	78
4.19	XRD pattern for (a) PL-1, (b) PL-3, (c) PL-4 and (d) PL-5	79
4.20	XRD pattern for Sb_2O_3	81
4.21	XRD pattern for (a) PLS-2, (b) PLS-6 and (c) PLS-8	82
4.22	XRD pattern for TiO_2	84
4.23	XRD pattern of (a) PLT-4, (b) PLT-8 and (c) PLT-10	85
4.24(a)	SEM micrograph of pure PVA at a magnification of 1000x	89
4.24(b)	SEM micrograph of PL-1 at a magnification of 1000x	89
4.24(c)	SEM micrograph of PL-3 at a magnification of 1000x	90
4.24(d)	SEM micrograph of PL-4 at a magnification of 1000x	90
4.24(e)	SEM micrograph of PL-5 at a magnification of 1000x	90
4.25(a)	SEM micrograph of PLS-2 at a magnification of 1000x	92
4.25(b)	SEM micrograph of PLS-6 at a magnification of 1000x	92
4.25(c)	SEM micrograph of PLS-8 at a magnification of 1000x	93
4.26(a)	SEM micrograph for PLT-4 at magnification of 1000x	94
4.26(b)	SEM micrograph of PLT-8 at a magnification of 1000x	95
4.26(c)	SEM micrograph of PLT-10 at a magnification of 1000x	95
4.27	DSC thermograms of (a) pure PVA, (b) PL-1, (c) PL-3, (d) PL-4 and (e) PL-5.	96
4.28	DSC thermograms of (a) PLS-2, (b) PLS-6 and (c) PLS-8	98
4.29	DSC thermograms of (a) PLT-4, (b) PLT-8 and (c) PLT-10	100
4.30	Thermogravimetric curves of pure PVA, PL-1, PL-3, PL-4 and PL-5.	102
4.31	Thermogravimetric curves of PLS-2, PLS-6 and PLS-8	105
4.32	Thermogravimetric curves of PLT-4, PLT-8 and PLT-10	106
5.1	LSV curve for PL-4	112
5.2	LSV curve for PLS-6	112
5.3	Cyclic voltammograms of (a) EDLC cell with PL-4 and (b) EDLC cell with PLS-6 at 10 mV s^{-1} scan rate.	113
5.4	Cyclic voltammograms of EDLC cell with PLS-6 with various scan rate at 10 mV s^{-1}, 30 mV s^{-1}, 50 mV s^{-1} and 100 mV s^{-1}.	115
5.5	Variation of specific capacitance and scan rate for EDLC assembled with PLS-6	116
5.6	Charge-discharge pattern for (a) EDLC cell with PL-4 and (b) EDLC cell with PLS-6 at current of 1 mA.	117
5.7	Specific capacitance retention versus cycle number for PL-4 and PLS-6 EDLC devices.	120
5.8	Typical impedance plot of (a) EDLC cell with PL-4 and (b) EDLC cell with PLS-6 at room temperature.	122
5.9	Specific capacitance versus frequency dependence of (a) EDLC	123

with PL-4 and (b) EDLC cell with PLS-6.
5.10 LSV curve for PLT-8 124
5.11 Cyclic voltammograms of (a) EDLC cell with PL-4 and (b) EDLC cell with PLT-8 at 10 mV s^{-1} scan rate. 126
5.12 Cyclic votammograms of EDLC cell with PLT-8 with various scan rate at 10 mV s^{-1}, 30 mV s^{-1}, 50 mV s^{-1} and 100 mV s^{-1} 127
5.13 Variation of specific capacitance and scan rate for EDLC assembles with PLT-8. 127
5.14 Charge-discharge pattern for EDLC cell with PLT-8 at current of 1 mA. 128
5.15 Specific capacitance retention versus cycle number for PLT-8 EDLC devices 129
5.16 Typical impedance plot of EDLC cell with PLT-8 at room temperature. 131
5.17 Specific capacitance versus frequency dependence of EDLC cell with PLT-8. 132

LIST OF ABBREVIATION

A	Area of disk electrodes in cm^2
C	Parallel capacitance in F (farad)
L	Thickness of the film in cm
f	Frequency in Hz
DSC	Differential scanning calorimetry
CV	Cyclic voltammetry
G	Conductance in S cm^{-1}
LSV	Linear sweep voltammetry
k	Boltzmann Constant
M'	Real part of dielectric modulus
M''	Imaginary part of dielectric modulus
SEM	Scanning electron microscope
TGA	Thermogravimetric analysis
XRD	X-ray diffraction
PVA	Poly (vinyl alcohol)
SPE	Solid polymer electrolyte
GPE	Gel polymer electrolyte
CPE	Composite polymer electrolyte
R_b	Bulk resistance in Ω
T_g	Glass transition temperature in ^oC
AC	Activated carbon

NMP	N-methyl-2-pyrrolidone
Z	Impedance
Z'	Real impedance in Ω
Z''	Imaginary impedance in Ω
ε'	Real part of dielectric constant
ε"	Imaginary part of dielectric constant
θ	Phase angle in degree
σ	Ionic Conductivity in S cm^{-1}
PVdF	Poly (vinylidene fluoride)
C_{spec}	Specific capacitance, F g^{-1}

CHAPTER 1

Introduction

1.1 Overview of polymer electrolyte

The science of polymer electrolytes is a highly specialized interdisciplinary field which encompasses the disciplines of electrochemistry, material science, organic chemistry, and inorganic chemistry. This field has attracted researchers in academia and industry, for the past two decades due to the potentially promising applications of such electrolyte, not only in all solid-state rechargeable lithium or lithium-ion batteries, but also in other electrochemical devices such as electric double layer capacitors, solar cells, and sensors (Song *et. al.*, 1999).

Polymer electrolytes (PE) are materials that have polymeric backbones with covalently bonded ionizing groups attached to them. It can also be defined as a membrane that possesses ion transport properties that can be compared with the common type of the liquid ionic solutions. The first generation polymer electrolyte also known as 'solid' polymer electrolyte or 'solvent-free' polymer electrolyte was prepared by Wright and co-workers where poly (ethylene oxide) (PEO) was employed as host polymer and sodium and potassium salts as dopant salts (Fenton *et al.*, 1973). However, first generation solid polymer electrolyte attained very low ambient temperature ionic conductivities of the order of 10^{-8} S cm^{-1}.

The low ionic conductivity is owing to the limitations on the systems as PEO shows a partial crystalline nature on oxyethylene chain and thus, an acceptable level of the ionic conductivity can only be achieved above the melting temperature. This is partly due to high degree of crystallinity of polymer electrolytes as ion conduction in polymer electrolytes are mostly in the amorphous region which containing the electrolyte salts. Consequently, a low ionic conductivity caused by slow kinetics of crystallization of polymer as ionic conduction in polymer electrolytes is dominated by the amorphous phase in the polymer matrixes (Kalita *et al.*, 2007).

The low ionic conductivity of polymer electrolyte also shows a low satisfaction on the performance of lithium batteries. Therefore, second and third types of polymer electrolytes were implemented by researchers. The second type of polymer is called "gel polymer electrolyte" or "plasticized polymer electrolyte" whereas the third type polymer electrolyte is known as "composite polymer electrolyte". The purpose of the development of new generation polymer electrolyte is to enhance the ionic conductivity of polymer electrolyte at ambient temperature.

1.2 Application of polymer electrolytes

The attentiveness in the investigation of polymer electrolyte is continuously increasing due to their varied application on electrochemical devices such as high energy density batteries, fuel cells, sensors and electrochromic devices (Baskaran *et. al.*, 2006). Recently, researchers are utilizing polymer electrolyte in the production of commercial secondary lithium batteries. Lithium batteries has widely concerned by

researchers because of wider range in applications that can be applied on small portable electronic and personal communications equipment such as laptop, mobile phone, MP3 player, PDA electric vehicle (EV) and starlight-ignition (SLI) which serves as traction power source for electricity (Gray, 1997a). In addition, researchers found that polymer electrolytes could act as separators and electrolytes in the electric double layer capacitors (Sivaraman *et. al.*, 2003).

1.3 Advantages and drawbacks of polymer electrolytes

Recently, liquid electrolytes were replaced by polymer electrolytes in some applications due to several advantages that had been found in polymer electrolytes. The advantages are no corrosive or powerful solvents are present in polymer electrolytes that may react with seals and containers, suppression of lithium dendrite growth, high flexibility, improved safety and enhanced the endurance to varying electrode volume during cycling. Another feature associated with polymer–electrolyte batteries is the manufacturing integrity; all elements, both the electrolyte and electrodes, of a cell can be laminated automatically via well-developed coating technology (Xu and Ye, 2005; Gray, 1991).

Although polymeric electrolytes have many promising applications, the ionic conductivity of the polymer electrolytes is still not ideal to be used in these applications. Based on previous research, PEO based polymer electrolytes attained ionic conductivity in the range of 10^{-8} S cm^{-1} at an ambient temperature. The low ionic conductivity value was owing to the crystalline nature of the polymer used and

poor flexibility of polymer backbone. Thus, most researchers are now attempting to find new approaches and materials that will provide a superior ionic conduction, high chemical stability, wide electrochemical stability window, long lifespan, and resistance to steady stress over a temperature range through different types of materials and types of approaches. Some of the approaches are synthesizing new polymers, cross-linking two polymers, blending two polymers, addition of plasticizers, addition of inorganic inert fillers and addition of mixed salts (Gaelle *et al.*, 2009).

1.4 Objectives of the study

Preparation of biodegradable polymer electrolytes by solution casting technique is the main objective in this study. In this research would be Poly (vinyl alcohol) (PVA) and Lithium perchlorate ($LiClO_4$) were used as host polymer and inorganic salt, respectively. The effect of different fillers such as Sb_2O_3 and TiO_2 on PVA-$LiClO_4$ based polymer electrolytes was analyzed using different techniques

Investigation of ionic conductivity is one of the main aspiration of this study. The effect of inorganic fillers on ionic conductivity of prepared polymer electrolytes was scrutinized by alternating current impedance spectroscopy. Impedance spectroscopy can also help us to understand the ion conduction mechanism by temperature dependence ionic conductivity study and to evaluate the dielectric relaxation characteristic of the solid polymer electrolytes.

Thin films were also subjected to X-ray diffraction (XRD) measurement in order to examine the crystalline nature of polymer electrolytes and to prove the complexation between polymer, inorganic salt and fillers. Scanning electron microscope (SEM) was used to understand the morphology of polymer electrolytes upon the addition of additives. Thermal properties of polymer electrolytes were examined using differential scanning calorimetry (DSC) and thermogravimetric analyzer (TGA). The electrochemical stability window or operational potential for a complete system was investigated by linear sweep voltammetry (LSV).

In addition, electric double layer capacitor was fabricated by sandwiching the thin films with two activated carbon electrodes. The capacitive behaviour of the EDLC was studied by using different techniques such as cyclic voltammetry (CV), impedance spectroscopy (EIS) and galvanostatic charge-discharge techniques.

Chapter 2

Literature Reviews

2.1 Solid state ionics

Generally, solid state ionics is the study of solid state electrolytes and their applications. Materials that fall into this category include inorganic crystalline solids, polycrystalline solids, ceramics, glasses, polymers and composites. Solid electrolytes are materials that show the occurrence of ionic conductivity inside the materials. These solid electrolytes must have rigid framework structure that own sets of ions from a mobile sub lattice. Apart from that, the conductivity of the solid electrolytes must be similar to those of strong liquid electrolytes, which is around 1 S cm^{-1}.

These solid state electrolytes are intermediates between typical ionic solids, where all ions are fixed on their lattice sites, and liquid electrolytes, in which all ions are mobile. The availability of empty sites for ions to hop and the smaller energy barrier for ions to hop between sites are other characteristics of the solid electrolytes. Besides, modest amounts of ionic conduction are common in the solid electrolytes, especially in non-stoichiometric or doped materials.

Several types of solid state electrolytes such as crystalline electrolytes, glass electrolytes, molten electrolytes and polymer electrolytes are described briefly in the following part in order to give a understanding of the fundamental differences between polymer electrolytes and other solid state electrolytes.

2.1.1 Crystalline electrolytes

Crystalline electrolyte is classified as solid state electrolyte which conduct H^+, Li^+, Na^+, K^+, Ag^+, Ti^+, F^-, O^{2-}, as well as numerous divalent and trivalent cations. Crystalline electrolyte possesses high ionic conductivity owing to high concentration of mobile ions and low activation energy for ionic motion from site to site. Generally, the conduction happens by means of a hopping mechanism from site to site along channels in the crystal structure.

2.1.2 Glass electrolytes

Glass electrolytes are generally known as amorphous solid conductors. Glass electrolytes are formed when liquids or solutions containing ions cooled without crystallizing. Basically, glasses able to transport a number of ions such as Li^+, Na^+, K^+, Cs^+, Rb^+, Ag^+ and F^-. Most glasses are obtained by quenching from the liquid state, and the resulting atomic structures varied from the original liquid. Glassy systems are made up from three basic constituent with some or all present in all conducting glasses. These components are known as network formers (covalent compounds), network modifiers (oxides or sulphide) and ionic salts (halides or sometimes sulphate) (Gray, 1997).

2.1.3 Molten electrolytes

Molten electrolytes are the molten of single salts or molten eutectic mixture, which generally exhibits high ionic conductivities (more than 1 S cm^{-1}). Examples of those molten electrolytes are the LiCl-KCl eutectic and the chloroaluminates ($AlCl_3$-MCl, where M = alkaline metal). In spite of having high ionic conductivity, the major

counterpart of molten electrolyte possesses a high maintenance at a high operating temperature. The usage of aggressive agents during this process may lead to corrosion and leakage.

2.1.4 Polymer electrolytes

In this study, we are concentrating on polymer electrolytes due to their low cost and easy in preparation. A polymer electrolyte consists of an inorganic salt dissolved in a polymer host. These conductive materials were first described in the early 1970' s and it was quickly adopted by the electrochemical community, who recognized the potential of a flexible, plastic, ion transporting medium for vital applications such as energy storage and electrochemical displays.

Generally, polymer electrolytes have mechanical properties which should allow the construction of practical all solid state electrochemical cells. High molecular weight amorphous material may exhibit macroscopic properties that have the attributes of a true solid but, at an atomic level, local relaxations provide liquid-like degrees of freedom that are not significantly different to those of a conventional liquid as they are not hard and brittle. These properties can ensure a good interfacial contact with electrode materials and, more importantly, maintain these contacts under stress such as the volume changes associated with cell charging and discharging.

2.2 Classification of polymer electrolyte

Polymer electrolytes can be classified as:

1. Solid polymer electrolyte
2. Gel polymer electrolyte
3. Composite polymer electrolyte

2.2.1 Solid polymer electrolyte (SPE)

A solvent-free electrolyte is created by mixing inorganic salts with a high molecular weight polar polymer matrix. In the present study, the solvent free electrolyte was prepared by using solution casting method. Both polymer and salt will be stirred thoroughly for at least 24 hours for the mixtures to reach homogeneity. The solution was then poured onto a petri dish and was allowed to evaporate slowly inside a fume hood until a thin film is formed. The resulting thin film is solvent free and essentially an ion complexed polymer electrolyte (Alamgir and Abraham, 1993).

SPE serves few important roles in a lithium rechargeable battery. Firstly, polymer electrolyte incorporated with lithium salt is a lithium ion carrier and can enhance the energy density. Besides, it acts as the electrode separator that insulates the anode from the cathode in the battery which removes the requirement of inclusion of inert porous spacer between the electrolyte and electrodes interface. SPE also plays the role as medium channel to generate ionic conductivity which ions are transported between the anode and cathode during charging and discharging. This leads to enhancement of energy density in the batteries with formation of thin film. In

addition, SPE works as binder to ensure good electrical contact with electrodes. Thus, high temperature process for conventional liquid electrolyte can be ignored (Kang Xu, 2004).

The lithium salt complexed with PEO and –poly (proplylene oxide) PPO are the most popular polymer electrolyte system to be investigated (Armand, 1987). The PEO was employed as polymer host will create stable complexes with lithium salt compared to other solvating polymers and possess higher ionic conductivities compared to other group. The PEO-salt complex is formed when the cation of lithium salt formed a coordinate bond with the oxygen donor. This complex formation of PEO host and salt is governed by the competition between solvation energy and lattice energy of both polymer and salts. Low lattice energy of the salt has been found to facilitate dissociation of the salt which in turn increases the number of free ion species in the polymer matrix.

In the early studies, although PEO based polymer electrolytes exhibit good mechanical properties, they show low ionic conductivity value (~10^{-8}S cm^{-1}) at room temperature. This is attributed to the high degree of crystallinity. Eventually, researchers had tried to seek for other synthetic polymers that possess electron-donating power such as poly (acrylonitrile) (PAN), poly (vinylidene fluoride) (PVdF), poly (ethylene glycol) (PEG) and poly (vinyl alcohol) (PVA). Watanabe and co-workers reported that ionic conducitivity value as high as 10^{-4} S cm^{-1} was achieved utilizing PPO complexed with $LiCF_3SO_3$system (Watanabe *et. al.*, 1998). This implies that the use of other polymers can also acts as conductors.

2.2.2 Gel polymer electrolyte (GPE)

Gels are generally defined as “polymers and their swollen matters with three dimensional network structures that are insoluble in any solvents” and gels exist under special condition which is not found in solid, liquid and gasses (Osada and Kajiwara, 2001). The gel polymer electrolyte contains organic liquid as plasticizers with which the inorganic salt remains encapsulated in a polymer matrix. Basically, gel polymer electrolyte is formed by dissolving a lithium salt in a plasticizer and mixed with polymers.

The characterization of this sample falls between the solid and liquid, and their properties vary from viscous liquids to hard solids. The properties of polymer gel depend upon the structure of the polymer network that makes up the gel as well as the interaction of the network and the solvent. Since the polymer networks are solvated by a large amount of trapped solvent thus gels generally possess high mobility. Since the first report on high conductivity in lithium ion conducting polymer gel electrolytes (Feuillade and Perche, 1975), the polymer gel appears as a promising alternative in producing high mobility membrane or medium in the development of polymer electrolytes. The interest in these materials is due to their potential applications in solid state batteries, electrochromic devices, fuel cells, supercapacitors etc. (Abraham and Alamgir, 1994).

Generally, gel-type polymer electrolytes were obtained from heavily plasticized polymers. This fabrication caught most of the researchers attention in line to some of their unique properties like high value of ionic conductivity at room

temperature (10^{-2} to 10^{-4} S cm^{-1}), ease in preparation, wide range of composition and hence wider control of properties, good adhesive properties suitable for lamination and good thermal/ electrochemical stability.

In general, the functions of plasticizers in polymer electrolyte are listed as follows (Kim and Smotkin, 2002):

1) Enhance ion dissociation resulting in higher number of free charge carriers that involve in ion transportation. Generally, the tendency of a salt to dissociate is high owing to the high dielectric constant of the added plasticizers.
2) Plasticizers can reduce the crystallinity of polymers by increasing more amorphous phases in polymer matrix.
3) Increase the polymer segmental mobility. The mobility of the ion was elevated when the viscosity of the plasticizer is low.
4) Addition of plasticizers can shift the glass transition temperature to lower temperature which increases the flexibility of polymer backbone. A flexible backbone can favor the ion migration.
5) Plasticizers have the ability to reduce the solvent leakage during the fabrication. This can improve the contact between electrodes and electrolytes.

2.2.3 Composite polymer electrolyte

The third category of polymer electrolyte is called composite polymer electrolyte. Composite polymer electrolyte is a polymer electrolyte where high surface area filler was incorporated into the dry solid polymer electrolyte. The

imperfection of SPE is overcome by introducing the inert fillers such as TiO_2, Al_2O_3, SiO_2, carbon nanotubes and MgO into polymer electrolyte. Inorganic filler has the capability to enhance conductivity, mechanical stability, electrochemical stability, cation transference number, lowering interfacial resistance, and high dielectric constant and thermal stability towards electrode materials (Chu and Reddy, 2003; Kim *et. al.*, 2002).

Ahmad and co–workers had reported that dispersion of 6 wt. % of SiO_2had attained the highest ionic conductivity with poly(methyl methacrylate) (PMMA) as host polymer, lithium triflate as salt and propylene carbonate (PC) as plasticizer. These CPEs are homogeneous and exhibit wide electrochemical stability window with excellent rheological properties at ambient temperature (Ahmad *et al*., 2006a).

In addition, Raghavan and co-workers found that nanocomposite polymer electrolyte comprising of a nanosized barium titanate ($BaTiO_3$) and ionic liquid [*n*-butyl-3-methylimidazolium bis (trifluoromethanesulfonyl) imide (BMITFSI)] hosted in electrospun poly (vinylidene fluoride-co hexafluoropropylene) (PVdF-HFP) shows improved ionic conductivity as well as energy density (Raghavan *et. al.*, 2010). The higher surface area of inorganic filler (smaller particle size) which may create a more conducting pathway of polymer-filler interface and thus, promotes the ionic transportation in the polymer matrix (Kumar *et. al*., 2009). However, Liu and co-workers had investigated the composite polymer electrolyte and found that suppression of lithium dendrite formation was observed upon the addition of inorganic filler. This is proven when low internal resistance is obtained from

impedance analysis (Liu *et. al.*, 2010). Inorganic filler is also capable in reducing the crystalline phase of polymer electrolytes and increasing the flexibility of polymer backbone that favors the ion migration (Ji *et. al.*, 2003).

In conclusion, the function of inorganic fillers could be summarized as below:

a) Addition of the filler powder in the suitable proportion retards the crystallization of the polymer electrolytes.
b) High surface area of filler will create new conducting pathways for ion migration. Fillers also assist in salt dissociation and increase the number of ion species in the polymer matrix.
c) Ceramic fillers can improve the mechanical stability and thermal stability of the polymer electrolytes.

2.3 Ionic conductivity in polymer electrolyte

The general expression of ionic conductivity of a homogenous polymer electrolyte is shown as

$$\sigma = \sum n_i z_i \mu_i \quad \text{(Equation 2.1)}$$

Where n_i is the number of charge carriers type of *i* per unit volume, z_i is the charge of ions type of *i*, and μ_i is the mobility of ions type of *i* which is the measure of the drift velocity in a constant electric field (Smart and Moore, 2005). Based on the equation, the number and mobility of charge carriers are the main aspects that could affects the ionic conductivity of polymer electrolytes as the charge of the mobile charge carriers

are the same and negligible.

There are several principal conditions that must be achieved in order to produce the ionic hopping process:

1. A massive number of ions of one species should be mobile
2. A large number of empty sites should be available for the ionic conduction. This is essentially a corollary of (1) because ions able to move only if there are vacant sites available for them to occupy.
3. The empty and occupied vacant sites should have similar potential energies with low activation energy for hopping between the neighboring sites. It is useless to have a large number of available vacant sites if either the mobile ions cannot get into them or if they are too small.
4. The structure should have a framework, three-dimensional, permeated by open channels through which mobile ions may migrate.
5. The anion substructure should be highly polarized (West, 1999a).

Direct current (dc) ionic conductivity is a parameter that evaluates conductivity of polymer electrolytes. An optimum ionic conductivity value is required in the range of 10^{-3} to 10^{-5} S cm^{-1}. The polymer electrolyte with high ionic conductivity is suitable to be used for application purposes. There are two factors that manipulate the magnitude of the ionic conductivity of polymer electrolyte:

a) Degree of crystallinity

b) Salt concentration

2.3.1 Degree of crystallinity

A semi-crystalline polymer with organized and closely packed areas of polymer molecules is known as “polymer crystals” in semi-crystalline polymers. Nevertheless, semi-crystalline polymers also possess an amorphous phase where the polymer chains have no well-defined order in either the solid or liquid states. Figure 2.1 shows the polymer matrixes with crystalline regions embedded in amorphous matrix.

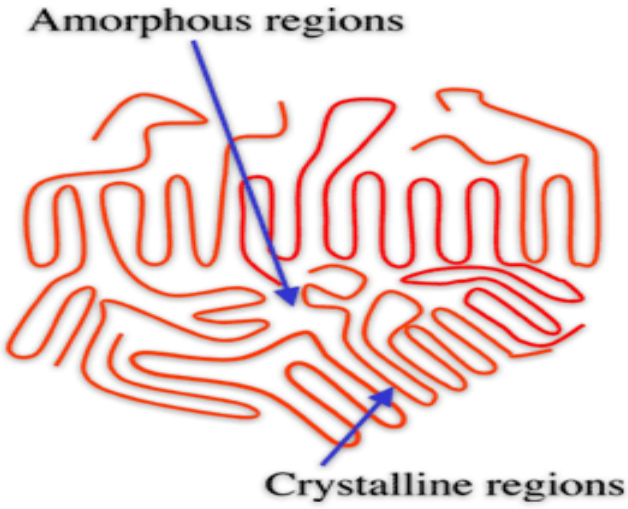

Figure 2.1: Schematic diagram of mixed amorphous and crystalline regions in semi-crystalline polymer structure.

In polymer electrolyte, the ionic conduction is more favourable when there is more amorphous portion in the polymer matrix. The amorphous region is not similar with crystalline region as the molecules indicate unordered arrangement and hence, the molecules in the polymer matrix are loosely packed in the lattice site. This leads to better flexibility of the polymer backbone which sustains the charge carriers in

transportation. In addition, as the degree of amorphous enhanced, it will provide more spaces and formation of void that assists in ionic hopping.

Another attributor that affects the crystallinity of polymers is temperature. As the temperature is increased, the crystalline region has high tendency to transform into amorphous region and hence, the charge density increases extensively. Eventually, this will create a better medium for ion species to migrate from one site to another (Gray, 1991b).

2.3.2 Salt concentration in polymer electrolyte

The movement of ions is closely correlated to the relaxation modes of the polymer host. This can be observed through the increase in glass transition temperature (T_g) of polymer systems as salt concentration is increased. The deterioration in segmental motion is usually interpreted as being a result of the effects of an increase in intramolecular and intermolecular coordinations between coordinating sites on the polymer or different polymer chains caused by the ions acting as transient crosslinks. The increase in T_g value will cause the ionic conductivity of the polymer electrolyte decreases. This is mainly owing to stiffening of the matrix; the availability of vacant coordinating sites is greatly reduced at higher wt. % of salt content (Gray, 1991b).

Based on Equation 2.1, the type of charge carriers includes the free ion species and neutral pair, such as ion aggregates. At low salt content, the mobility of ions is relatively unaffected by concentration, as the transient crosslink density will be low

and therefore the ionic conductivity will be controlled by the number of charge carriers (Yu et. al., 2007). Formation of neutral ion pairs and mobile higher aggregates can be expected when the salt content keep increasing. These aggregates may form a less mobile cluster and act as transient cross linking species. As a result, the availability of vacant sites for ionic conduction is enormously decreased (Braun, 2005a) and the mobility of ion species was restricted. Eventually, the ionic conductivity of polymer electrolyte decreases due to these factors.

2.4 Basic requirement for lithium salt

An ideal electrolyte solute or salt for electrochemical devices should attain the following minimal requirements. Firstly, it should be able to completely dissolve and dissociate in the non-aqueous media, and the solvated ions (especially lithium cation, Li^+) should be able to move in the non- aqueous medium with high mobility. Second, the anion of salt should be stable against oxidative decomposition at the cathode and remain stable against thermally induced reactions with electrolyte solvents and other cell components. Third, the anion of salt is inert to electrolyte solvents to avoid the chemical changing between salt and solvent. Fourth, both the anion and the cation should remain inert toward the other cell components such as separator, electrode substrate, and cell packaging materials to prevent interaction between these components. The anion should be nontoxic to avoid the harmful leakage from the cell (Kang Xu, 2004).

2.4.1 Thermodynamics of salt dissolution in polymer matrix

As mentioned above, polymer electrolyte consists of a polymer host and inorganic salt. When inorganic salt is dissolved into a polymer matrix, the free energy change is given by standard Gibbs free energy expression

$$\Delta G_{mixing} = \Delta H_{mixing} - T\Delta S_{mixing} \qquad \text{(Equation 2.2)}$$

From the equation, when $\Delta G_{mixing} < 0$, the mixing process happens spontaneously. It is very obvious that one must consider changes in both entropy and enthalpy.

The entropy change, ΔS, is an important parameter, consisting of a positive value from lattice energy of the salt, and a negative value from ionic coordination to the polymer. For a complete mixing, the ions should therefore not bind too efficiently to one another, but form bonds with the polar atom from polymers. This means that cations should coordinate electrostatically to the polymer backbone, while the anions should diffuse freely in the matrix, with a minimum of interaction with the polymer and especially with the cations. A salt with small univalent cation and a large anion seems to fulfill these requirements: low lattice enthalpy, weak ion-ion bonding and strong cation-polymer coordination.

The entropy change is more complicated to study. First, there is a positive entropy contribution from the break up of the crystal latttice of the ionic salt, and the subsequent disordering of the ions in the system. This effect is compensated for by an increased rigidity in the polymeric system when the cations cross-linking with different parts of the polymer, thereby reducing its translational and rotational motion. In addition, salt dissolution facilitates more polymer configurations via multidentate

coordination to the cation – an effect which leads to an increase in entropy. In spite of that, when ΔS is negative, Gibbs free energy automatically must possess positive value at higher temperatures, where out salting will occur – the very opposite effect of dissolution in most liquid systems (Gray, 1997).

2.4.2 Hard/Soft Acid Base (HSAB Principle)

The solvation enthalpy of a salt in a polymer solvent is relying on the interaction between the cation and polar atom in polymers. Solubility can be discussed in terms of the acid-base interactions between solvent and solute molecules, which each solvent being classified as hard or soft. The bonding between the polymer solvent and salt can be classified according to the hard or soft acid-base principle. The strongest interactions able to exist by coordinating hard acids with hard bases or soft acids with soft bases. The classifications are shown as following (Gray, 1997):

a) Hard/soft acids

Hard acids are small cations without any valence electrons which can polarized or removed easily, for example, alkali and Mg^{2+} while soft acids must possess larger cations with several valence electrons that are easily distorted or removed (partially filled '*d*' orbital and to a lesser extent '*f*' orbital), for example, Hg^{2+}.

b) Hard/soft bases

Hard bases are non-polarizable ligands with high electronegativity, for example, oxygen in ether. Soft bases are more polarizable groups, for example, the thio group of the thioether.

In water or hydrogen-bonded solvent such as alcohols, the anions are solvated and stabilized by the hydrogen bonds, but it is a totally different situation for the less polar solvents. The stability of the anions depends very much on charge dispersion for the less polar solvents. Examples of less polar solvents are tetrahydrofuran and acetonitrile. Large anions with delocalized charge require little solvation, and it can be either 'soft' (I^-) or 'hard' ($CF_3SO_3^-$) bases (Gray, 1997).

Salts of singly charged polyatomic anions such as in $LiCF_3SO_3$ or $LiClO_4$ would dissolve easily in polyethers. Salts containing monoatomic anions may be soluble in polyethers, provided they are large and polarizable, for examples, I^-, and Br^-. The large salvation energies of 2^+ and 3^+ cations can induce the formation of polymer complexes, even with the small Br^- anions. However, the larger I^- anion is required for less-solvated monovalent cations such as K^+. An addition factor that will aid dissolution is that salts with large monovalent anions having low lattice energies.

The most appropriate salts for polymer electrolytes are those of a small cation and a large anion of delocalized charge, which will minimize the lattice energy. The salt affects the overall conductivity through the crystalline complex formation, intramolecular cross-linking of the polymer chains and the degree of salt dissociation (the number or charge carriers). The anion, in particular, has a major influence on the phase composition and conductivity (Gray, 1997).

2.5 Characteristic and reviews of Poly (vinyl alcohol)

PVA was discovered in 1924 by W.O. Herman and W. Haehnel at the consortium Fur Elektrochemische Industrie. Figure 2.2 shows the chemical structure of PVA. Generally, polymer electrolyte that uses PVA as host polymer can give a excellent film with high tensile strength and flexibility. Beside, PVA also shows other properties such as resistant to oil, grease and solvent.

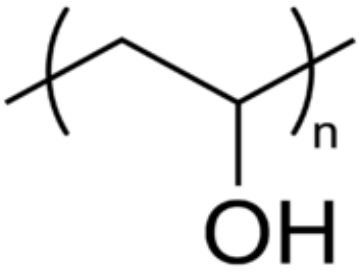

Figure 2.2: Chemical structure of PVA

The physical and chemical properties of PVA depend on the method of preparation. PVA is usually prepared by hydrolysis of poly (vinyl acetate) (PVAc), where the acetate (CH_3COO) side groups are replaced by hydroxyls (-OH). Choosing a suitable polymerization and hydrolysis conditions can provide PVA with different physical and chemical properties.

In this study, Poly (viny alcohol) (PVA) with hydrolysed 99%+ was used which has a hydrophilic synthetic polymer that classified as green polymer due to high degree of hydrolysis, which can undergo biodegradable process. PVA is a

versatile polymer with plenty of industrial application due to its biodegradability, biocompatibility, chemical resistance and excellent physical properties.

Saroj and Singh found that PVA based polymer electrolytes possess good mechanical property and high ionic conductivity value (Saroj and Singh, 2012). In addition, Lewandoski and co-workers found that the ionic conductivity of the PVA based polymer electrolyte was in the order of 10^{-3} S cm^{-1} at room temperature (Lewandoski *et. al.*, 2000). Nevertheless, in recent century, PVA based polymer electrolytes were used in several applications such as fuel cells, lithium batteries, supercapacitors and electrochromic displays. One of the research team had fabricated an electrochromic display using PVA mixed with H_3PO_4 and H_2SO_4 as electrolytes. The result reveals the PVA is a promising candidate to be used in electrochromic devices (Singh *et. al.*, 1995). Other researchers also reported that PVA based alkaline polymer electrolyte prepared by solution casting technique is a promising candidate for supercapacitor where the polymer film acts as a transporting medium for ion species (Sun and Yuan, 2009).

2.5.1 Properties of PVA

The properties of PVA can be characterized as below:

i) Solubility

The high level of hydrogen bonding manipulates the water solubility of the polymer. Even though the amorphous region of the polymer may be swollen by the ingress of water, the polymer will not dissolve until the crystal structure is broken down.

Dissolution must require the replacement of polymer-polymer hydrogen bonds with polymer-water hydrogen bonds. The solubility of PVA in water depends on the degree of hydrolysis and molecular weight. Full hydrolyzed PVA is soluble only in hot to boiling water, whereas partially hydrolyzed grades (88%) are soluble in water only at room temperature. PVA with 80% of degree hydrolysis is soluble only at water temperatures between 10 ^{o}C to 40 ^{o}C (Lindeman, 1971).

ii) Molecular weight

PVA can be obtained in different molecular weights from a few thousands up to about a million. The upper limit is largely defined through chain termination by acetaldehyde in the polymerization of vinyl acetate and by other impurities in other type of polymerization.

iii) Crystallinity

PVA shows a broad peak at 2θ= 19.8° in the XRD pattern (Gupta *et. al.*, 1996; Assender and Windle, 1998b). This diffraction peak reveals the semi-crystalline nature of PVA.

iv) Melting point temperature (T_m)

T_m for PVA is difficult to be determined due to no sharp melting peak but rather from about 220^{o}C to 240 ^{o}C (Lindemann, 1971). PVA possesses a high T_m attributed to high amount of hydrogen bonding that exist in the polymer matrix.

v) Glass transition temperature (T_g)

The T_g of PVA has been determined at 85 ^{o}C. However, other studies also revealed the $T_g$value at 70 ^{o}C. This is mainly owing to different heating rate and other experimental problems (Lindemann, 1971).

2.6 Lithium perchlorate ($LiClO_4$)

Lithium salts had attracted the most attention from researchers due to its small ionic radius, greatest electrochemical potential and largest energy content. The use of this alkali metal has two distinct characteristics as Li metal shows the most electronegative value compared to other metal and it is lightest metal in the world that can reduce the weight of the devices. The small ionic radii which assist in dissolution when bonded with larger size of anion and at the same time the small size of Li^+ ions can moves more freely with high mobility. $LiClO_4$ has been a popular electrolyte solute due to high solubility in most ionic solvents and high ionic conductivity (~9.0 mS cm^{-1}). $LiClO_4$ also indicates a high anodic stability up to 5.1V (Tarascon and Guyomard, 1994). Figure 2.3 shows the chemical structure for $LiClO_4$

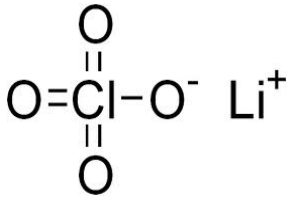

Figure 2.3: Chemical structure of $LiClO_4$

Compared with other lithium salts, $LiClO_4$ also has the merits of being relatively less hygroscopic and is stable to ambient moisture. Guilherme and co-workers reported that solid polymer electrolyte consist of polyethylene-*b*-poly

(ethylene oxide) as host polymer and lithium perchlorate as electrolyte had attained the ionic conductivity value approximately ~10^{-4} S cm^{-1} which is suitable to be used in lithium batteries (Guilherme *et. al.*, 2007).

2.7 Antimony trioxide (Sb_2O_3)

In this study, a new type of inorganic filler, Sb_2O_3 has been incorporated into the polymer-salt system. In the global production of antimony trioxide, in 2005 the production of Sb_2O_3 was 120,000 tonnes, an increase from 112,600 tonnes in 2002. The result reveals the demand increased tremendously from year to year.

Antimony trioxide is mainly produced via the smelting of stibnite ore, which is oxidized to crude Sb_2O_3using furnaces operating at temperature range of 850 ^oC to 1000 ^oC. The reaction is expressed as below:

$$2\ Sb_2S_3 + 9\ O_2 \rightarrow 2\ Sb_2O_3 + 6\ SO_2$$

The crude Sb_2O_3 obtained is then purified by sublimation. Purification is conducted to separate the volatile compound which is arsenic trioxide. This step is important as the crude Sb_2O_3 contains massive amount of arsenic.

Generally, the primary application in the United States and Europe of Sb_2O_3 is flame retardants. The combination of the halides and the antimony can provide the flame-retardant action polymer. This feature enhances the thermal stability of polymer

electrolytes and heat resistant. Sb_2O_3 is an amphoteric oxide where the molecules are able to react as an acid as well as a base. Therefore, addition of Sb_2O_3 into polymer electrolyte will promote lewis-base interaction and as a cross-linking center result in the reduction in the formation of ion aggregates.

2.8 Titanium dioxide (TiO_2)

Titanium dioxide is used as another inorganic filler in this study. TiO_2 exists in nature with 3 types of minerals which is rutile, anatase and brookite. For production, mixing the ilmenite with sulfuric acid can produce the TiO_2. The by-product then is crystallized and filtered-off to yield only the titanium salt in the digestion solution. The titanium salt is processed in the same way to give a more pure TiO_2 product. There are several applications such as pigements, sunscreen, UV absorber, as a catalyst and electronic data storage medium.

In polymer electrolyte studies, TiO_2 is classified as inactive filler which do not involve in the lithium ion transport process. The dispersion of nano-sized TiO_2 into polymer matrix can magnify the mechanical properties such as modulus, tensile strength and abrasion resistance of the polymer electrolytes. In addition, incorporation of filler can enhance the ionic conductivity and amorphous characteristics of polymer electrolyte. Based on previous studies, Shin and co-workers had investigated the addition of TiO_2 into poly (ethylene oxide) based polymer electrolyte can induce to low interfacial resistance of lithium batteries (Shin *et. al.,* 2002). Besides, addition of TiO_2 leads to improved thermal stability and has a wider electrochemically stable

potential window compared to SPE.

2.9 Electric double layer capacitors (EDLC)

Helmholtz, Guoy, Chapman and Stern had revealed the charges could be separated and stored at the interface between a conductor and liquid electrolyte. The first EDLC device was developed by Boos in 1971 (Tabuchi *et. al.*, 1993). EDLC cell stores the mobile charge carrier in a similar manner to the conventional capacitors. Figure 2.4 shows a typical EDLC cell. The distance between opposite sign charges at the interface is about 1 to 2 angstroms. Hence, by applying a high surface area of electrodes able to raise the size of charge stored not only at the interface but also in the entire electrode volume. The EDLC exhibits the highest capacitance value compared to other types of capacitor. For example, conventional capacitors provide capacitance in the range of picofarad to microfarad, whereas EDLC is shown in Farad.

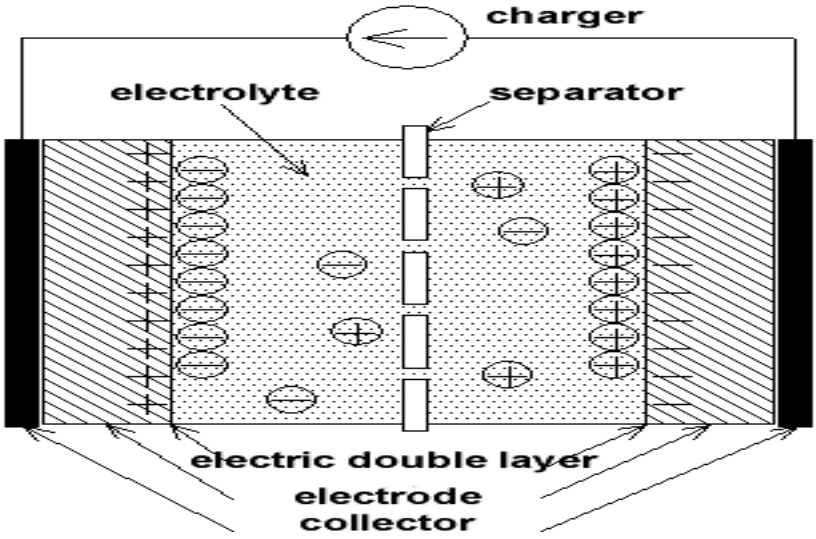

Figure 2.4: Schematic diagram of an EDLC cell

Previous studies had stated the EDLC is a unique electrical storage device, which can store much more energy than conventional capacitors and offer much high power density, fast charging time, long durability (>10^5 cycles), and environment-friendly features than batteries (Vieira *et. al.*, 2007; Zhang and Zhao, 2009). EDLC works on the principle of double-layer capacitance at the electrode/electrolyte interface where electric charges are accumulated on the electrode surfaces and ions of opposite charge are arranged on the electrolyte side. In the early of 90's, researcher had utilized the polymer electrolyte as electrolyte in the EDLC devices. Kanbara and co-workers reported that PVA based polymer electrolytes with different lithium salts were fabricated with electrodes to create EDLC cell and it show a good charge/discharge behavior with large capacitance of 2.5-3.5 Farad (Kanbara *et. al.*, 1991). Researchers have reported various types of lithium based polymer electrolyte and electrode materials that is used to fabricate EDLC cell as shown in Table 2.1. These results had proven that polymer electrolyte is a promising candidate to be used in such application.

Table 2.1: Specific capacitance of EDLC using different lithium based polymer electrolytes

Polymer electrolytes	Electrode materials	Specific capacitance ($F\ g^{-1}$)	Ref.
PVdF-$TEABF_4$-EC-PC	Acetylene black	2.56	(Osaka *et. al.*, 1998)
PEO-LiTf-EmITf	Multiwalled carbon nanotube	2.0	(Pandey *et. al.*, 2011)
PEO-NPPP-$LiClO_4$	Nano structured carbon black	14.3	(Lavall *et. al.*, 2008)
PUR-$LiClO_4$-EC-PC	Carbon cloth	5.0	(Latham *et. al.*, 2002)

2.9.1 Electrode materials

EDLC employed two electrodes, a separator and an electrolyte. Electrolytes can be solid, gel or liquid. In solid polymer electrolytes, separator is not required. The electrode consists of a current collector to which the active material is adhesive. The function of current collector in EDLC is to conduct electrons while the active material plays a role to absorb charge carrier form the electrolyte.

Generally, performance of EDLC is influenced by two factors which are the ionic conductivity of polymer electrolytes and surface area of the electrode materials. The materials to prepare the electrode consist of active material, binder and solvent. The active material can be active carbon, carbon black, carbon cloth, carbon fiber, carbon nanotubes, glassy carbon, and carbon aerogels (Zhu *et. al.*, 2004; Niu *et. al.*, 2006). In this study, activated carbon was used to prepare the electrode materials. The electrode material most frequently used in electrochemical capacitors is activated carbon with various modifications. The purpose for using activated carbon as electrode is due to low cost, high surface area, big pore size, environmental safety, and established electrode production technologies (Chandasekaran *et. al.*, 2008).

Li and co-workers reported the various types of activated carbon (AC) based on different types of starch. They had evaluated the physical properties of AC and investigated the electrochemical performance of capacitor based on the starch-derived AC using 30 wt. % of KOH aqueous solution. Li and co-workers reported the AC produced with various specific surface areas. From the results obtained, a high specific surface area of AC exhibits higher specific capacitance compared to low

specific surface area of AC. This implies a high surface area of activated carbon is more preferable.

Besides, other researchers reported the AC alone as electrode material is not suitable for the polarizable electrodes owing to its low electrical conductivity (Show and Imaizumi, 2007). Hsieh and Teng explained the AC has high electrical resistance due to the binders. The binder such as PVdF shows blocking effect on the ion species when ions are attempted to enter pores in the porous AC (Hsieh and Teng, 2002). As a result, the capacitance of EDLC decreases due to the blocking effect.

In this study, carbon black (CB) is added in the electrode mixture during the preparation. Lust and co-workers reported that addition of CB could reduce the ohmic resistance of the electrolyte (Lust et. al., 2004). Nevertheless, other researcher also reported that CB has the capability to enhance the electrical conductivity by forming conducting bridges between particles of the active materials (Sheem *et. al.*, 2006).

CHAPTER 3

Experimental Procedure

3.1 Materials

Poly (vinyl alcohol) (PVA) with an average molecular weight of 130000 (99%+ hydrolyzed) purchased from Aldrich was used as polymer host. Lithium perchlorate ($LiClO_4$) purchased from Merck was used as electrolyte salt. Antimony trioxide (Sb_2O_3) with particle size less than 250 nm was purchased from Aldrich. Titanium oxide (TiO_2) with particle size less than <100nm was purchased from Aldrich as well. These materials were used as-received without further treatment or purification. Distilled water was used as solvent. All the polymer electrolytes were prepared by solution casting technique.

The electrode preparation requires activated carbon (BP20) (obtained from Magna), Carbon black known as Super P and poly (vinylidene fluoride) (PVdF) (obtained from Sigma Aldrich). The N-methyl-2-pyrrolidone (NMP) (Obtained from Merck, Germany) was act as solvent to dissolve the carbon materials and polymer.

3.2 Preparation of polymer electrolyte

In this study, there are 3 systems of polymer electrolyte being prepared by solution casting technique, whereby the first system is started with mixing PVA and $LiClO_4$ to form solid polymer electrolytes. Before proceeding to prepare the second

and third system of polymer electrolytes, it was required to find out the highest ionic conductivity in PVA-$LiClO_4$ system. After investigation, the highest ionic conducting polymer electrolyte from PVA-$LiClO_4$ system was used for further investigation. The solid polymer electrolyte was then incorporated with Sb_2O_3 in second system and TiO_2 in third system.

3.2.1 First system (PVA-$LiClO_4$ based polymer electrolyte)

Preparation of first polymer electrolyte system was utilized to find out the most compatible ratio for PVA with $LiClO_4$. The system containing host polymer and salt will form solid polymer electrolyte. The compositions prepared were [xPVA-(1-x)$LiClO_4$] where x is 0.1, 0.2, 0.3, 0.4 and 0.5. The compositions of PVA and $LiClO_4$ and their designation are listed in table below.

Table 3.1: Designation and composition of first polymer electrolyte system (PVA-$LiClO_4$).

Designation	Composition	
	Weight percentage of PVA (%)	Weight percentage of $LiClO_4$ (%)
PL-1	90.0	10.0
PL-2	80.0	20.0
PL-3	70.0	30.0
PL-4	60.0	40.0
PL-5	50.0	50.0

3.2.2 Second system (PVA-$LiClO_4$-Sb_2O_3 based polymer electrolyte)

After investigating the first system, 60 wt. % of PVA and 40 wt. % of $LiClO_4$ noted as PL-4 gives the highest ionic conductivity and therefore, this ratio was used to further studies with the addition of inorganic fillers. To prepare second polymer

electrolyte system, an appropriate amount of PVA, $LiClO_4$ and Sb_2O_3were mixed in distilled water and stirred for few hours until Sb_2O_3 was well dispersed in the solution. The solution was poured on petri dish and dried inside an oven at 70 ℃ to produce solid thin films. This procedure yields mechanically stable and free-standing films. Designation and composition of polymer electrolytes with different ratio of Sb_2O_3 was tabulated in table 3.2.

Table 3.2: Designation and composition of second polymer electrolyte system (PVA-$LiClO_4$-Sb_2O_3).

Designation	Composition		
	Weight percentage of PVA (%)	Weight percentage of $LiClO_4$ (%)	Weight percentage of Sb_2O_3 (%)
PLS-2	58.8	39.2	2.0
PLS-4	57.6	38.4	4.0
PLS-6	56.4	37.6	6.0
PLS-8	55.2	36.8	8.0
PLS-10	54.0	36.0	10.0

3.2.3 Third system (PVA-$LiClO_4$-TiO_2 based polymer electrolyte)

In the third system, TiO_2 was incorporated into PL-4 to prepare composite polymer electrolyte using the same procedures as mentioned in 3.2.2. The composite polymer electrolytes were formed by dispersing TiO_2 particles in the distilled water. Table 3.3 shows the designation and composition with different ratio of TiO_2.

Table 3.3: Designation and composition of third polymer electrolyte system (PVA-$LiClO_4$-TiO_2).

Designation	Composition		
	Weight percentage of PVA (%)	Weight percentage of $LiClO_4$ (%)	Weight percentage of TiO_2 (%)
PLT-2	58.8	39.2	2.0
PLT-4	57.6	38.4	4.0
PLT-6	56.4	37.6	6.0
PLT-8	55.2	36.8	8.0
PLT-10	54.0	36.0	10.0

3.3 Impedance spectroscopy

Complex impedance measurement of polymer electrolytes was carried out by using HIOKI 3532-50 LCR Hi-tester as shown in Figure 3.1 with the AC frequency in the range from 50 Hz to 5 MHz at room temperature. The thickness of the films was measured by means of a micrometer screw gauge. The thickness of the films is a parameter which the values were used to calculate the ionic conductivities of polymer electrolyte. The thin films were sandwiched between two stainless steel electrodes which having an area of 4.92 cm^2. A complex impedance plot, the imaginary axis (*Z''*) was plotted versus the real axis (*Z'*) at each excitation frequency can be obtained.

Figure 3.1: Impedance spectroscopy

Ionic conductivity value was determined by the equation below:

$$s = \frac{L}{R_b A} \qquad \text{(Equation 3.1)}$$

where L, A and R_b, are the thickness, area and bulk resistance of the solid polymer electrolytes, respectively. Figure 3.2 displays a typical complex impedance plot. The semicircle fitting was achieved to obtain the R_b value. As shown in Figure 3.1, R_b is determined from interception of the semicircle and the spike at x-axis. By substituting this value to the equation, ionic conductivity value of polymer electrolyte can be determined. In addition, temperature dependence ionic conductivity of polymer electrolytes were measured from room temperature to 80 ^{o}C.

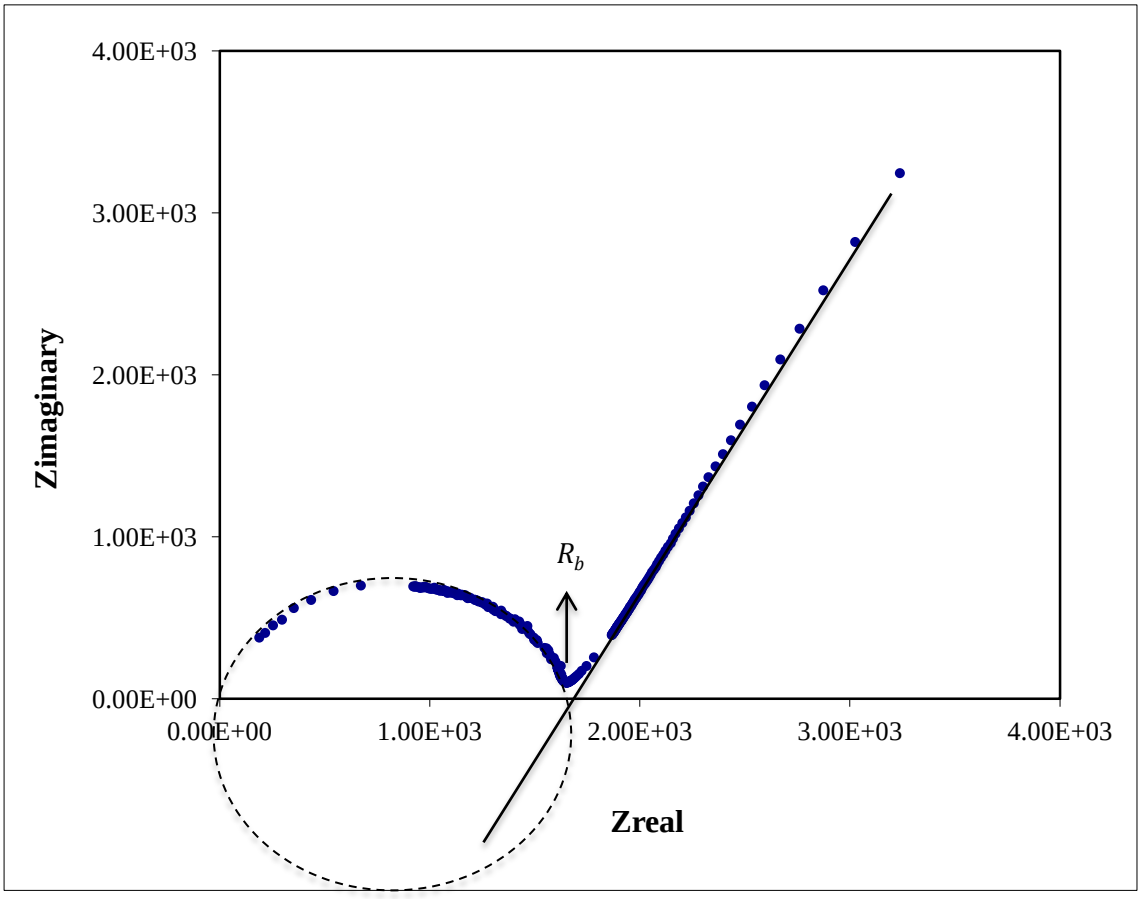

Figure 3.2: A typical complex impedance plot of polymer electrolyte

The impedance spectroscopy can be used to obtain various types of data as well and most of this data can be used for the dielectric analysis. Some examples of the data are the conductance, G (S cm^{-1}) and the parallel capacitance, C_p. From the new data which was obtained, the real (ε') dielectric constant and loss tangent ($\tan\delta$) of a sample can be determined by following relationship:

$$\sigma = \frac{GL}{A} \qquad \text{(Equation 3.2)}$$

$$\varepsilon' = \frac{C_p \times L}{\varepsilon_0 \times A} \qquad \text{(Equation 3.3)}$$

$$\tan\delta = \frac{\varepsilon''}{\varepsilon'} \qquad \text{(Equation 3.4)}$$

where G is the conductance in S cm^{-1}, L is the thickness of the sample (cm), A is the electrode contact area (cm^2), ε_0 is the permittivity of the free space with the value of 8.856 $\times$ 10^{-14} F cm^{-1}, C_p is the parallel capacitance, and ω is $2\pi f$, where f represents the frequency in Hz.

3.4 X-ray diffraction (XRD)

XRD analysis was carried out to investigate the crystalline nature of the polymer electrolytes. The XRD patterns were recorded using a Siemens D 5000 diffractometer with Cu-Kα radiation (λ = 1.54060 Å) as shown in Figure 3.3, over the range of 2θ=5-80^o at ambient temperature. The crystallite size of Sb_2O_3 has been calculated from the Scherrer equation:

$$L = \frac{0.9\lambda}{\beta\cos\theta} \qquad \text{(Equation 3.5)}$$

where λ is the wavelength of the impinging X-ray beam, β is the full width at half maximum intensity (FHMW) of the XRD peak and θ is the glancing angle.

Figure 3.3: X-ray Diffractometer

3.5 Scanning electron microscope (SEM)

Morphology of polymer electrolytes was investigated using Leica S440 digital scanning electron microscope as shown in Figure 3.4. The morphology images of selected polymer electrolytes were captured using Leica's SEM with the model S440 at 10 kV. The micrographs for polymer electrolytes were captured with the magnification factor of 1000 ×. Prior to proceed capturing the surface image, a thin layer of gold was coated on the thin films which are a step to prevent electrostatic charging when the samples surface being subjected with a high-energy beam of electrons.

Figure 3.4: Scanning electron microscope

3.6 Differential scanning calorimetry (DSC)

In this study, the prepared polymer electrolytes were subjected to DSC analysis to determine glass transition temperature (T_g). DSC analysis was carried out using TA instrument Q200 as shown in Figure 3.5.

Nitrogen purge gas was used with 50.0 ml min^{-1} flow rate. Sample with approximately 5 mg was sealed in a 40 µl aluminium crucible. Before analysis, the samples were equilibrated at 105 ℃ for 5 min to remove any traces of water. The

samples were then cooled rapidly to -50 ℃ and then reheated to 180 ℃ at 30 ℃ min^{-1}. The last heating scan was performed to determine the T_g value of the sample.

Figure 3.5: Differential scanning calorimetry

3.7 Thermogravimetric analysis (TGA)

The thermogravimetric analysis (TGA) was performed to measure the weight change from the sample with thermal energy. TGA is commonly used to determine polymer degradation temperatures, residual solvent levels, moisture content, and the amount of inorganic (non-combustible) filler in polymer or composite material.

Thermal stability of polymer films was evaluated by using TA instrument Q500 as shown in Figure 3.6

Figure 3.6: Thermogravimetric analyzer

A mass approximately 5.0 mg of sample was weighed and placed in a 40 µl aluminium crucible and the sample was heated from 30 ℃ to 400 ℃ in nitrogen gas atmosphere with the heating rate of 10 ℃ /min.

3.8 Linear sweep voltammetry (LSV)

Electrochemical stability window of polymer electrolytes was determined using the Autolab PGSTAT 12 potentiostat/galvanostat as shown in Figure 3.7. The instrument is in conjunction with the General Purpose Electrochemical System (GPES) software Version 4.9.005. Polymer films were sandwiched between stainless steel electrodes. The scan rate was 10 mV s^{-1} and the potential applied was in the range from -4 to 4 V at room temperature.

Figure 3.7: Autolab PGSTAT 12 potentiostat/galvanostat

3.9 Fabrication of EDLC

The electrodes were prepared by mixing 80 wt.% of activated carbon (BP20) purchased from Magna, 10 wt.% of carbon black (known as Super P) and 10 wt.% of poly (vinylidene fluoride) (PVdF) in 50 ml of N-methyl-2-pyrrolidone (NMP). The mixture was stirred until a homogenous slurry was formed. The aluminium grid was washed using acetone prior to use. The slurry was spread on the aluminium grid by dip-coating method. The prepared electrode was then dried at 80 ℃ in the oven for 30 minutes and the electrode was pressed up to 300 mbar to make a good contact between aluminium grid and electrode. EDLC was fabricated by sandwiching the polymer electrolyte film between two activated carbon electrodes and pressed under 150 mbar pressure to make an intimate contact between each other.

3.10 Characterisation of EDLC

3.10.1 Cyclic voltammetry test (CV)

CV measurements were performed on the EDLC cells using the Autolab PGSTAT 12 potentiostat/galvanostat in conjunction with the General Purpose Electrochemical System (GPES) software Version 4.9.005. Various scan rate was tested at 10 mV s^{-1}, 30mV s^{-1}, 50 mV s^{-1} and 100 mV s^{-1} in the potential region 0 to 1 V at room temperature.

3.10.2 Galvanostatic charge-discharge technique

Galvanostatic charging-discharging tests were performed by Neware battery cycler in the voltage range between 0 to 1 V at constant current of 1 mA as shown in Figure 3.8. Charge-discharge was used to understand the capacitive behavior of an EDLC. Charge-discharge profile can provide some essential information such as capacitance of EDLC and internal resistance.

Figure 3.8: Neware battery cycler

3.10.3 Low frequency impedance spectroscopy

Low frequency impedance measurements on EDLC cells were carried out using the HIOKI 3522-50 Z Hi-tester in the frequency range from 10 mHz to 100 kHz at room temperature.

3.11 Summary

The tables below depict the various methods to characterize the polymer electrolytes and EDLC,

Table 3.4: The function of instrument for characterization of polymer electrolytes

Instrument	Function
Impedance spectroscopy (EIS)	i. Determine ionic conductivity of polymer electrolytes at ambient temperature and varied temperature ii. Study dielectric properties of polymer electrolytes
X-ray Diffration (XRD)	Investigate the crystalline nature of the polymer electrolytes.
Scanning electron microscope (SEM)	Examine the changes of morphology of polymer electrolytes.
Differential scanning calorimetry (DSC)	Determine the glass transition temperature (T_g) of polymer electrolytes.
Thermogravimetric analysis (TGA)	Measure the weight change from the sample with thermal energy.

Linear sweep voltammetry (LSV)	To check the electrochemical stability region of polymer electrolytes.

Table 3.5: The function of instrument for characterization of EDLC device

Instrument	**Function**
Cyclic voltammetry (CV)	To study the capacitive behavior of an EDLC.
Galvanostatic charge-discharge technique	
Low frequency impedance spectroscopy	

CHAPTER 4

Results and Discussion I

4.1 Electrical properties

4.1.1 Impedance studies

Electrochemical impedance spectroscopy (EIS) is one of the most effective and reliable methods to extract information about electrochemical characteristics of the electrochemical system, double-layer capacitance, diffusion impedance, determination of the rate of charge transfer and charge transport processes, and solution resistance (Barsoukov and Macdonald, 2005). In this research, the ionic conductivity of prepared polymer electrolytes was determined at the temperature from room temperature to 80 ^{o}C.

4.1.1.1First system (PVA-$LiClO_4$ based polymer electrolytes)

Figures 4.1and 4.2 depicts the nyquist plot for the PL-1 and PL-4 samples. The R_b value of both samples was determined from the nyquist plot in the intercept of the semicircle at high frequency region on the Z_{real} axis and was used to calculate the ionic conductivity of the polymer eletrolytes. The nyquist plot of PL-1 exhibits a semicircle at high frequency region while in the nyquist plot for PL-4 displays the smaller semicircle at high frequency compared to PL-1. The small size of semicircle is owing to the increase in the salt concentration, and the total conductivity is mainly the result of the ionic conduction.

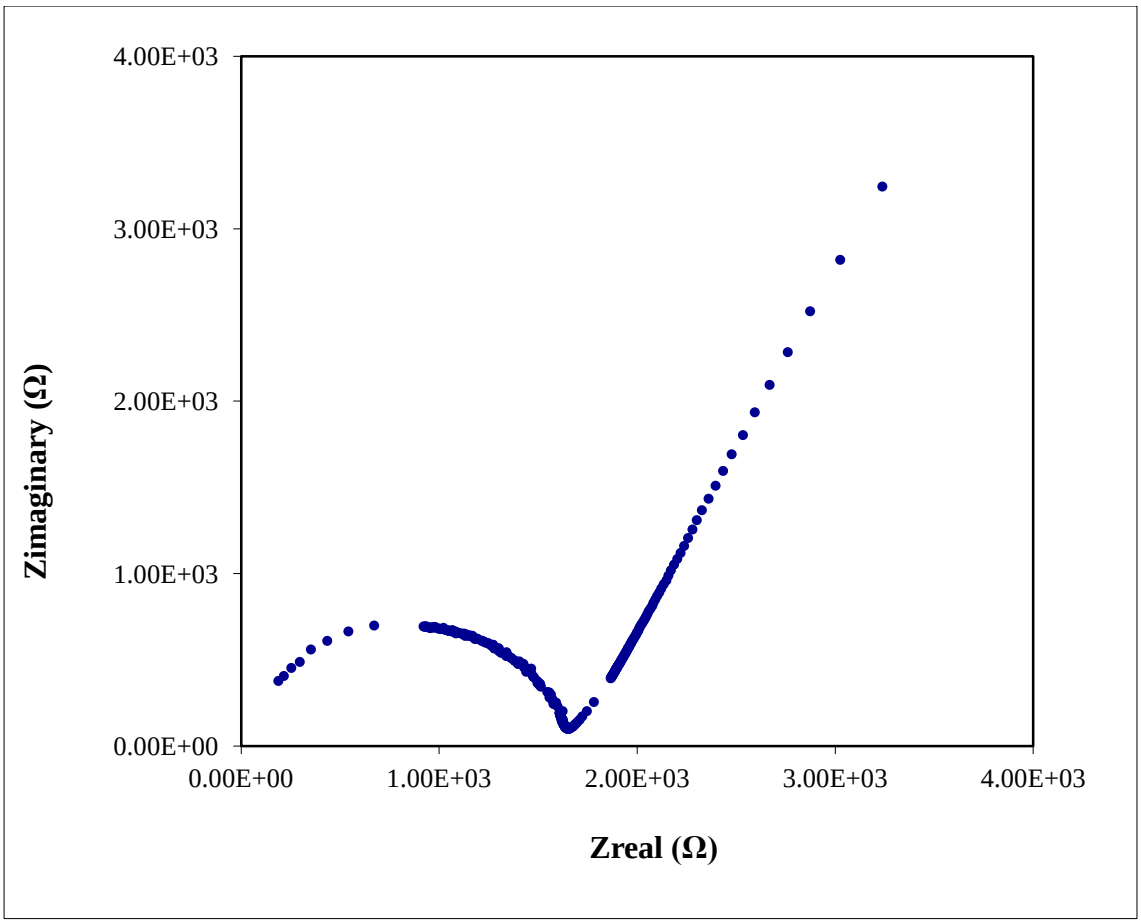

Figure 4.1: Complex impedance plot for PL-1.

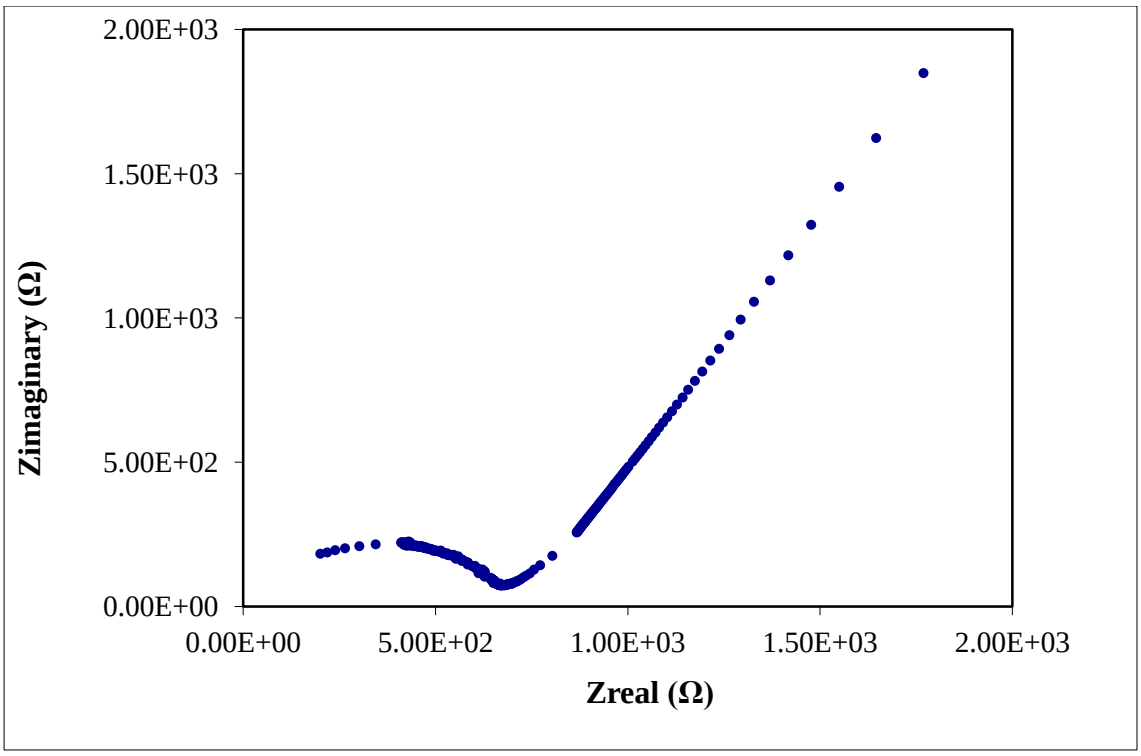

Figure 4.2: Complex impedance plot for PL-4.

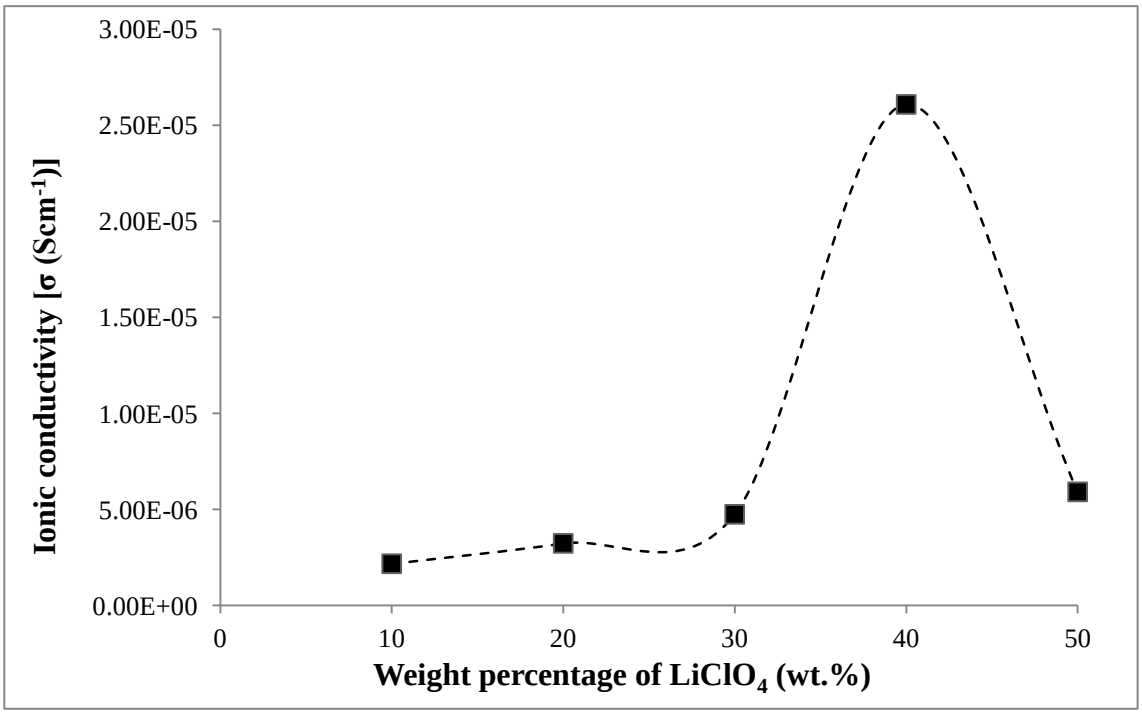

Figure 4.3: The variation of ionic conductivity values as a function of $LiClO_4$concentration.

The relationship between $LiClO_4$ content and the ionic conductivity of the polymer electrolytes is shown in Figure 4.3. The ionic conductivity of an electrolyte depends on the number of charge carriers and their mobility in the electrolyte and is often defined as follows:

$$\sigma = \sum n_i z_i \mu_i \quad \text{(Equation 4.1)}$$

where n_i, z_i and μ_i represent the number of charge carriers, the ionic charge and the ionic mobility respectively. Figure 4.3 shows that the ionic conductivity of the polymer electrolyte increases gradually as the weight percentage of $LiClO_4$ is increased up to 40 wt. %. The ionic conductivity increased is owing to the increase in the number of charge carriers, n_i with the addition of $LiClO_4$. Beyond this point the ionic conductivity decreases with the increase of the weight percentage of $LiClO_4$. The decrease in ionic conductivity can be attributed to the formation of neutral ion pair and also owing to the coagulation of $LiClO_4$. When excessive amount of $LiClO_4$ incorporated into polymer matrix, it will increase the number of cation and anion and reduce the free space in the polymer matrix. As the number of free charge carrier increased, it will increase the rigidity of polymer electrolyte and the tendency of formation of neutral ion pair and aggregates will occur more easily. Eventually, this phenomenon will reduce the ion mobility in PL-5 for transportation as well as the ionic conductivity (Rajendran *et. al.*, 2007).

4.1.1.2 Second system (PVA-$LiClO_4$-Sb_2O_3 based polymer electrolyte)

Figure 4.4 displays the variation of ionic conductivity of the samples with different weight percentage of Sb_2O_3. It is observed that, the ionic conductivity of the polymer electrolyte increases gradually as the weight percentage of Sb_2O_3 is increased

up to 6 wt. %. This is due to the increase in the number of charge carriers with the addition of Sb_2O_3 and it can be concluded that the filler aids to dissociate the lithium salt more easily. Mobility of Li^+ is enhanced by reduction of the tendency of Li^+ coordinate with the oxygen atom in PVA.

Sb_2O_3 also has the ability to penetrate into the polymer matrix and promotes an interaction between Sb_2O_3, $LiClO_4$, and PVA chains. Consequently, the cohesive force between the polymer chain is reduced which provides a more flexible chain segmental motion (Best *et. al.*, 1999). Moreover, the active sites on the Sb_2O_3 surface aid in lowering the ionic coupling and dissociate the $LiClO_4$ aggregate into free charge carriers (Chu et. al., 2003). In addition, Lewis acid–base type oxygen and OH surface groups on the antimony grains interact with the charge carriers (cation and anion). This provides cross-linking centers for PVA segment and anions. This modifies the network structure, leading to lowering of PVA reorganizing tendency and promoting cation–conducting pathways along the filler surface within the network. The creation of Lewis acid-base centers with ionic species results in the ease of dissociation of lithium salt. This will increase the number of charge carriers as well as ionic conductivity (Stephan et al. 2006). The idea of disperse fillers which may act as ‘solid plasticizers’ are capable of enhancing the composite polymer electrolyte’s transport properties without affecting its mechanical and interfacial stability.

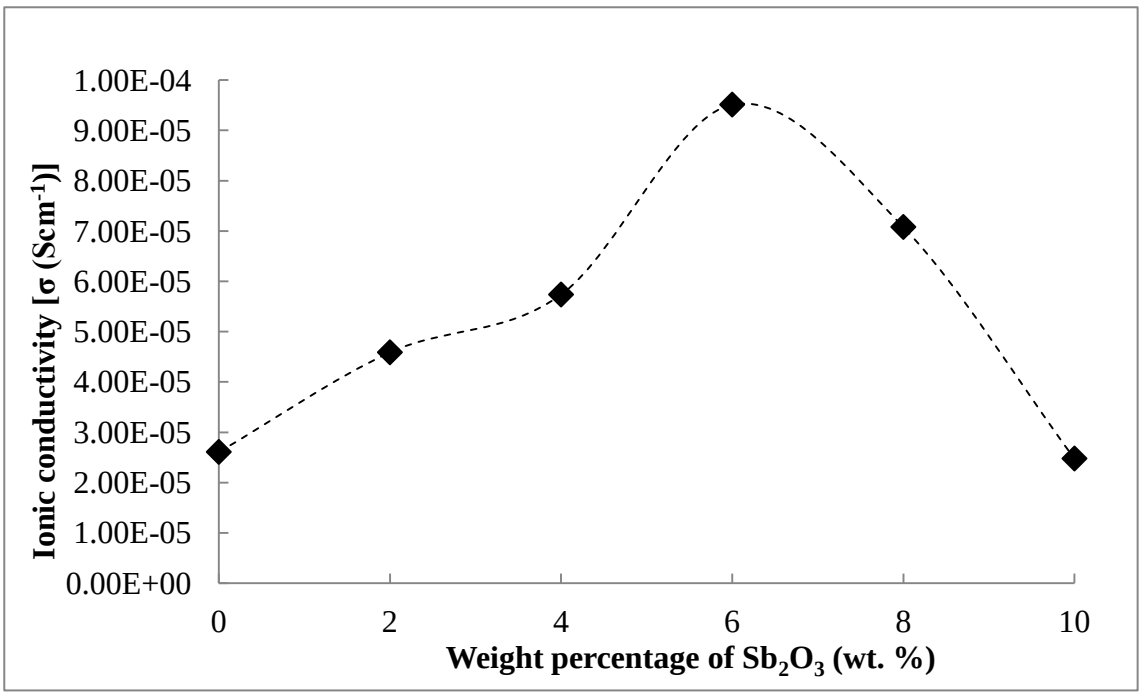

Figure 4.4: The variation of ionic conductivity values as a function of Sb_2O_3 concentration.

PLS-6 exhibits the highest ionic conductivity value of 9.51 x 10^{-5} S cm^{-1} at room temperature. However, as the weight percentage of nanosized Sb_2O_3 increased up to 8 wt. %, the ionic conductivity of the polymer electrolytes starts to drop. This can be attributed to the aggregation of Sb_2O_3 nanoparticles leading to blocking effect on conducting pathway, hence immobilizing the polymer chain (Wen *et. al.*, 2003).

4.1.1.3Third system (PVA-$LiClO_4$-TiO_2 based polymer electrolyte)

Figure 4.5 indicates the variation of ionic conductivity of the samples with different weight percentage of TiO_2. Results show that the ionic conductivity of the polymer electrolyte decreases upon the addition of 2 wt. % of TiO_2. Then it started to increase gradually when more filler is added into the polymer system.

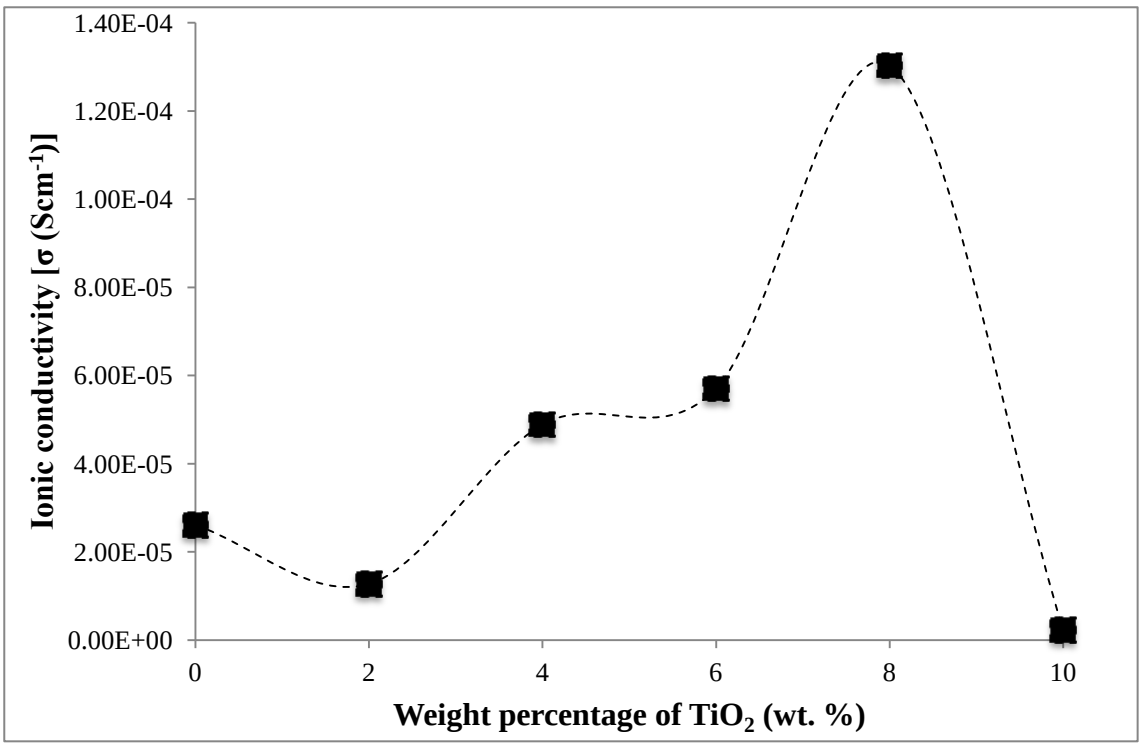

Figure 4.5: The variation of ionic conductivity values as a function of TiO_2 concentration.

The highest ionic conductivity is observed for PLT-8 at which the ionic conductivity value calculated is 1.30×10^{-4} S cm^{-1}. The enhancement of ionic conductivity might due to the incorporation of TiO_2 which resulted in the dissociation of ion-pair and depending on the surface acid–base property of such particles, anions or cations that are adsorbed on the surface leading to higher counter ion (Li^+) concentration in the vicinity of the oxide (space charge layer) (Appetecchi *et. al.*, 2001). At TiO_2 surface, the oxygen atoms act as empty coordination sites which responsible to compete with Li^+ ions to coordinate with PVA segments (Nookala *et. al.*, 2002). Such coordination prevents PVA molecules from crystallizing and leads to increment of the number of free Li^+ ions. Moreover, the ClO_4^- anions are also bound to the Lewis acidic sites (oxygen vacancies) through coordination, which prevent ion-

ion interaction. Eventually, this phenomenon had increased the number of dissociated Li^+ ions as charge carriers. Besides, TiO_2 act as solid plasticizer, which increases the flexibility of amorphous phase of polymer for charge carriers to transfer and favors the ion migration. Hence the ionic conductivity of polymer electrolytes increases (Capiglia *et. al.*, 2002).

The aggregation of the fillers results in blocking effect that imposed by TiO_2 particles. These nanoparticles are getting closer to each other as the neutral filler become larger and rigid. Eventually, TiO_2 aggregate could interact with long polymer chains and immobilizing the polymer chain in the process hence the ionic conductivity starts to drop.

4.1.2 Temperature dependence ionic conductivity studies

4.1.2.1 First system (PVA-$LiClO_4$ based polymer electrolytes)

The temperature dependence ionic conductivity studies provide useful insights in the mechanism of ion transport and associated activation energy for ion hopping (Basak and Manorama, 2004). Figure 4.6 indicates the Arrhenius plot for various compositions of polymer electrolytes at different temperatures. The linear relationship between log ionic conductivity and reciprocal temperature suggests that all the samples obeyed the Arrhenius rule, as their regression value is approximate to unity. Hence, the temperature dependent ionic conductivity can be expressed by the Arrhenius equation:

$$\sigma = A\exp\left(\frac{-E_a}{kT}\right) \qquad \text{(Equation 4.2)}$$

Where A is a constant which is proportional to the amount of charge carriers, E_a is activation energy, k is Boltzmann constant and T represents the absolute temperature in K.

Figure 4.6 shows that the ionic conductivity of samples increased with increase in temperature. As temperature increases, polymer chain acquires faster internal modes in which hopping mechanism is favored. The rise of temperature increases the rate of ion transportation; it means the increment of speed of an ion to transport from one vacant site to another one. Consequently, the increase of temperature enhances the mobility of ions as well as ionic conductivity (Armand *et. al.*, 1979). The coordination site of PVA for Li^+ is oxygen atom; the dipole-dipole interaction between these two atoms had been weakened by the increase in temperature that causes the Li^+ to be loosely bound to the oxygen atom. At higher temperature, the backbone of the polymer has a higher tendency to create vacant sites where the adjacent site of ions will then occupy (Kumar and Scanlon, 2001).

The activation energy, E_a value for PL-1, PL-3, PL-4 and PL-5 is 22.8 kJ mol^{-1}, 22.1 kJ mol^{-1}, 17.9 kJ mol^{-1} and 21.9 kJ mol^{-1}, respectively, which is highly dependent on the doping ration. The E_a value for PVA-$LiClO_4$ polymer electrolyte is on the order of 17.9-22.8 kJ mol^{-1}. One of the researcher reported that the E_a value for polymer electrolyte without inorganic filler is 20 kJ mol^{-1} (Yang, 2006). After incorporation of $LiClO_4$ into polymer matrix, E_a value slightly decreases which may be due to lesser energy to weaken the dipole-dipole interaction. The E_a value is decreases with increase in the content of $LiClO_4$. PL-4 has the lowest E_a value

compared to PL-0 and PL-3; this deduces that PL-4 requires lesser energy to break the physical and chemicals bonds and, therefore ionic conduction is more favorable on PLS-6 sample. On the other hand, E_a value for PL-8 is found to increase. This can be attributed to the formation of lithium aggregates and ion pairs which require higher energy to overcome the energy barrier.

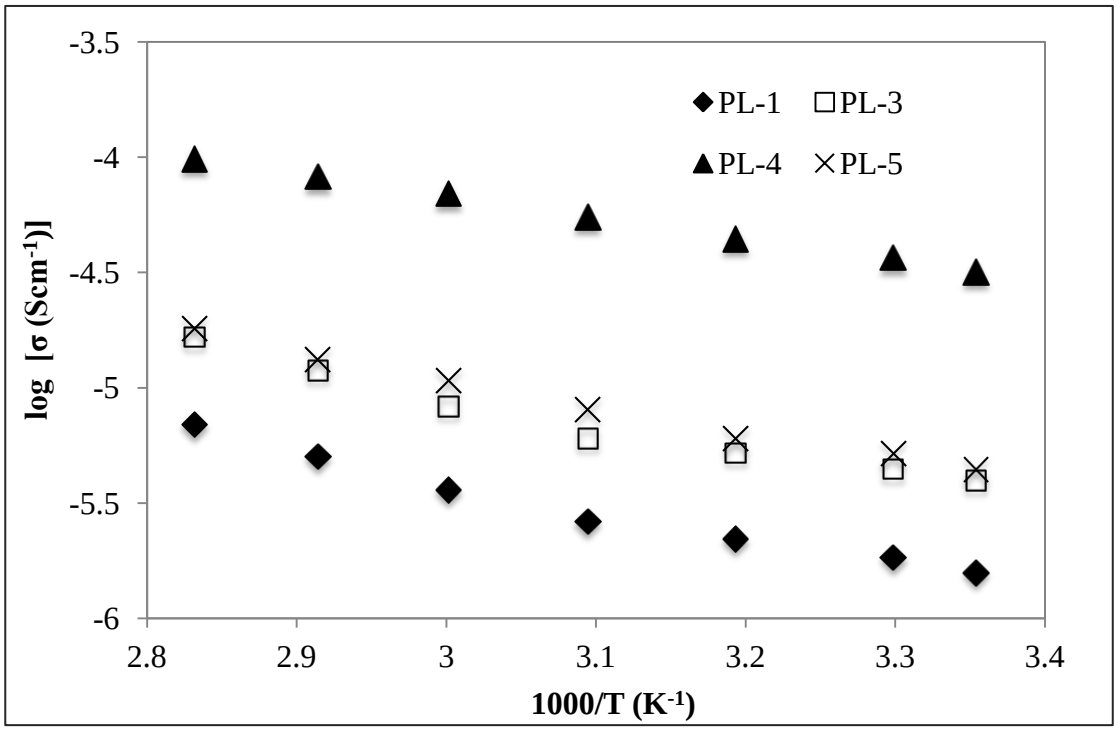

Figure 4.6: Arrhenius plots of ionic conductivity of PL-1, PL-3, PL-4 and PL-5.

4.1.2.2 Second system (PVA-$LiClO_4$-Sb_2O_3 based polymer electrolytes.)

Figure 4.7 depicts the temperature dependence of ionic conductivity for PL-4, PLS-2, PLS-6 and PLS-8 at different temperature. The ionic conductivity for various compositions of polymer electrolytes increases with increasing temperature (Armand *et. al.*, 1979). It was found that the linear relationship between log ionic conductivity and reciprocal temperature and regression value is nearly unity, which describes the

polymer electrolytes obey the Arrhenius rule. Polymer electrolytes that obey Arrhenius behavior disclose the conductivity isotherm was assisted by thermal energy. In addition, Arrhenius behavior describe there is no phase transition that take place in the polymer matrix. The transition can be understood from the trend of ionic conductivity when increasing temperature, as there is no rapid jump on the ionic conductivity value. This resulting the polymer matrix possesses a fully amorphous structure.

The calculated E_a for PL-4, PLS-2, PLS-6 and PLS-8 is 20.6 kJ mol^{-1}, 19.6 kJ mol^{-1}, 16.8 kJ mol^{-1} and 19.4 kJ mol^{-1}, respectively. As mentioned in 4.1.2.1, lower E_a will possess higher ionic conductivity value as it favor faster ion conduction. Low E_a value signifies the energy required to weaken the dipole-dipole interaction is lesser compared to high E_a value. Therefore, ion conduction was favoured at low E_a. PLS-8 shows higher E_a value owing to formation of ion pairs that requires higher energy to weaken the chemical bonding. Hence, the ionic conductivity of PLS-8 decreases beyond the addition of 6 wt. % of Sb_2O_3.

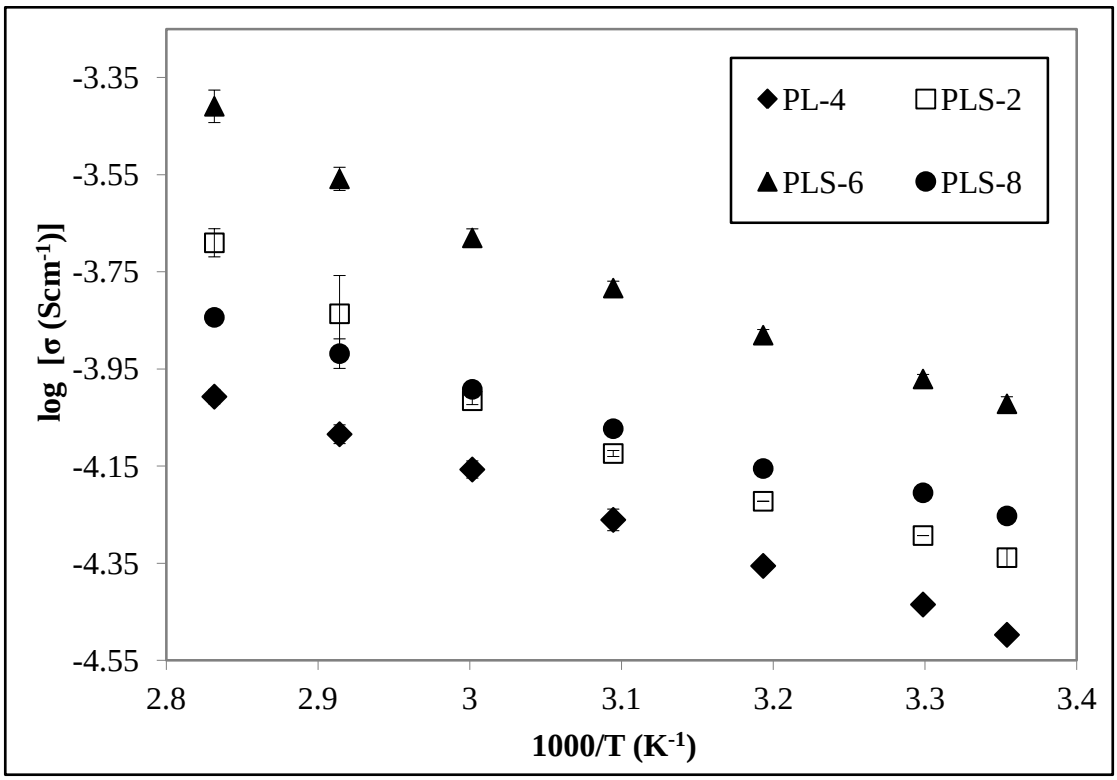

Figure 4.7: Arrhenius plots of ionic conductivity of PL-4, PLS-2, PLS-6 and PLS-8

4.1.2.3 Third system (PVA-$LiClO_4$-TiO_2 based composite polymer electrolytes)

Figure 4.8 displays the Arrhenius plots of the ionic conductivity of PVA–$LiClO_4$–TiO_2 polymer complexes in the temperature range of room temperature to 80 ^oC. Figure 4.8 indicates the ionic conductivity of PL-4, PLT-6, PLT-8 and PLT-10 increases with increasing temperature and suggesting that the process is thermally active to all samples (Armand *et. al.*, 1979). The linear relationship, regression value approximate to unity and no phase transition are identical as shown in Figure 4.6 and 4.7. This behavior indicates the polymer electrolyte obeys the Arrhenius rule. This rule elucidate migration of the cation (Li^+) in polymer matrix probably occurs quite similar to that in solid crystals, where ions jump from a vacant site to another and this phenomenon known as ion hopping mechanism.

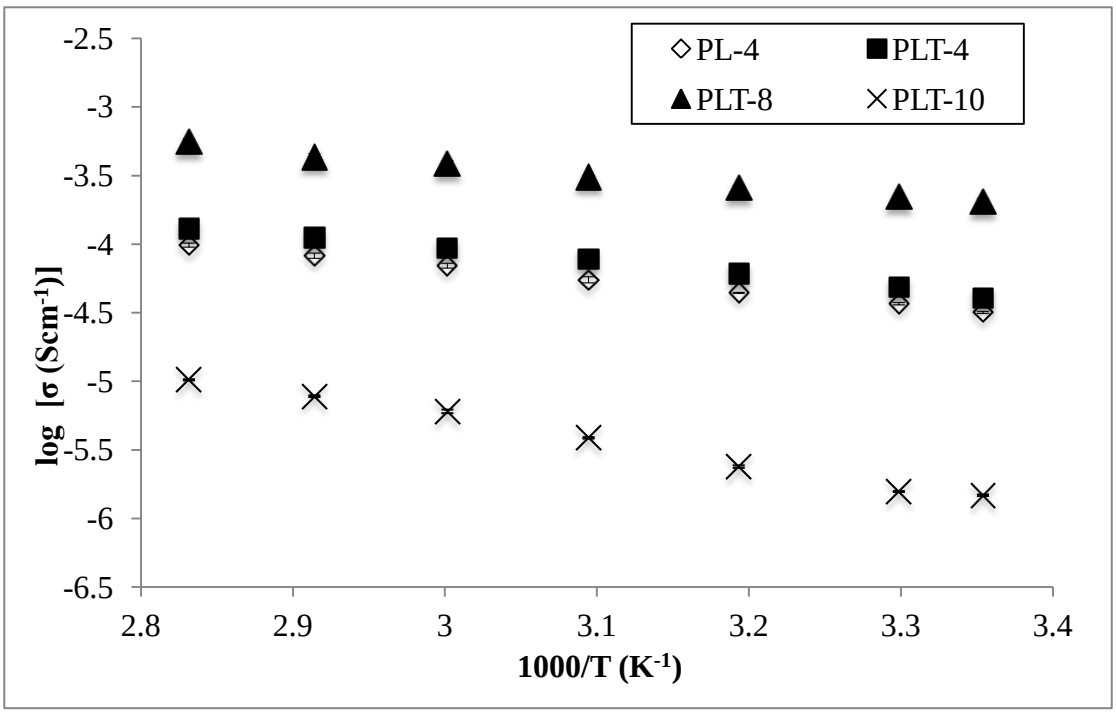

Figure 4.8: Arrhenius plots of ionic conductivity of PL-4, PLT-4, PLT-8 and PLT-10

The calculated E_a value for PL-4, PLT-4, PLT-8 and PLT-10 is 17.9 kJ mol^{-1}, 17.8 kJ mol^{-1}, 15.7 kJ mol^{-1} and 21.8 kJ mol^{-1}, respectively. As expected, PLT-8 exhibits the highest ionic conductivity in the system owing to lowest E_a value, which favors fast ion conduction as lesser energy is required to weaken the dipole-dipole interaction between oxygen atom and Li^+.

4.1.3 Dieletric behaviour studies

4.1.3.1 First system (PVA-$LiClO_4$ based polymer electrolytes)

4.1.3.1.1 Dielectric relaxation studies

Generally, the ionic conductivity behavior can be examined by dielectric studies because dielectric constant is a measure of stored charge (Ramesh *et. al.*,

2002). The variation of real parts of the dielectric constant as a function of frequency for PL-1, PL-3, PL-4 and PL-5 are shown in Figure 4.9. The dielectric constant for the samples was evaluated using equation 3.3. The observed variation in ε' with frequency could be attributed to the formation of a space charge region at the electrode and electrolyte interface, which is known as non-Debye type of behavior. The space charge region with connection to the frequency is elucidated in terms of ion diffusion. Dispersion occur in low frequency region is attributable to electrode polarization where an accumulation of ions near the electrodes (Karan *et. al.*, 2008). The decrease in ε' with increasing frequency can be associated to the inability of dipoles to rotate rapidly leading to a lag between frequency of oscillating dipole and that of the applied field (Awadhia *et. al.*, 2006). Hence, the periodic reversal of the electric field occurs too fast that there is almost no ion diffusion in the direction of the field. Therefore, the ion species that accumulate at electrode during polarization become lesser causing the ε' to decreases towards the higher frequency.

PL-4 shows the highest dielectric constant value among others and this can be ascribed to high charge density. High value of ε' for the PL-4 polymer electrolyte was favored by the addition of $LiClO_4$ into polymer matrix. Number of charge carrier increases with increasing the weight percentage of $LiClO_4$. Consequently, the increment in density of hopping ion species causes a high value of ε' in low frequency region. As 50 wt. % of $LiClO_4$ was added into polymer electrolyte the ε' value declines. This is due to the formation of ion pairs that reduce the number of free charge carrier during polarization and therefore, excess of $LiClO_4$ added into polymer matrix causes the ε' decreases.

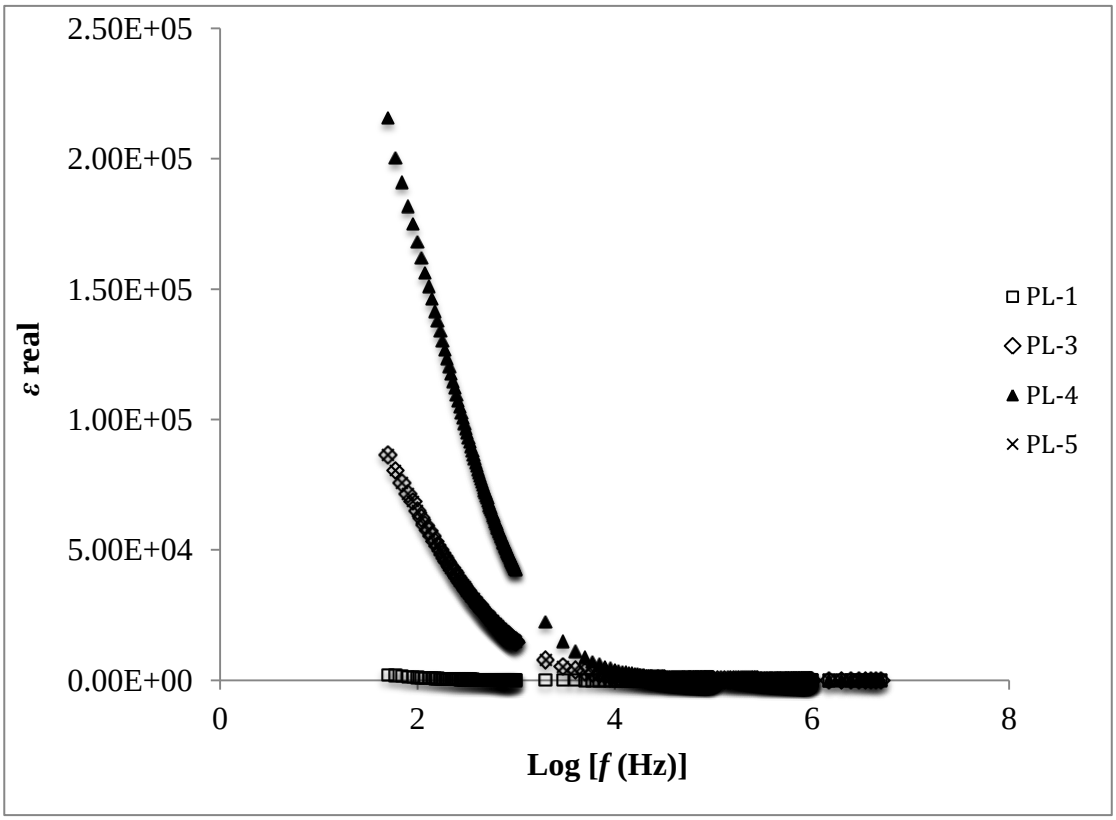

Figure 4.9: Variation of real part of dielectric constant (ε') with frequency at ambient temperature for PL-1, PL-3, PL-4 and PL-5.

4.1.3.1.2 Frequency-dependence ionic conductivity studies

Figure 4.10 depicts the frequency dependent conductivity for PL-1, PL-3, PL-4 and PL-5 with two distinct regions, which is low frequency region and high frequency region. The frequency dependent conductivity plot shows a frequency independent plateau at mid-frequency region and exhibits dispersion at the high frequency (Pradhan *et. al.*, 2009). Besides, the reason of dispersion at low frequency is attributed to the interfacial resistance and the space charge polarization inside the polymer electrolytes (Venkateswarlu *et. al.*, 2000). As the frequency decreases, the

tendency of charges that being accumulated at the electrodes and electrolyte interfaces becomes higher and this is related to the slow periodic reversal of the electric field. Consequently, the number of free mobile ions decreases at low frequency as well as the conductivity.

The plateau region signifies that the conductivity is equal to dc conductivity of polymer electrolytes (Ramesh *et. al.*, 2008). The dc conductivity of the prepared polymer electrolyte samples has been determined by extrapolating the plateau region on the *x*-axis. The dc conductivity values from the frequency dependence ionic conductivity plots are in good agreement with ionic conductivity studies. From Figure 4.10, it was observed that PL-4 exhibits the highest ionic conductivity followed by PL-5, PL-3 and PL-1. On top of that, ionic conductivity of polymer electrolytes is found to increase with increasing frequency. At higher frequency, the conductivity increases with frequency as the greater mobility of charge carriers and faster hopping of ions.

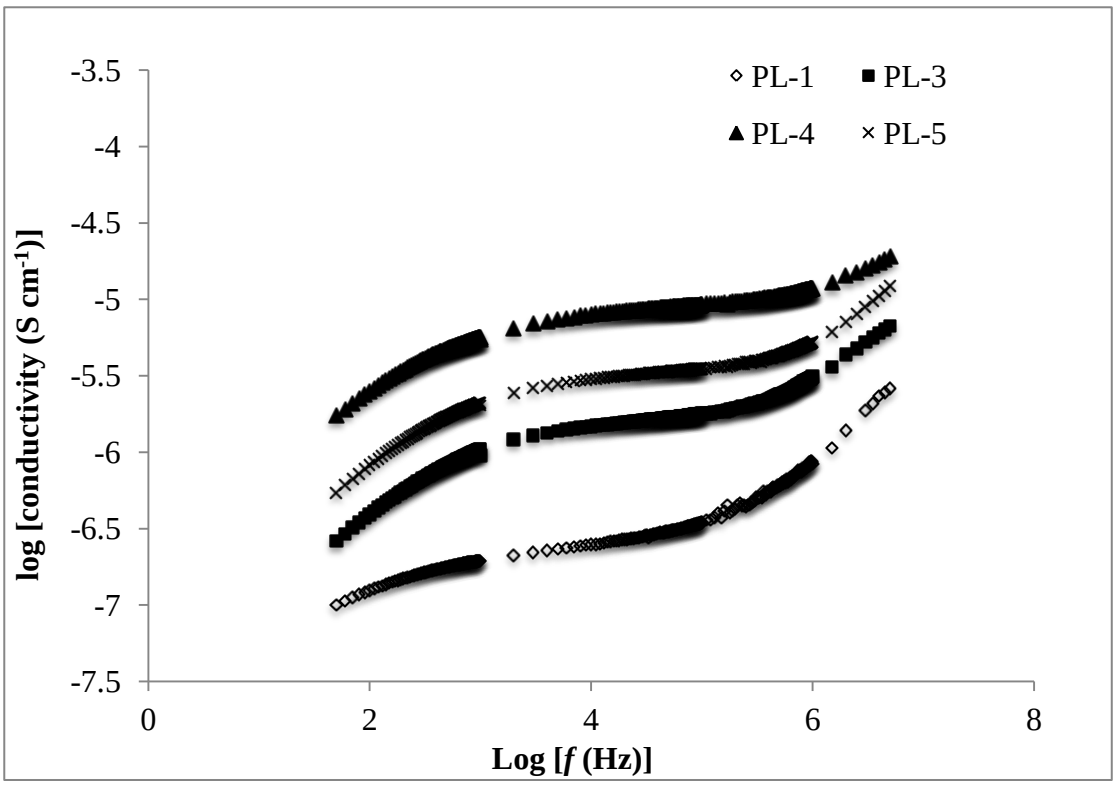

Figure 4.10: Variation of logarithm conductivity as a function of frequency for PL-1, PL-3, PL-4 and PL-5.

4.1.3.1.3 Frequency dependence of loss tangent

The loss tangent (tan δ) is the ratio of loss factor to the dielectric constant, also a measure of the ratio of the electrical energy lost to the energy store in a periodic field. Figure 4.11 depicts the variation of loss tangent as a function of frequency for polymer electrolyte incorporated with various wt. % of $LiClO_4$ at room temperature. It can be observed that as the wt. % of $LiClO_4$ increases gradually, the tangent loss peaks are shifted to higher frequency. From the Figure 4.11, tan δ increases with frequency until a maximum, and following that decreases with further increase in frequency. The occurrence of peak for every sample can be seen in Figure 4.11, this is ascribed to the presence of relaxation dipoles in Li^+ ions in all the tested samples. Presence of loss tangent peak had separated the bulk material and the electrode

surface polarization phenomena in the low frequency dielectric dispersion. Electrode polarization phenomenon occurs due to the formation of blocking layer.

As the wt. % of $LiClO_4$ increases gradually, tangent loss peaks are shifted to higher frequency. As the peak shifts towards higher frequency side, the relaxation time is reduced (Pradhan *et. al.*, 2008). The shifting of peak to higher frequency illustrates the increase in the cations mobility upon reduction in the relaxation time.

In terms of peak intensity, the intensity of the loss tangent peak is to correlate with the number of free charge carrier for the sample. The increase of peak intensity upon the doping of $LiClO_4$ implies to increase the area under the loss tangent peak (Azizi Samir *et. al.*, 2004). As the intensity of loss tangent peak become higher with increases the $LiClO_4$ content, more number of free Li^+ ions has participates in relaxation process to enhance the ionic conductivity of the polymer electrolytes. From Figure 4.11, the loss tangent peak for PL-4 displaced to highest frequency and biggest area under the curve which means more number of charge carriers contributes in relaxation process compared to other sample. Eventually, the ionic conductivity of PL-4 increases.

However beyond the optimum level, above 40 wt. % of $LiClO_4$, the loss tangent peak shifts to lower frequency. This phenomenon implies the increase in relaxation time. Longer relaxation time might reduce the Li^+ ion mobility that inhibits the ion conduction due to the formation of neutral ion pair or aggregates, leading to the formation of thick interfacial layer within the grain boundary. Consequently, the

intensity of loss tangent peak decreased as shown in the Figure 4.11 and thus, this suggest the number of free charge carrier has been decreased when the addition of 50 wt. % of $LiClO_4$. As a result, ionic conductivity of PL-5 decreased beyond the optimum level.

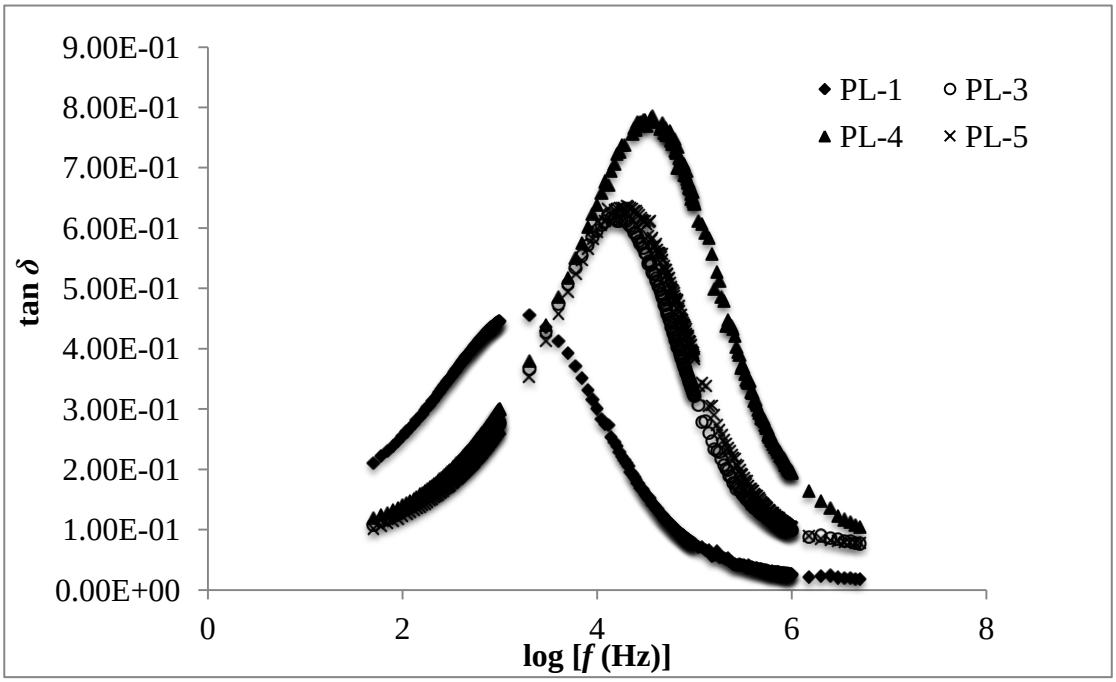

Figure 4.11: Variation of tan d with frequency for PL-1, PL-3, PL-4 and PL-5 at room temperature.

4.1.3.2 Second system (PVA-$LiClO_4$-Sb_2O_3 based polymer electrolytes)

4.1.3.2.1 Dielectric relaxation studies

The variation of real parts of the dielectric constant as a function of frequency for PL-4, PLS-2, PLS-6 and PLS-8 are shown in Figure 4.12. It can be observed that the dielectric constant increased drastically after the incorporation of Sb_2O_3. The variation of ε' with frequency was seen in Figure 4.12 which signifies the polymer electrolytes are non-Debye type of behaviour. Dispersion occurs in low frequency

region is attributable to electrode polarization where an accumulation of ions near the electrodes. The decrease in ε' with increasing frequency can be associated to the inability of dipoles to rotate rapidly leading to a lag between frequency of oscillating dipole and that of the applied field. Hence, the periodic reversal of the electric field occurs too fast that there is almost no ion diffusion in the direction of the field. Therefore, the ion species that accumulate at electrode during polarization become lesser causing the ε' decreases towards the frequency.

In this polymer electrolyte system, PLS-6 exhibits the highest dielectric constant value among others and this is owing to the highest charge density. High value of ε' for the PLS-6 electrolyte was favored by the addition of Sb_2O_3 into polymer matrix. The role of Sb_2O_3 in the polymer matrix has the capability to dissociate lithium aggregates into free ion species that contribute in polarization. Consequently, the increment in density of hopping ion species causes a high value of ε' in low frequency region.

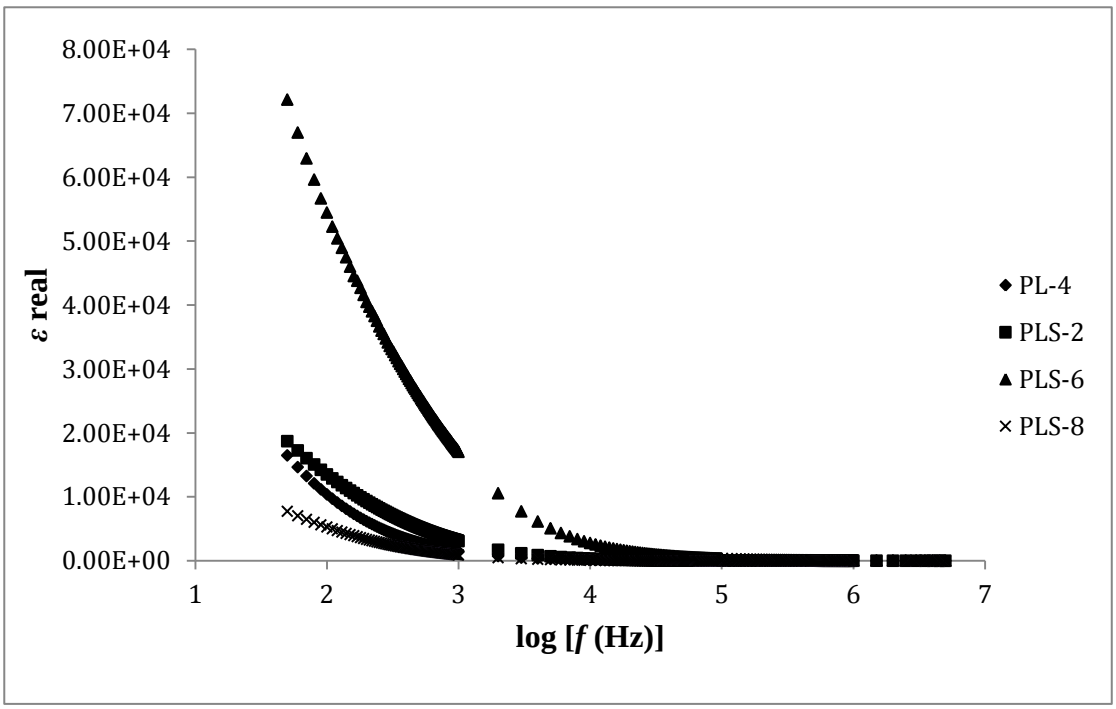

Figure 4.12: Variation of real part of dielectric constant (ε') with frequency at ambient temperature for PL-4, PLS-2, PLS-6 and PLS-8.

4.1.3.1.2 Frequency-dependence ionic conductivity studies

Figure 4.13 depicts the frequency dependent conductivity for PL-4, PLS-2, PLS-6 and PLS-8 with two distinct regions, which is low frequency region and high frequency region. The frequency dependent conductivity plots show a frequency independent plateau at mid-frequency region and exhibits dispersion at the high frequency. Besides, the reason of dispersion at low frequency is attributed to the interfacial resistance and the space charge polarization inside the polymer electrolytes. As the frequency decreases, the tendency of charges that being accumulated at the electrodes and electrolyte interfaces becomes higher and this is related to the slow periodic reversal of the electric field. Consequently, the number of free mobile ions decreases at low frequency as well as the conductivity.

The plateau region signifies that the conductivity is equal to dc conductivity of polymer electrolytes. The dc conductivity of the prepared polymer electrolyte samples has been determined by extrapolating the plateau region on the *y*-axis. The dc conductivity values from the frequency dependence ionic conductivity plots are in good agreement with those obtained in ionic conductivity studies. From Figure 4.13, it was observed that PLS-6 exhibits the highest ionic conductivity followed by PLS-4, PL-4 and PLS-8. On top of that, ionic conductivity of polymer electrolytes is found to increase with increasing frequency. At higher frequency, the conductivity increases with frequency as the greater mobility of charge carriers and faster hopping of ions.

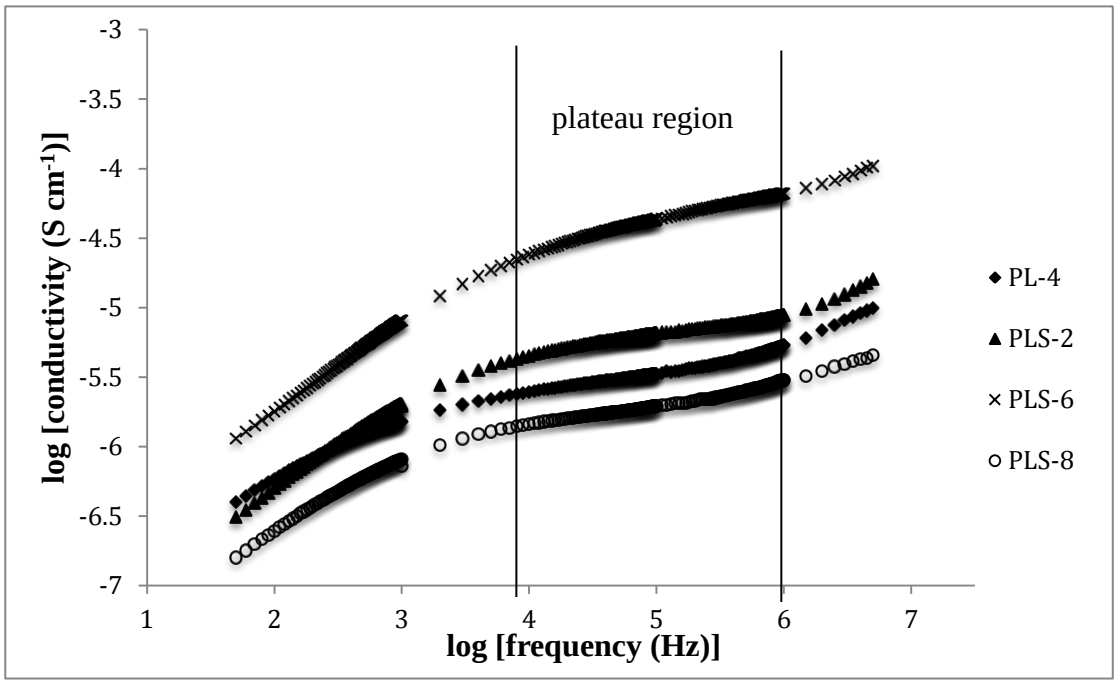

Figure 4.13: Variation of logarithm conductivity as a function of frequency for PL-4, PLS-2, PLS-6 and PLS-8.

4.1.3.2.3 Frequency dependence of loss tangent

Figure 4.14(a) and (b) display the variation of loss tangent as a function of frequency for PL-4, PLS-2, PLS-6 and PLS-8 at room temperature. It can be observed that as the wt. % of Sb_2O_3 increases gradually, the tangent loss peaks are shifted to higher frequency. Beyond the 6 wt. % of Sb_2O_3, the tangent loss peak was shifted to lower frequency. From the Figure 4.14(a) and (b), tan δ increases with frequency until a maximum, and following that decreases with further increase in frequency. The loss tangent peak for every sample can be observed in Figure 4.14, this is owing to the presence of relaxation dipoles in Li^+ ions in all the tested samples. Presence of loss tangent peak had separated the bulk material and the electrode surface polarization phenomena in the low frequency dielectric dispersion. Electrode polarization phenomenon occurs due to the formation of blocking layer.

As the wt. % of Sb_2O_3 increases, tangent loss peaks are shifted to higher frequency. As the peak shifts towards higher frequency, the relaxation time is reduced. The shifting of peak to higher frequency illustrates the increase in the cations mobility upon reduction in the relaxation time. Based on relaxation time value, the relaxation time is inversely proportional to ionic conductivity of polymer electrolyte. As more inorganic filler is added, the crystalline region will reduced and therefore, polymer segment is now more flexible to orient. Eventually, the relaxation time becomes faster.

The increase of peak intensity upon the addition of Sb_2O_3 implies to increase the area under the loss tangent peak. As the intensity of loss tangent peak become

higher with increases the Sb_2O_3 content, more number of free Li^+ ions has contributes in the relaxation process to enhance the ionic conductivity of the polymer electrolytes. PLS-6 shows the highest peak intensity and biggest area under the curve that implies PLS-6 has more number of free charge carriers that contribute in relaxation process as well as ionic conductivity value.

However beyond the optimum level, above 6wt. % of Sb_2O_3, the loss tangent peak shifts to lower frequency. This phenomenon implies the increase in relaxation time. Longer relaxation time might reduces the Li^+ ion mobility that inhibits the ion conduction due to the formation of neutral ion pairs or aggregates, leading to the formation of thick interfacial layer within the grain boundary. Consequently, the intensity of loss tangent peak decreased as shown in the Figure 4.14(a) and thus, this suggest the number of free charge carrier has been decreased with the addition of more than 6 wt. % of Sb_2O_3. As a result, ionic conductivity of PLS-8 decreased beyond the optimum level.

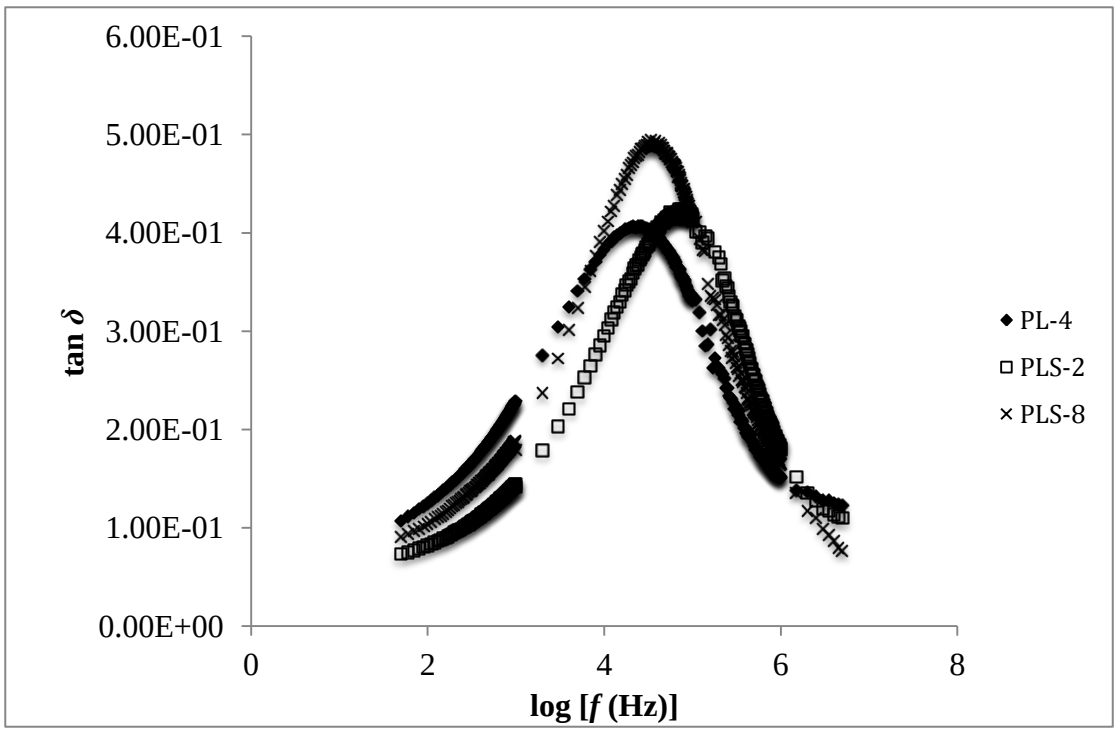

Figure 4.14(a): Variation of tan δ with frequency for PL-4, PLS-2 and PLS-8 at room temperature.

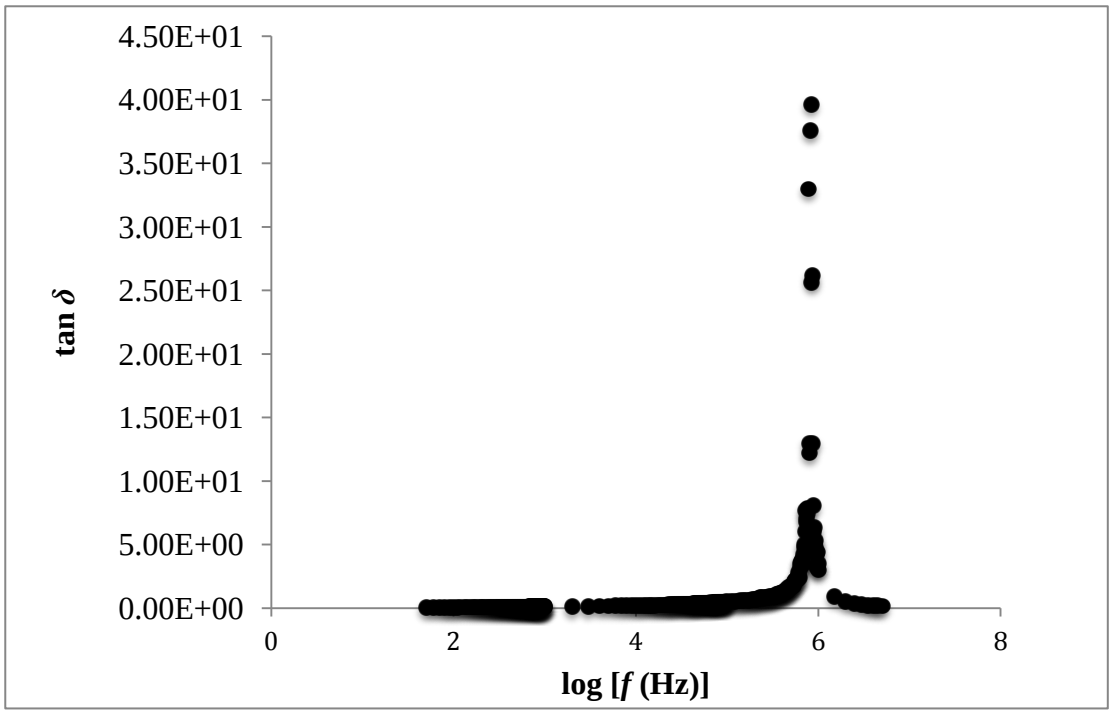

Figure 4.14(b): Variation of tan δ with frequency for PLS-6 at room temperature.

4.1.3.3 Third system (PVA-$LiClO_4$-TiO_2 based polymer electrolytes)

4.1.3.3.1 Dielectric relaxation studies

The variation of real parts of the dielectric constant as a function of frequency for PL-4, PLT-4, PLT-8 and PLT-10 are shown in Figure 4.15. As mentioned in the section of 4.1.3.2.1, the incorporation of filler had increased the dielectric constant of polymer electrolyte. The similar trend also can be seen when the TiO_2 was doped into polymer matrix. The variation of ε' with frequency as shown in Figure 4.15 also proves that the polymer electrolytes exhibit non-Debye behaviour. Dispersion occurs in low frequency region is attributable to electrode polarization where an accumulation of ions near the electrodes. The fall of ε' with increasing frequency can be associated to the inability of dipoles to rotate rapidly leading to a lag between frequency of oscillating dipole and that of the applied field. Therefore, the periodic reversal of the electric field occurs too fast that there is almost no ion diffusion in the direction of the field. Eventually, the ion species that assemble at electrode during polarization become lesser causing the ε' decreases towards the frequency.

In this polymer electrolyte system, PLT-8 exhibits the highest dielectric constant value among others and this is owing to the highest charge density. High value of ε' for the PLT-8 electrolyte was favored by the addition of TiO_2 into polymer matrix. TiO_2 has the capability to dissociate lithium aggregates into free ion species that contribute in polarization. Consequently, the increment in density of hopping ion species causes a high value of ε' in low frequency region.

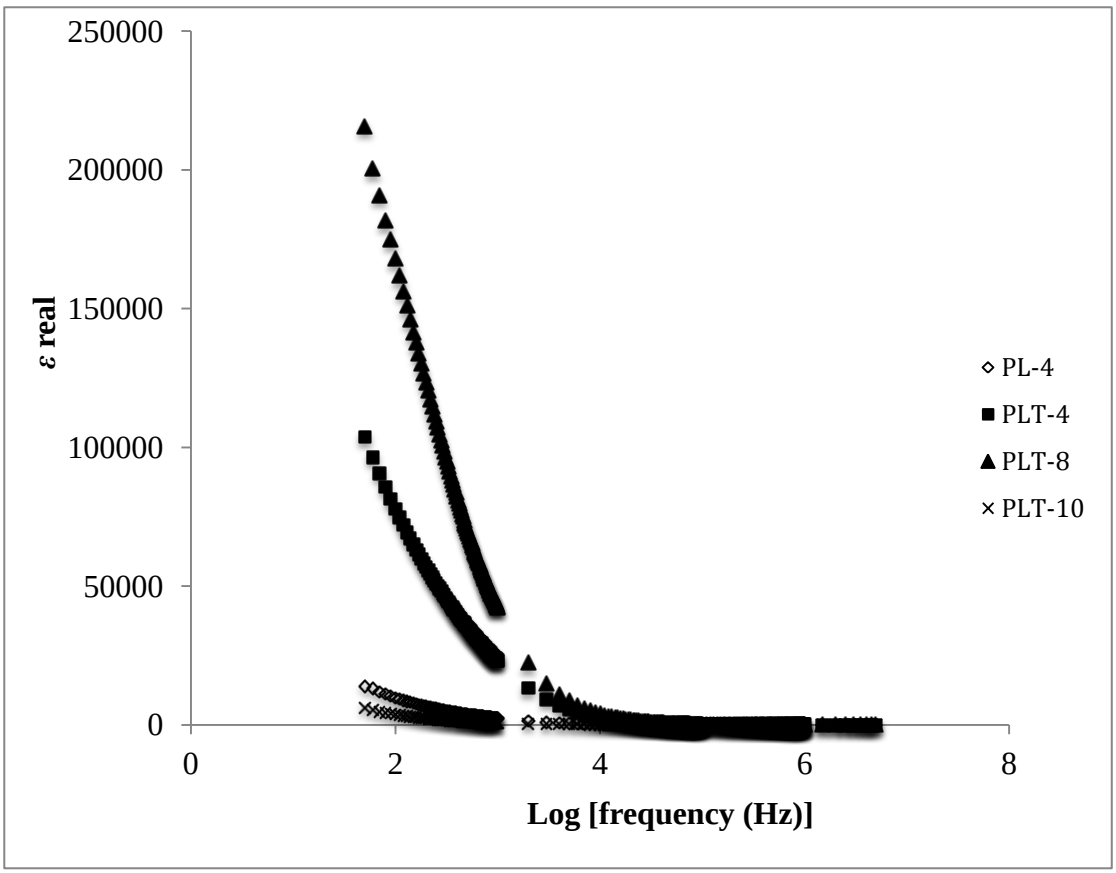

Figure 4.15: Variation of real part of dielectric constant (ε') with frequency at ambient temperature for PL-4, PLT-4, PLT-8 and PLT-10.

4.1.3.3.2 Frequency-dependence ionic conductivity studies

Figure 4.16 depicts the frequency dependent conductivity for PL-4, PLT-4, PLT-8 and PLT-10. All samples also display two distinct regions, which is low frequency region and high frequency region that similar in previous studies. The frequency dependent conductivity plot shows a frequency independent plateau at mid-frequency region and exhibits dispersion at the high frequency. The dispersion at low frequency region is owing to the interfacial resistance and the space charge polarization inside the polymer electrolytes. As the frequency decreases, the tendency of charges that being accumulated at the electrodes and electrolyte interfaces becomes

higher and this is related to the slow periodic reversal of the electric field. Consequently, the number of free mobile ions decreases at low frequency as well as the conductivity.

The plateau region signifies that the conductivity is equal to dc conductivity of polymer electrolytes. The dc conductivity of the prepared polymer electrolyte samples has been determined by extrapolating the plateau region on the *y*-axis. The dc conductivity values from the frequency dependence ionic conductivity plots are in good agreement with those obtained in ionic conductivity studies. It is clearly known that PLT-8 exhibits the highest ionic conductivity and followed by PLT-4, PL-4 and PLT-10. Apart of that, ionic conductivity of polymer electrolytes is found to increase with increasing frequency. At higher frequency, the conductivity increases with frequency as the greater mobility of charge carriers and faster hopping of ions.

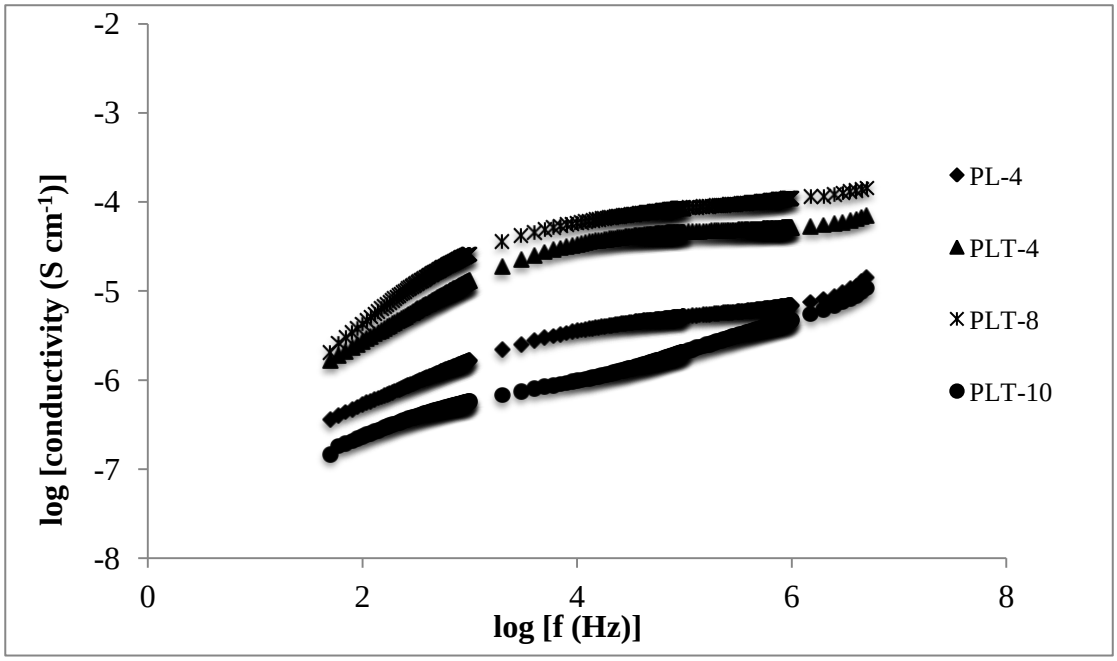

Figure 4.16: Variation of logarithm conductivity as a function of frequency for PL-4, PLT-4, PLT-8 and PLT-10.

4.1.3.3.3 Frequency dependence of loss tangent

Figures 4.17 (a) and (b) depict the variation of loss tangent as a function of frequency for PL-4, PLT-4, PLT-8 and PLT-10 at room temperature. It can be observed that as the wt. % of TiO_2 increases gradually, the tangent loss peaks are shifted to higher frequency. Beyond the 8 wt. % of TiO_2, the tangent loss peak was shifted to lower frequency. From the Figure 4.17(a) and (b), tan δ increases with frequency until a maximum, and following that decreases with further increase in frequency. The occurrence of peak for every sample can be seen in Figure 4.17, this is ascribed to the presence of relaxation dipoles in Li^+ ions in all the tested samples. Presence of loss tangent peak had separated the bulk material and the electrode surface polarization phenomena in the low frequency dielectric dispersion. Electrode polarization phenomenon occurs due to the formation of blocking layer.

As the wt. % of TiO_2 increases gradually, tangent loss peaks are shifted to higher frequency. As the peak shifts towards higher frequency side, the relaxation time is reduced. The shifting of peak to higher frequency illustrates the increase in the cations mobility upon reduction in the relaxation time. Based on the reported relaxation time value, the relaxation time is inversely proportional to ionic conductivity of polymer electrolyte. As more inorganic filler is added, the crystalline region will become lesser and therefore, polymer segment is now more flexible to orient. Eventually, the relaxation time becomes faster.

In terms of peak intensity, the intensity of the loss tangent peak is to correlate with the number of free charge carrier for the sample. The increase of peak intensity

upon the addition of TiO_2 implies to increase the area under the loss tangent peak. As the intensity of loss tangent peak become higher with increases the TiO_2 content, more number of free Li^+ ions has participates in the relaxation process to enhance the ionic conductivity of the polymer electrolytes. The loss tangent peak for PLT-8 as shown in Fig. 4.17(b) shows highest peak intensity and biggest area under the curve compared to other samples. This implies PLT-8 has more number of free charge carriers that contribute in relaxation processes as well as ionic conductivity value.

However beyond the optimum level, above 8 wt. % of TiO_2, the loss tangent peak shifts to low frequency. This phenomenon implies the increase in relaxation time. Longer relaxation time might reduce the Li^+ ion mobility that inhibits the ion conduction due to the formation of neutral ion pairs or aggregates, leading to the formation of thick interfacial layer within the grain boundary. Consequently, the intensity of loss tangent peak decreased as shown in the Figure 4.17(a) and thus, this suggest the number of free charge carrier has been decreased when the addition beyond 8 wt. % of TiO_2. As a result, ionic conductivity of PLT-10 decreased beyond the optimum level.

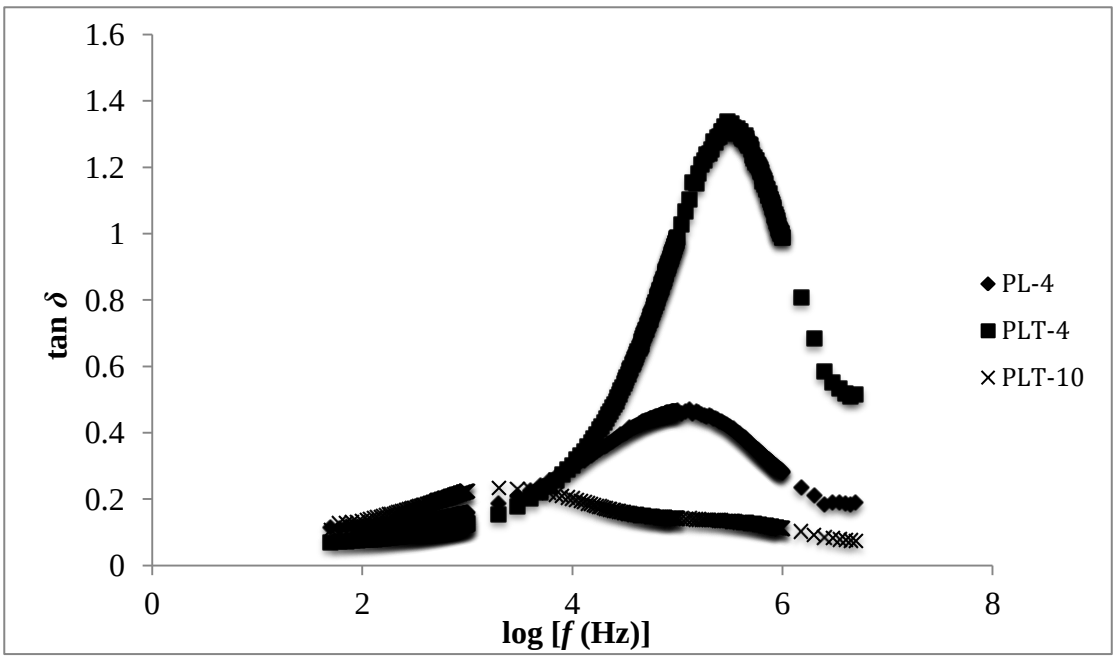

Figure 4.17 (a): Variation of tan d with frequency for PL-4, PLT-4 and PLT-10 at room temperature.

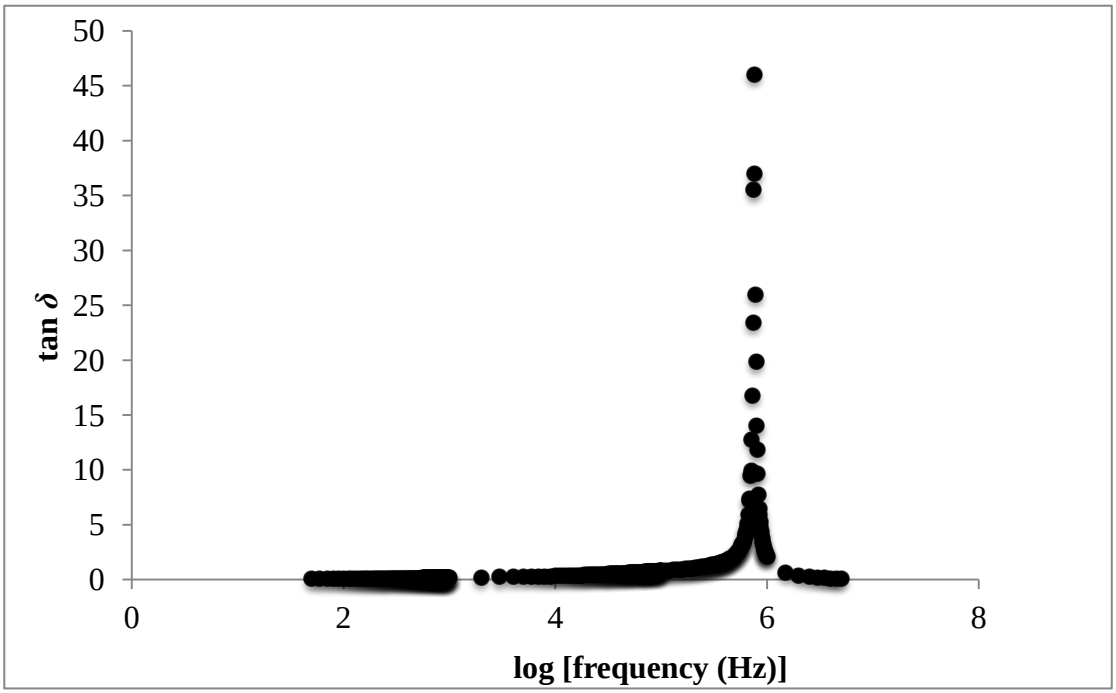

Figure 4.17 (b): Variation of tan d with frequency for PLT-8 at room temperature.

4.2 XRD studies

Many polymers consist of crystalline and amorphous region. Researchers had reported that polymers with low crystallinity will exhibit more amorphous characteristic of polymer matrix (Bertheir *et. al.*, 1983). Consequently, the polymer electrolytes with higher degree of amorphousness exhibit higher ionic conductivity value. In addition, XRD instrument was used to investigate the complexation between the polymer and doping materials. In this study, X-ray diffraction measurement was also performed to examine the crystalline nature of the PVA thin films.

4.2.1 First system (PVA-$LiClO_4$ based polymer electrolyte)

Figure 4.18indicates the XRD diffractograms of pure PVA, and $LiClO_4$. The XRD diffratograms of PL-1, PL-3, PL-4 and PL-5 is shown in Figure 4.19. From Figure 4.18 (a), the crystalline peak of PVA is obtained at glancing angle of $2\theta=19.8°$ which reveals the semi-crystalline nature of PVA. The crystalline peaks for $LiClO_4$ was obtained at angles of $2\theta= 21.1°, 23.2°, 31.3°, 31.4°, 35.7°$ and $39.3°$ as shown in Figure 4.18 (b). Results show that the relative peak at $2\theta= 19.8°$ for pure PVA had shifted to $2\theta=19.0°, 20.7°, 20.3°$ and $19.9°$ in PL-1, PL-3, PL-4 and PL-5, respectively. The peak intensity of relative diffraction peak is an indicator to study the structural characteristic of polymer electrolytes. As the peak intensity of relative diffraction peak becomes lower and broader, the polymer electrolytes have more amorphous characteristic, hence enhancing the ionic conductivity (Yang, 2007). It can be seen by comparing Figure 4.18(a) with Figure 4.19 that the relative diffraction peak intensity of PVA decreases upon the addition of $LiClO_4$. Results imply that the

crystallinity of polymer electrolyte decreases and therefore increases the amorphous nature in polymer electrolytes which gives a higher ionic conductivity (Vassal *et. al.*, 2000).

The decrement in peak intensity of the diffraction peak indicates that the addition of $LiClO_4$ disrupted the arrangement in the polymer backbone of PVA (Ramesh and Arof, 2001). Peaks corresponding to pure $LiClO_4$ have been found to be absent in the complex indicating a complete dissociation of salt in the polymer matrix for PL-1 and PL-3, which is shown in the Figure 4.19 (a) and (b). Absence of these crystalline peaks in polymer electrolytes indicates that the electrolytes are in amorphous region. The complexation of polymer electrolyte has been further confirmed based on the changes in peak intensity.

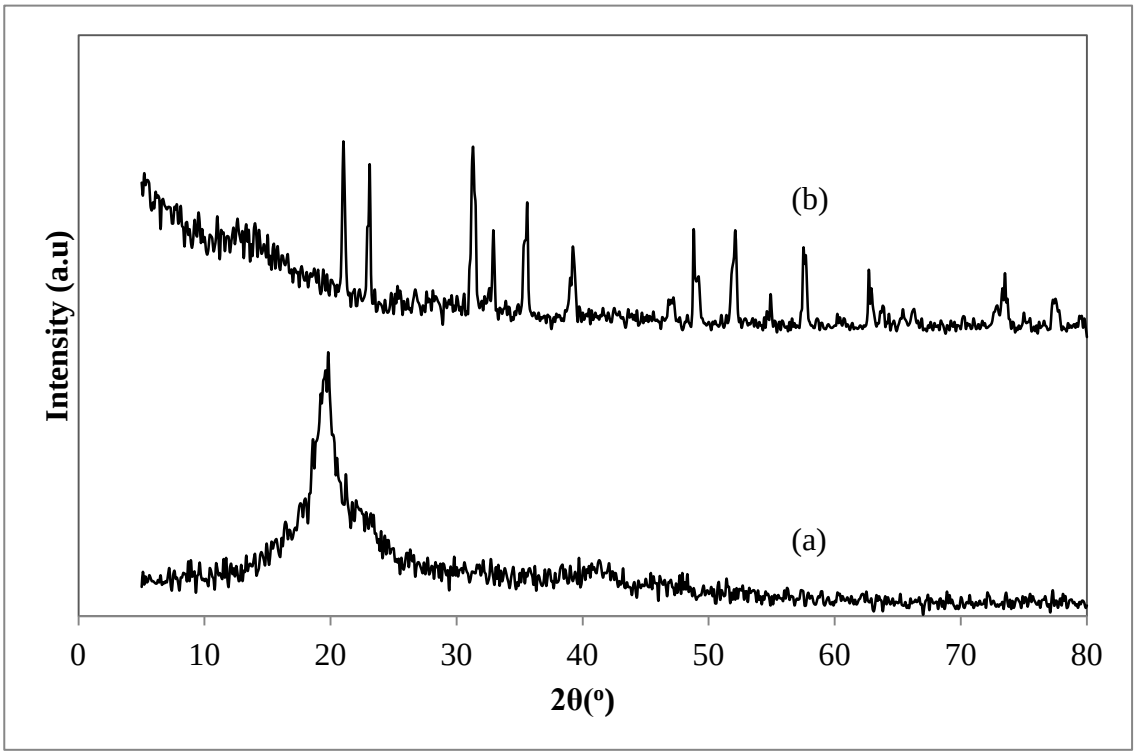

Figure 4.18: XRD patterns for (a) pure PVA and (b) $LiClO_4$

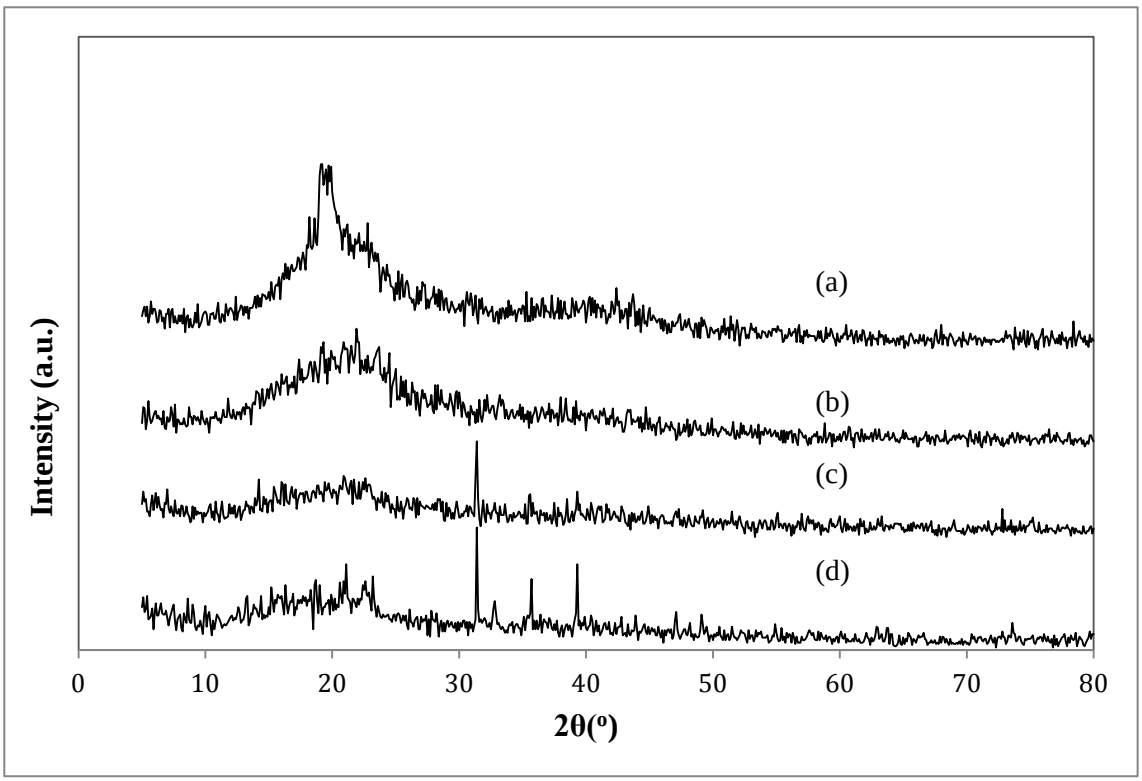

Figure 4.19: XRD patterns for (a) PL-1, (b) PL-3, (c) PL-4 and (d) PL-5

By comparing to the peak intensity of each sample in Figure 4.19. PL-4 gives the lowest peak intensity among others and inferred that PL-4 has highest ionic conductivity and most amorphous character compared to other samples. The enhanced amorphous character increases the ion mobility in the polymer matrix and therefore, PL-4 possesses higher ionic conductivity. There is an intense peak present for PL-4 sample at $2\theta = 31.3°$ that corresponds to the crystalline peak of $LiClO_4$. Presence of sharp peaks in PL-4 as shown in Figure 4.19 (c) is ascribed to the crystalline peak of $LiClO_4$. This is owing to the lithium salt that does not undergo fully dissolution in the polymer matrix. At higher wt. % of $LiClO_4$, aggregates start to form and it is hardly to dissociate in the solvent. Whereby this crystalline peak does not affect the ionic

conductivity of polymer electrolyte, as the relative diffraction peak at angle of 2θ=19.8 ° becomes less intense although crystalline peak is exist.

The crystallite size was calculated using the peak at $2\theta=19.8^{o}$ and equation (3.5). The calculated crystallite size calculated for PL-1, PL-3, PL-4 and PL-5 are presented in Table 4.1. The calculated crystallite size of PVA decreased upon the increment of wt. % of $LiClO_4$ by increasing the value of FWHM. This means the crystallinity of polymer has been decreased and thus enhanced amorphous characteristic of PVA. Upon the addition of $LiClO_4$, the amorphosity of polymer has increased, leading to a flexible polymer backbone. Consequently, it produces a greater ionic diffusivity resulting in high ionic conductivity. PL-4 has the lowest crystallite size and thus, PL-4 possesses higher degree of amorphous nature as well as ionic conductivity.

Table 4.1: Crystallite size of PL-1, PL-3, PL-4 and PL-5 for diffraction peak at $2\theta=19.8^{o}$

Sample	**Crystallite size (Å)**
PL-1	85.8
PL-3	66.7
PL-4	46.9
PL-5	58.6

4.2.2 Second system (PVA-$LiClO_4$-Sb_2O_3 based polymer electrolyte)

Figure4.20 shows the XRD diffractogram of Sb_2O_3. The crystalline peaks for $Sb_2O_3$are observed at angles of 2θ= 25.3°, 28.4°, 44.2°, 50.3 ° and 54.4 °. Figure 4.21indicates the XRD patterns of PLS-2, PLS-6 and PLS-8. Results show that the relative peak at 2θ= 19.8° for pure PVA had shifted to 2θ=19.4, 19.0 and 19.3 in PLS-2, PLS-6 and PLS-8, respectively. The shifting of peaks is attributed to the incorporation of Sb_2O_3. This phenomenon shows that complexation has occurred between PVA, $LiClO_4$ and Sb_2O_3.

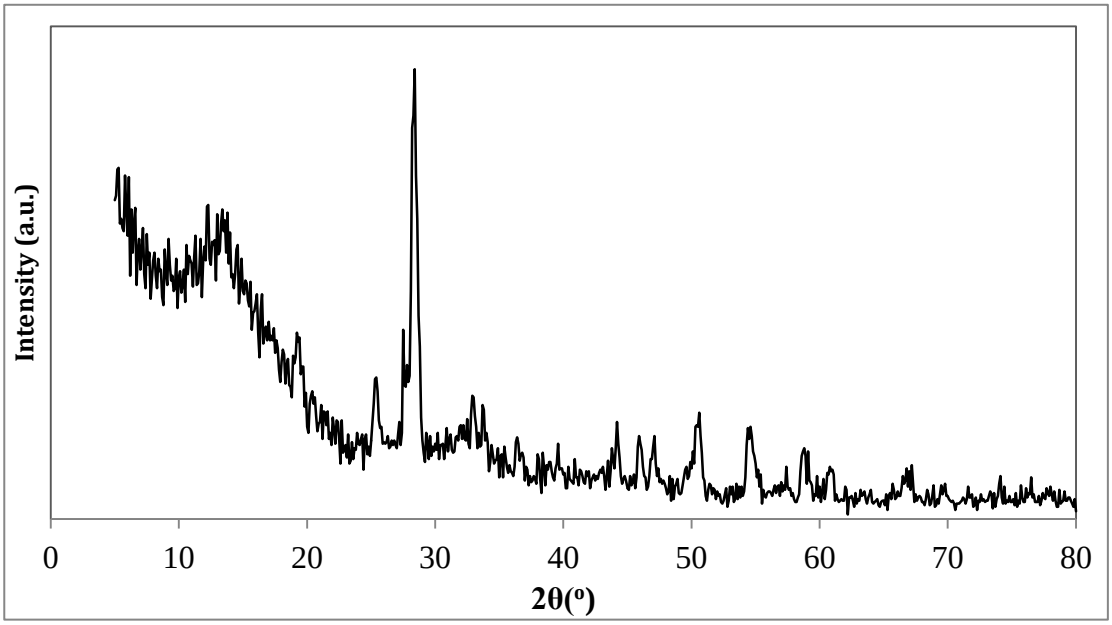

Figure 4.20: XRD pattern for Sb_2O_3

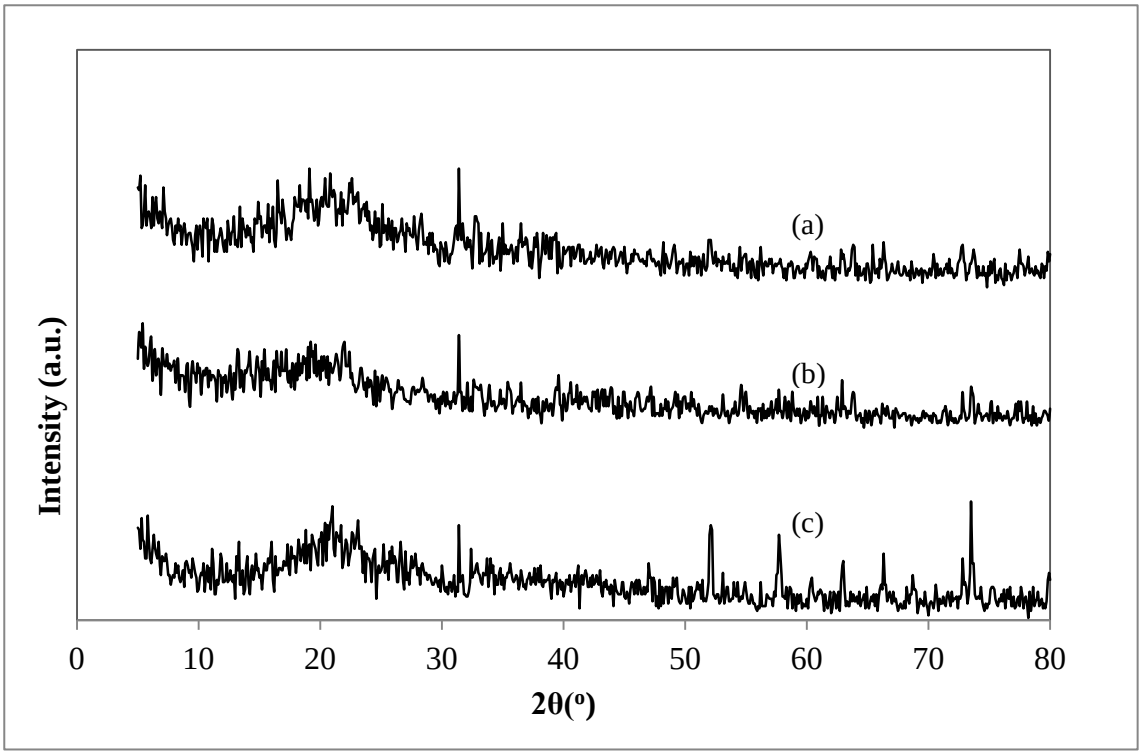

Figure 4.21: XRD patterns for (a) PLS-2, (b) PLS-6 and (c) PLS-8

PLS-2, PLS-6 and PLS-8 indicate decrease in intensity of the crystalline peak of PVA at 2θ=19.8° upon the addition of Sb_2O_3.Addition of 2 wt. % of Sb_2O_3 does not show any significant changes in relative peak intensity. This implies that small amount of filler does not enhance the degree of amorphousness of the sample. The relative peak intensity of PVA had become slightly less intense with further addition of 6 wt. % and 8 wt. % of Sb_2O_3 which implies that the amorphous nature of the polymer electrolyte is enhanced. This, in turn enhances the polymer chain flexibility as well as the ionic conduction. Figure 4.21(b) indicates that PLS-6 has more amorphous character compared to other samples. By comparing to Figure 4.21(b) and (c), the relative peak intensity for PLS-6 is observed to be less intense than PLS-8. Few crystalline peaks were present from the XRD diffractogram with further addition

of Sb_2O_3 up to 8 wt.%. This is attributed to excessive amount of Sb_2O_3 that does not undergo complexation with the PVA-$LiClO_4$ matrix.

Results also show that Sb_2O_3 decreases the intensity of crystalline peak at $2\theta = 30.3°$ which correspond to $LiClO_4$. This behaviour shows that lithium salt dissociates into free charge carrier upon the addition of Sb_2O_3, which is in good agreement with ionic conductivity studies.

The calculated crystallite size for PLS-2, PLS-6 and PLS-8 is tabulated in Table 4.2. Based on Scherrer equation, the higher the value of FWHM, the smaller the crystallite sizes. Addition of Sb_2O_3into polymer matrix had reduced the crystallite size as well as the crystallinity of the polymer electrolytes. PLS-6 which gives the highest ionic conductivity has the smallest crystallite size. The crystallite size was increased with the incorporation of 8 wt. % Sb_2O_3 due to excessive amount of filler content. This is attributed to the formation of aggregates. This is proven by the existence of the crystalline peak for PLS-8 as shown in Figure 4.21(c).

Table 4.2: Crystallite size of PLS-2, PLS-6 and PLS-8 for diffraction peak at $2\theta = 19.8^o$

Sample	**Crystallite size (Å)**
PLS-2	28.1
PLS-6	2.1
PLS-8	23.4

4.2.3 Third system (PVA-$LiClO_4$-TiO_2 based polymer electrolyte)

Figure 4.22 illustrates the XRD diffractogram for TiO_2.The characteristic peak of TiO_2 was obtained at angles of 2θ=25.2°, 27.4°, 36°, 41.1°, and 54.2°. XRD diffractogram of PLT-4, PLT-8 and PLT-10 were shown in Figure 4.23.Results show that the relative peak at angle of 2θ=19.8° for pure PVA had shifted to 2θ=20.6°, 21.2° and 20.9° in the PLT-4, PLT-8 and PLT-10, respectively. The shifting of relative diffraction peak was observed in PLT-4, PLT-8 and PLT-10 are mainly due to the incorporation of TiO_2. This situation discloses complexation has occurred in between the PVA, $LiClO_4$ and TiO_2.

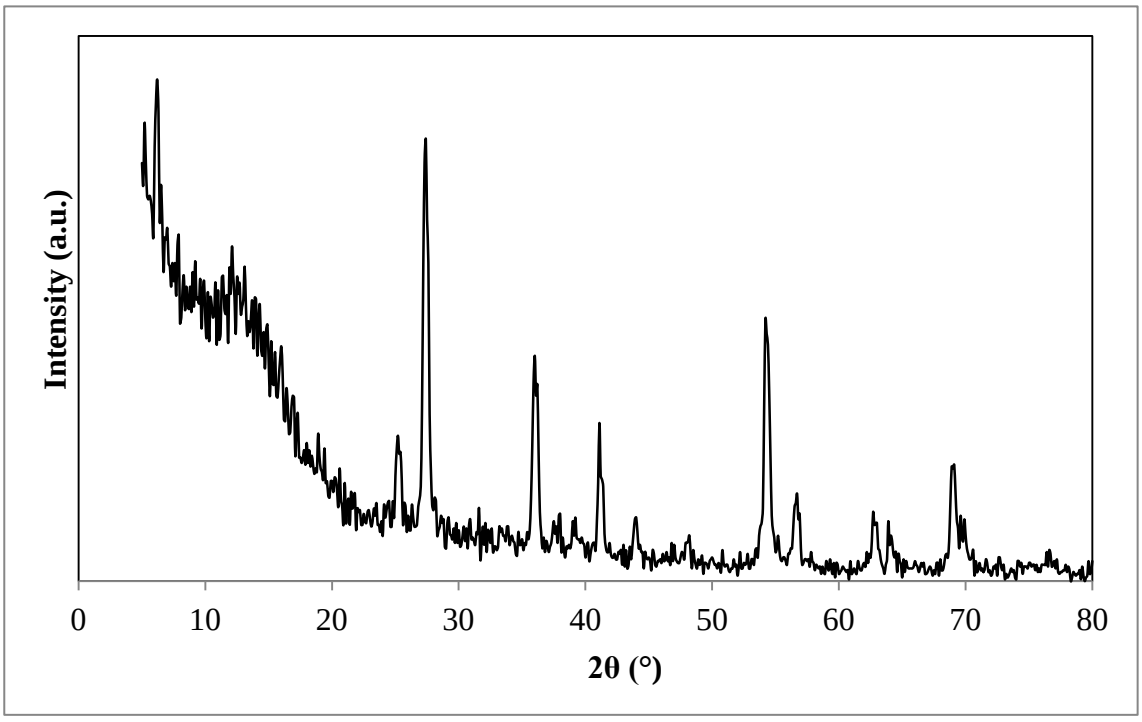

Figure 4.22: XRD pattern for TiO_2

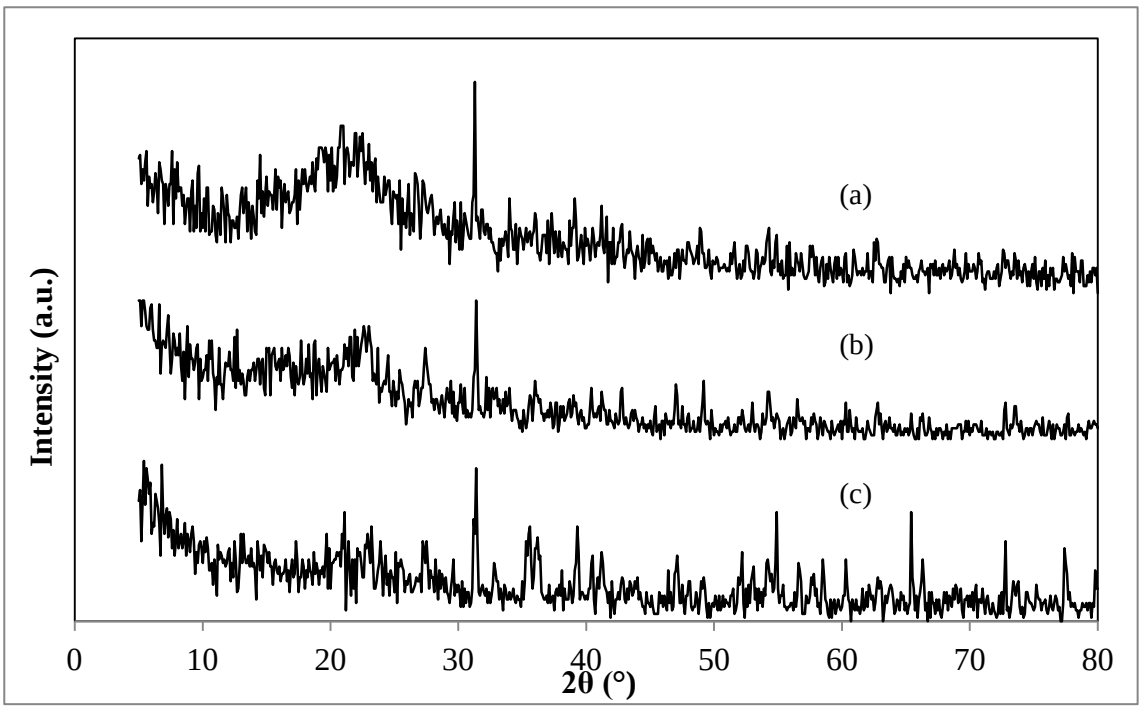

Figure 4.23: XRD patterns of (a) PLT-4, (b) PLT-8 and (c) PLT-10

Incorporation of 4 wt. % of TiO_2 into polymer matrix indicates no discernible effect on the reduction of peak intensity at diffraction peak at angle of 2θ=19.8 °. This is owing to the inadequate amount to dislocate the polymer network which causes an insignificant increase in amorphous degree among the polymer backbone. Upon the addition of 8 wt. % and 10 wt. % of TiO_2, the relative peak intensity was reducing greatly. This result clearly suggested that the crystalline region of PVA decreased with increasing the wt. % of TiO_2.

Generally, high degree of crystallinity of pure PVA was due to the hydroxyl groups in its side-chain (Benavente *et. al.*, 2002). The crystallinity of PVA decreased as the hydroxyl group in its side chain had reacted with the Li^+ conducting species and TiO_2. Hence the number of hydroxyl group remaining in the PVA decreases and

results in the crystallinity of PVA decreasing as well (Ramesh *et. al.*, 2011). Consequently, a decrease in relative peak intensity at angles of $2\theta=19.8°$ can be seen in every sample. The reduced peak intensity results in increase in the amorphous characteristic of polymer electrolyte; causing polymer electrolytes to have a flexible backbone that results in greater ionic diffusivity and ion mobility as well. Therefore, polymer electrolyte with flexible backbone and good ion mobility will favor the ionic conduction. By comparing the peak intensity among the samples, PLT-8 displays the lowest peak intensity compared to other samples. This implies PLT-8 exhibits the highest ionic conductivity.

However, several crystalline peaks were seen in PLT-10. This is attributed to excessive amount of TiO_2 particle and causes the formation of aggregates. The formation of aggregates debilitates TiO_2 to dissociate more lithium salt into free ions. As a consequence, $LiClO_4$ recrystallize in polymer matrix leading to the reduction in ionic conductivity. This result was in good agreement with ionic conductivity studies. Results also show that TiO_2 decreases the peak intensity of crystalline peak at $2\theta= 31.3°$ which correspond to $LiClO_4$. This behaviour shows lithium salt dissociates into free charge carrier upon the addition of TiO_2.

The calculated crystallite size of PLT-4, PLT-8 and PLT-10 at relative diffraction peak for each samples are presented in Table 4.3. The results signify that the incorporation of TiO_2 reduces the crystallite size as well as the crystallinity of polymer electrolytes. Smaller crystallite size can produce a more flexible polymer segment which favors the ionic transportation. It also deduces that the PLT-8 which

gives the smallest crystallite size will induces the highest ionic conductivity compared to other samples. Whereby, PLT-10 has bigger crystallite size compared to PLT-8, this is attributed to the excessive amount of TiO_2 have been added into the polymer matrix. Consequently, the ionic conductivity decreases.

Table 4.3: Crystallite size of PLS-2, PLS-6 and PLS-8 for diffraction peak at $2\theta=19.8^{o}$

Sample	**Crystallite size (Å)**
PLT-4	38.1
PLT-8	23.5
PLT-10	65.2

4.3 Morphological studies

SEM is one of the most versatile instrument available for the examination and analysis of the microstructure morphology for conducting polymer surfaces. In this study, SEM analyses were conducted to investigate the effect of doping such as $LiClO_4$, Sb_2O_3 and TiO_2 particles on structure and surface morphology of the conducting polymers.

4.3.1 First system (PVA-$LiClO_4$ based polymer electrolyte)

Figures 4.24 (a), (b), (c), (d) and (e) show the SEM micrographs for pure PVA, PL-1, PL-3, PL-4 and PL-5, respectively. Figure 4.24 (a) reveals the semi-crystalline structure of pure PVA. Whereas Figure 4.24 (b), (c), (d) and (e) clearly display homogeneity surface morphology of the PVA-$LiClO_4$. Upon addition of 10

wt. %, 30 wt. %, 40 wt. % and 50 wt. % of $LiClO_4$ the surface morphology of polymer electrolyte alters significantly. The surface morphology is uniform and no phase separation is seen. This infers an excellent distribution of lithium salt in the polymer matrix. Thus complexation between PVA and $LiClO_4$ is confirmed. The surface morphology of PL-1, PL-3, PL-4 and PL-5 becomes rougher compared to surface morphology of pure PVA. Whereby, the particles start to undergo coagulation as 40 wt. % and 50 wt. % of $LiClO_4$ were added into polymer matrix, and it can be seen that the PL-4 and PL-5 shows uneven surface compared to PL-3. In ionic conductivity studies, beyond the optimum level, ionic conductivity drops which elucidate by excess amount of $LiClO_4$ was added into polymer matrix. Therefore, the SEM image for PL-5 is an evidence and it was clearly observed that the excess amount of $LiClO_4$ shows the uneven surface and a very rigid surface owing to coagulation of $LiClO_4$. This occurrence inhibits the ion transportation and reduction in number of charge carrier. Despite that, PL-4 also shows a rough surface but small voids were seen on the surface morphology. Voids are the conducting pathway which allow the ions to migrate. Therefore, it can be deduced that 40 wt. % of $LiClO_4$ is an optimum amount to be added into PVA matrix.

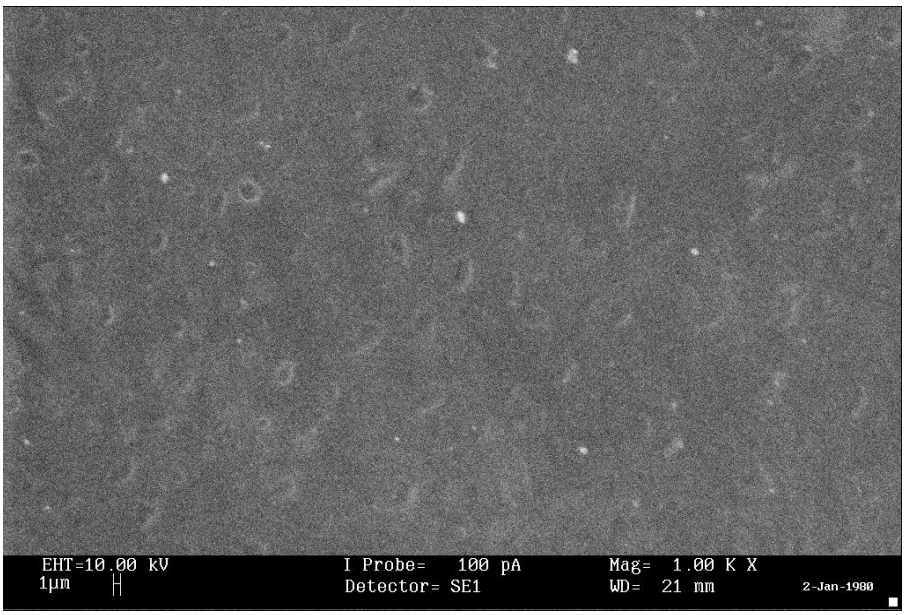

Figure 4.24 (a): SEM micrograph of pure PVA at magnification of 1000x

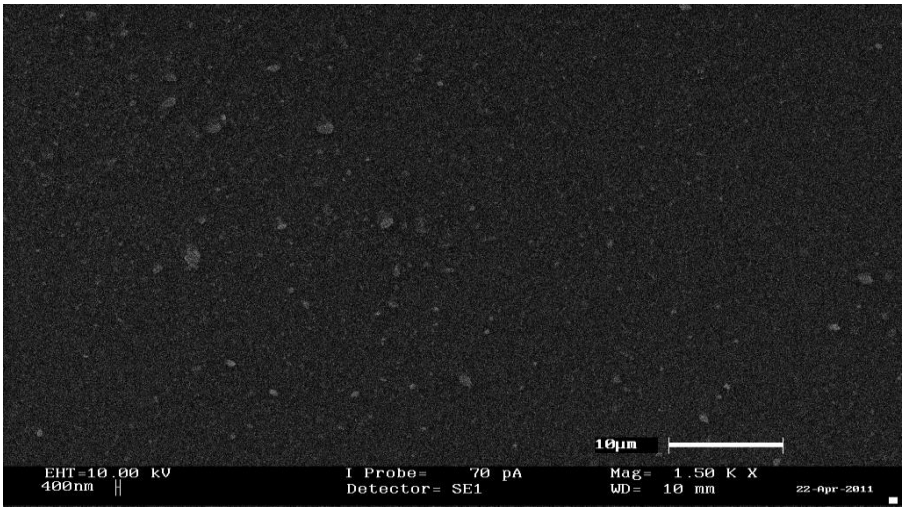

Figure 4.24 (b): SEM micrograph of PL-1 at magnification of 1000x

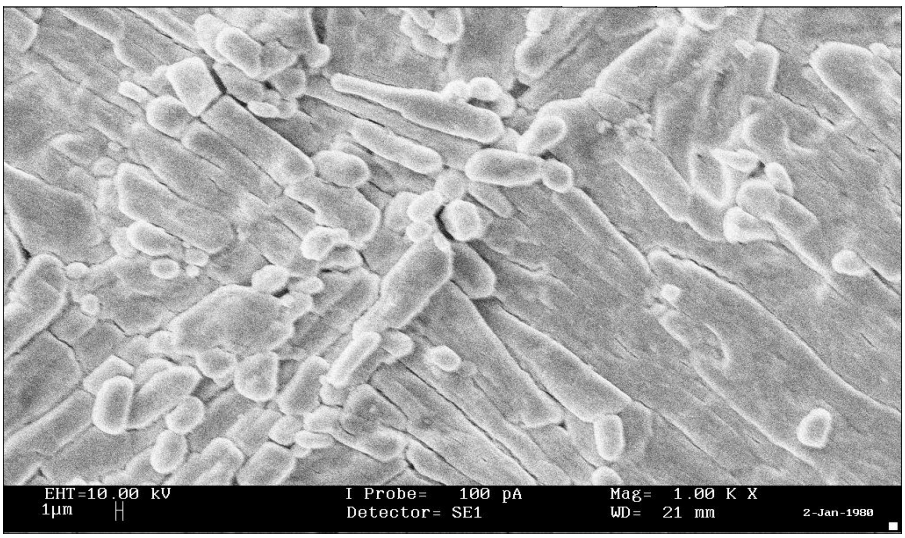

Figure 4.24 (c): SEM micrograph of PL-3 at magnification of 1000x

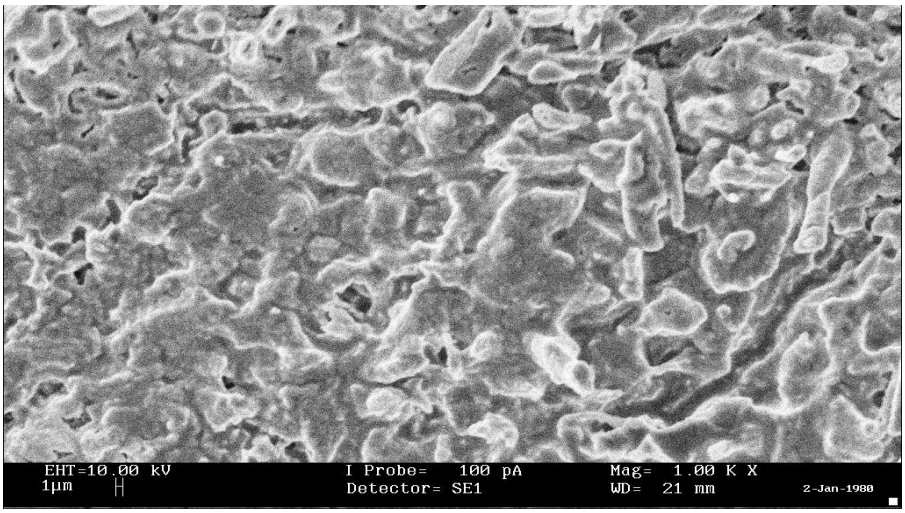

Figure 4.24 (d): SEM micrograph of PL-4 at magnification of 1000x

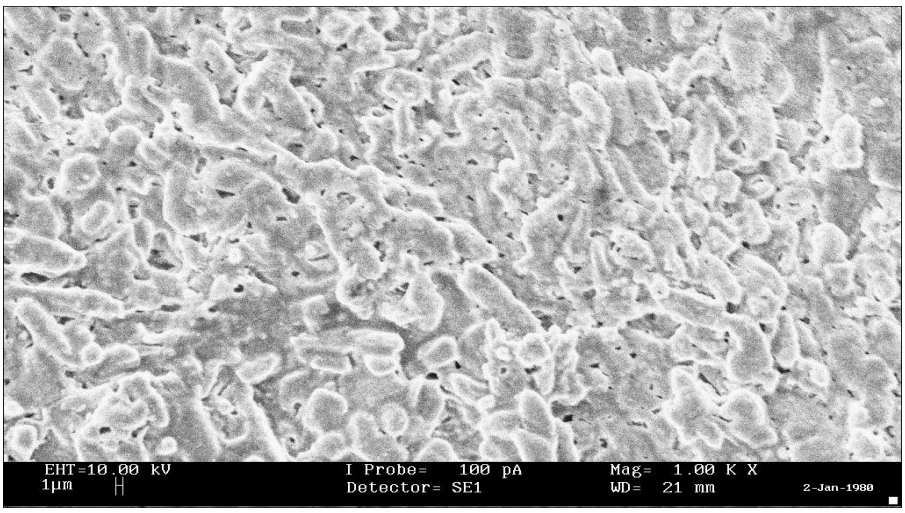

Figure 4.24 (e): SEM micrograph of PL-5 at magnification of 1000x

4.3.2 Second system (PVA-LiClO4-Sb_2O_3 based polymer electrolyte)

The crystallite size of polymer electrolytes can be further validated by referring to SEM micrographs. The surface morphology ofPLS-2, PLS-6 and PLS-8 is shown in Figure 4.25 (a), (b) and (c), respectively. Upon the addition of Sb_2O_3, the particles of Sb_2O_3 are well dispersed on polymer matrix and uniform throughout the surface of polymer matrix. This complexation between filler and polymer host is revealed in SEM micrographs, where the shape of particle or surface morphology is altered compared to polymer electrolyte without filler.

The dispersed Sb_2O_3 particles play an active role in the growth of microstructures resulting in different morphology. PLS-2 and PLS-8 have larger crystallite size compared to PLS-6 as shown in Figure 4.25 (b). Coagulation that happen in PLS-2 is attributed to the small amount of filler that does not disperse separately whereas formation of aggregates in PLS-8 is due to excessive amount of Sb_2O_3 that have been added. The ionic conductivity of PLS-2 and PLS-8 is not affected by coagulation and aggregates as the formation of voids can be seen in the SEM images. Formation of voids creates conducting pathway in the polymer matrix and enhance the mobility of ions. Eventually, it increases the ionic conductivity. PLS-6 exhibits the highest ionic conductivity; this is ascribed to small crystallite size that leads to higher surface area. Small crystallites tend to create high void surface area compared to bulk crystallites. This will ease the Li^+ ion to conduct in the polymer matrix. In terms of number of voids, the higher the number of voids, the more conducting pathways created. Hence, the ionic conductivity for PLS-6 increases.

These results were in agreement with the ionic conductivity studies where PLS-6 exhibits the highest ionic conductivity.

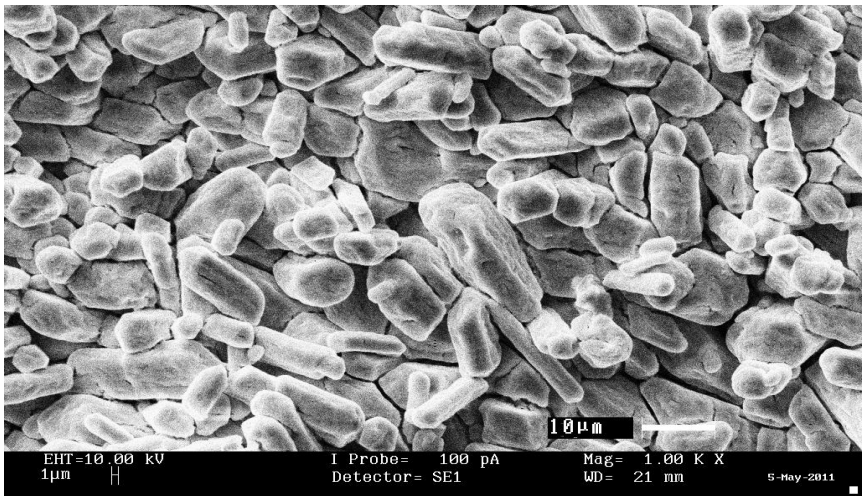

Figure 4.25 (a): SEM micrograph of PLS-2 at magnification of 1000x

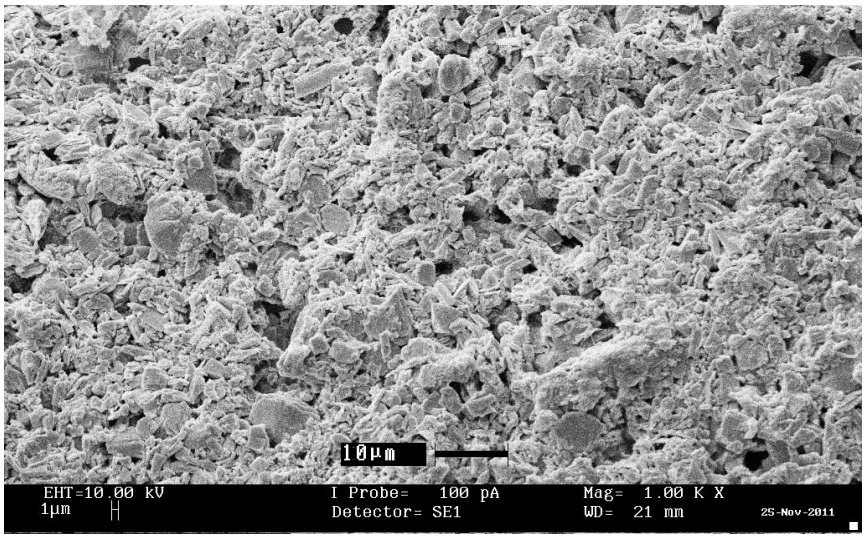

Figure 4.25 (b): SEM micrograph of PLS-6 at magnification of 1000x

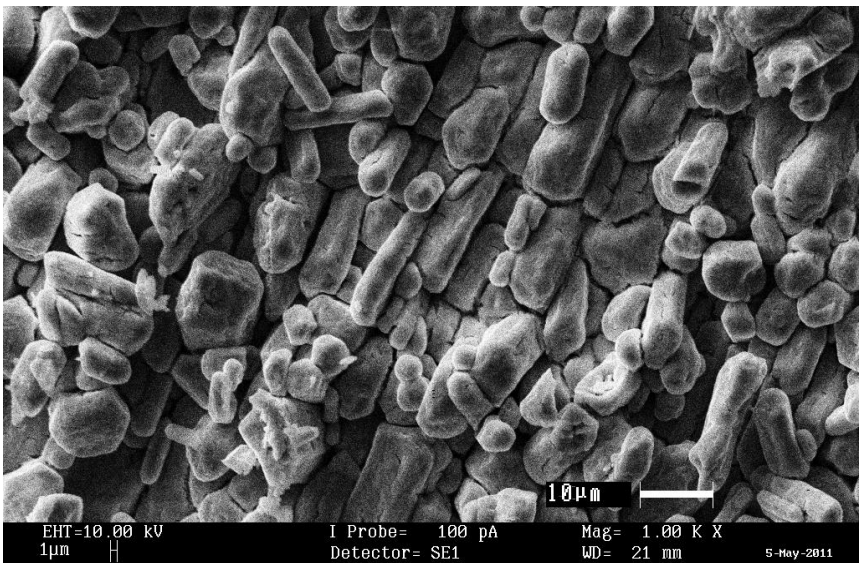

Figure 4.25 (c): SEM micrograph of PLS-8 at magnification of 1000x

4.3.3 Third system (PVA-$LiClO_4$-TiO_2 based polymer electrolyte)

Figure 4.26 display SEM images of the surfaces of several typical PVA-$LiClO_4$-TiO_2 thin films with different wt. % of TiO_2. As shown in Figure 4.26 (a), (b) and (c), it was found that the TiO_2 particles were well dispersed on the polymer matrix and uniform across the surface of polymer matrix. Referring to SEM micrographs, alteration on surface morphology of PLT-4, PLT-8 and PLT-10 as shown in Figure 4.26 has implies that there is complexation occur between PVA, $LiClO_4$ and TiO_2. In other words, TiO_2 particles play an active role in the growth of microstructures leading to modification on morphology of polymer electrolytes.

The ionic conductivity of PLT-4, PLT-8 and PLT-10 is not influenced by coagulation and aggregates as the formation of voids can be seen in the SEM images. Formation of voids creates conducting pathway in the polymer matrix and enhances

the mobility of ions. Eventually, it increases the ionic conductivity. As highlighted in the Figure 4.26(b), PLT-8 shows higher number of voids compared to PLT-4 and PLT-10 and this implies PLT-8 promotes more conducting pathway for ions transportation and enhance the mobility of ions. Eventually, this increases the ionic conductivity of polymer electrolytes (Southall *et. al.*, 1996). Based on the size of voids, the average diameter of voids in PLT-8 was found approximately 4 μm. In terms of the size of voids, PLT-8 shows larger voids compared to PLT-4 and PLT-10. This will cause the elevation in number of charge carrier that able to transport though out the polymer matrix as well as the ionic conductivity.

Besides, the ionic conductivity shows decline as the weight percentage of TiO_2 increased up to 10 wt. %. This can be seen in Figure 4.26 (c), where the surface morphology in PLT-10 has high level of rigidity and little voids were found resulting in blocking effect on ions transportation as well as the mobility of ions. Therefore, blocking effect leads to the decreases in ionic conductivity.

Figure 4.26 (a): SEM micrograph of PLT-4 at magnification of 1000x

Figure 4.26 (b): SEM micrograph of PLT-8 at magnification of 1000x

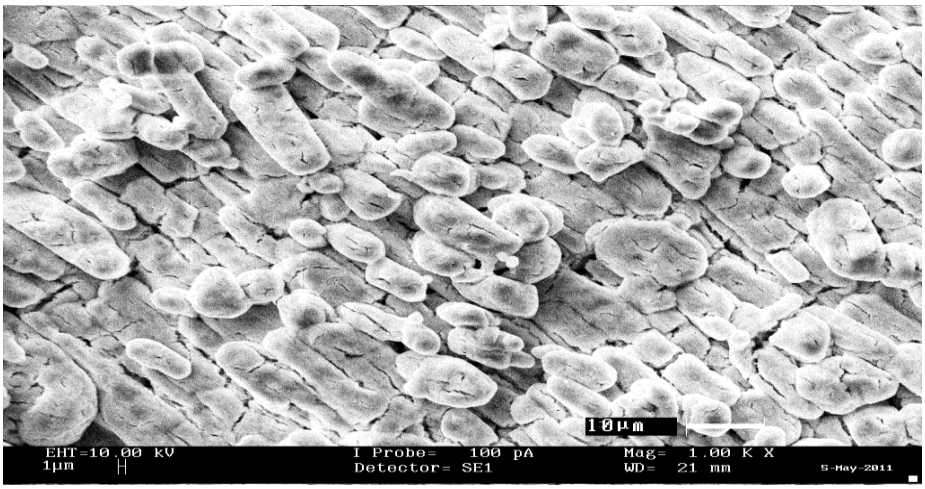

Figure 4.26 (c): SEM micrograph of PLT-10 at magnification of 1000x

4.4 DSC studies

DSC was used to determine the glass transition temperature (T_g). In general, a low glass transition temperature enhances the amorphous nature of the polymer as well as the flexibility. The flexibility of the polymeric chain is directly related to the glass transition temperature (T_g). The lower the value of T_g, the higher the flexibility of the polymeric chains or segments.

4.4.1 First system (PVA-$LiClO_4$ based polymer electrolyte)

Figure4.27shows the DSC curves for pure PVA, PL-1, PL-3, PL-4 and PLS-5 in the temperature range of 30 ^oC to 180 ^oC. The endothermic reaction of T_g can be observed in Figure 4.27. No melting temperature (T_m) exists in the DSC plot, which means that the polymer electrolyte shows amorphous structure in the temperature range of 30 ^oC to 180 ^oC as lithium ionic transport takes place in the amorphous phase (Nogueira *et. al.*, 2004). Table 4.4 shows the glass transition temperature of PVA, PL-1, PL-3, PL-4 and PL-5. The glass transition of PVA obtained from DSC analysis is 80.2 ^oC.

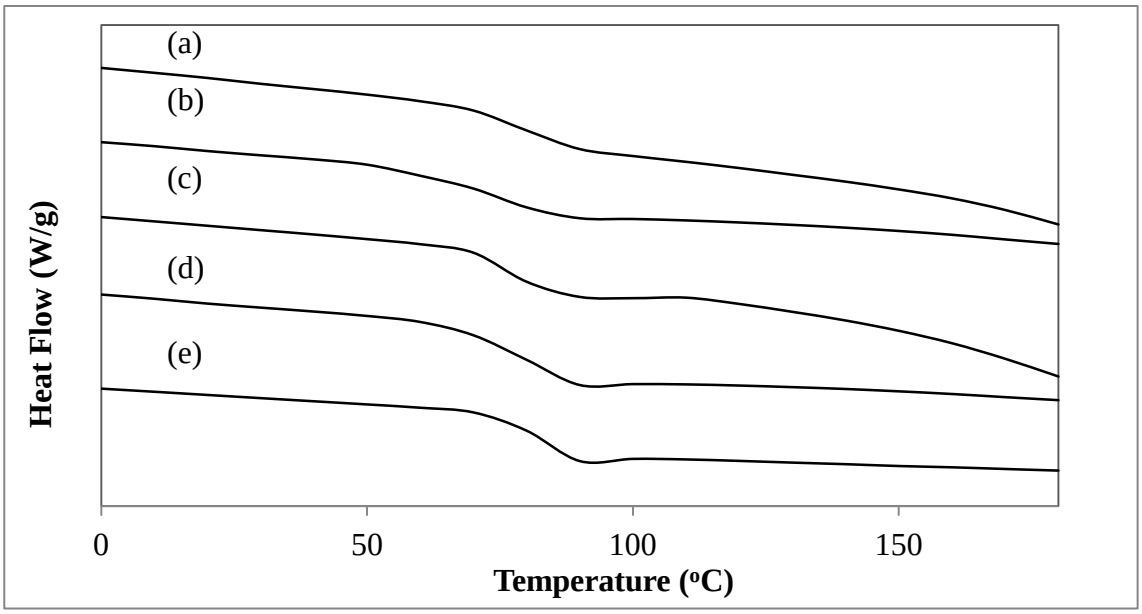

Figure 4.27: DSC thermograms of (a) pure PVA, (b) PL-1, (c) PL-3, (d) PL-4 and (e) PL-5.

Incorporation of 10 wt. % and 20 wt. % of $LiClO_4$into the polymer matrix indicates no appreciable change in the T_g as shown in table 4.4. It can be concluded

that T_g is not influenced by the low content of $LiClO_4$. When the weight percentage of $LiClO_4$ is increased, the glass transition of the polymer shifts to a higher temperature value of 84.2 ℃ and 83.2 ℃ for PL-4 and PL-5, respectively. The shifting of T_g suggests that there is an interaction between $LiClO_4$ and polymer backbone. Besides, transition temperature shifted to a higher value upon the addition of 40 wt. % and 50 wt. % of $LiClO_4$. This phenomenon indicates that the salvation of the lithium cation with the oxygen atom of the PVA is partially interrupted with the local motion of the polymer segment through the formation of transient crosslink of rotation. This causes an increase in the T_g value (Souquet *et. al.*, 1994). Hence, it can be said that the solvation of Li^+ reduces the flexibility of the polymer chain.

Table 4.4: Glass transition temperature (T_g) in DSC analyses for pure PVA, PL-1, PL-3, PL-4 and PL-5

Sample	**Glass transition temperature, T_g (^oC)**
Pure PVA	80.2
PL-1	78.6
PL-3	79.6
PL-4	84.2
PL-5	83.2

4.4.2 Second system (PVA-$LiClO_4$-Sb_2O_3based polymer electrolyte)

Figure4.28shows the DSC thermograms for PLS-2, PLS-6 and PLS-8 in the temperature range of 30 ^oC to 180 ^oC. The endothermic reaction of T_g can be observed in Figure4.28. No melting temperature (T_m) exists in the DSC plot, which means that the polymer electrolyte shows amorphous structure in the temperature range of 30 ^oC to 180 ^oC as lithium ionic transport takes place in the amorphous phase. Table 4.5 shows the glass transition temperature of PLS-2, PLS-6 and PLS-8. The glass transition temperature of PL-4 that obtained in 4.4.1 is 84.2 ^oC.

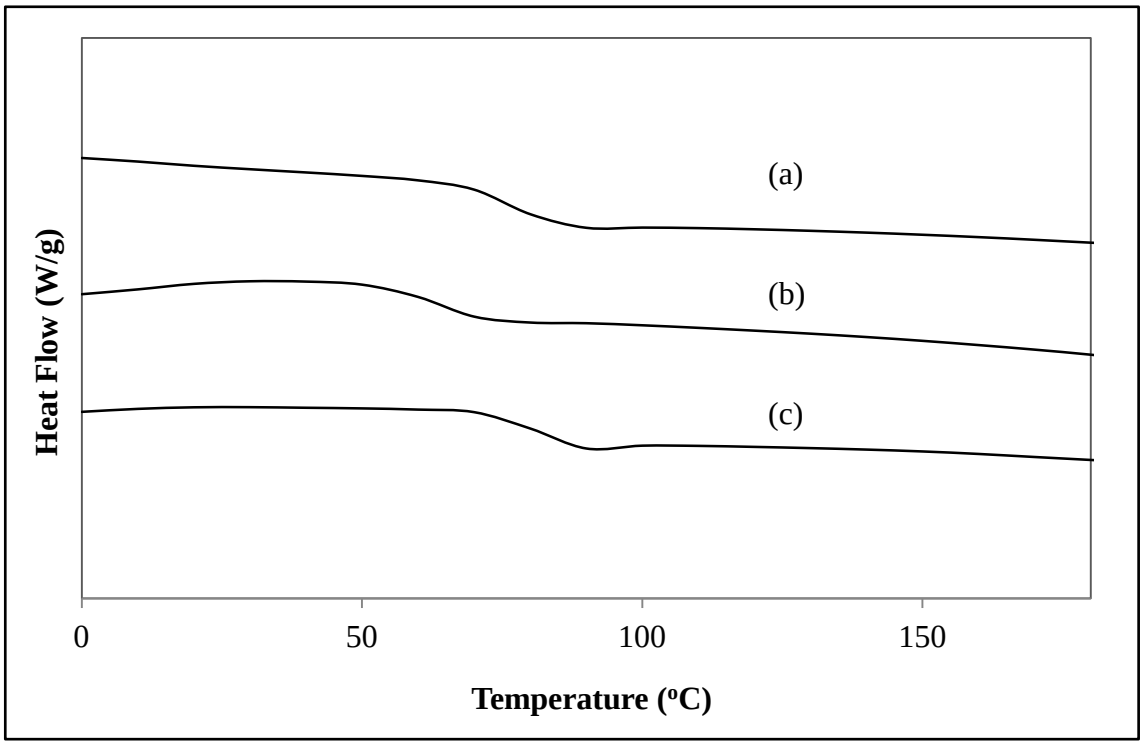

Figure 4.28: DSC thermograms of (a) PLS-2, (b) PLS-6 and (c) PLS-8.

Incorporation of 2 wt. % of Sb_2O_3 into the polymer system indicates no appreciable change in the T_g as shown in table 4.5. It can be concluded that T_g is not influenced by the low content of Sb_2O_3. When the weight percentage of Sb_2O_3 is

increased to 6 wt. %, the glass transition of the polymer shifts to a lower temperature value of 72.1 ℃. The shifting of T_g suggests that there is an interaction between Sb_2O_3 and polymer backbone. PLS-6 obtains the lowest glass transition temperature compared to other samples. This is due to addition of Sb_2O_3 that weakens the dipole-dipole interactions, which enable the easy flow of ions through polymer chains network when there is an applied electric field compared to other samples (Ramesh and Arof, 2001). As T_g lowers, the amorphous phase becomes more flexible and provides fast ion conduction, hence increasing the ionic conductivity of polymer electrolyte. This implies that the addition of Sb_2O_3 has enhanced the ionic conductivity of the polymer electrolytes.

As the weight percentage of Sb_2O_3 is increased to 8 wt. %, the T_g shifts to a slightly higher temperature of 82.9 ^oC. The increase in T_g with the addition of Sb_2O_3 is due to the stiffening of the polymeric segments, thereby suppressing the polymeric chain motion. Hence ionic conductivity of polymer electrolyte decreases.

Table 4.5: Glass transition temperature (T_g) in DSC analyses for PLS-2, PLS-6 and PLS-8

Sample	**Glass transition temperature, T_g (^oC)**
PLS-2	79.6
PLS-6	72.1
PLS-8	82.9

4.4.3 Third system (PVA-$LiClO_4$-TiO_2 based polymer electrolyte)

DSC thermograms for PLT-4, PLT-8, and PLT-10 in the temperature range of 30 to 180 ^oC is presented in Figure 4.29. The endothermic reaction of T_g can be observed in Figure 4.29 and the T_g value is tabulated in table 4.6. No crystalline peak was observed in the studied temperature range, which means the polymer electrolyte investigated in this work is predominantly amorphous as the lithium ionic transport takes place in amorphous phase. The discrepancy of T_g value of pure PVA upon addition of lithium salt and inorganic filler allows us to understand the miscibility and interaction between polymer, lithium salt and inorganic filler. The glass transition temperature of PL-4that obtained in 4.4.1 is 84.2 ^oC.

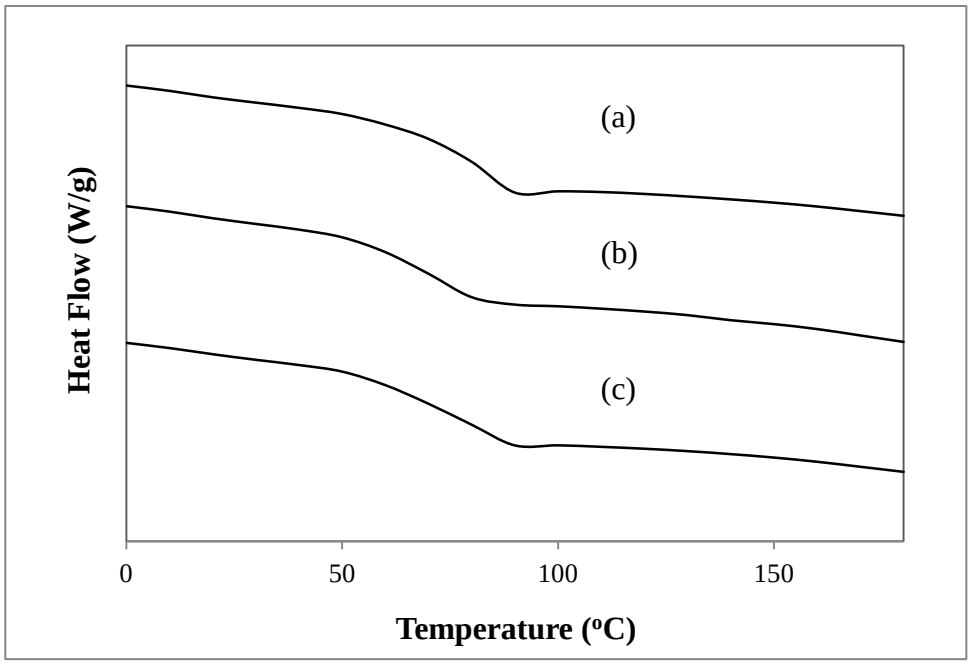

Figure 4.28: DSC thermograms of (a) PLT-4, (b) PLT-8 and (c) PLT-10

As mentioned earlier, low content of filler indicates no significant change in T_g value. A similar situation has been observed in PLT-4. Addition of 8 wt. % of TiO_2

into polymer system had shifted the transition temperature from 84.2 ^{o}C to 76.2^{o}C. The shifting of T_g suggests there is an interaction between TiO_2 and polymer backbone. The decrease in transition temperature implies that the incorporation of TiO_2 weakens the dipole-dipole interactions between the oxygen atom of PVA and Li^+. This will favor the ion migration throughout the polymer chain when there is an applied electric field. At lower T_g value, the amorphous phase becomes more flexible and yields fast ion conduction, hence increasing the ionic conductivity of PLT-8. Therefore, addition of 8 wt. % of TiO_2 into polymer matrix possesses a higher ionic conductivity.

As the weight percentage of TiO_2 is increased to 10 wt. %, the T_g shifts to a slightly higher temperature of 83.3^{o}C. The increase in T_g with the addition of TiO_2 is owing to the stiffening of the polymeric segments, thereby suppressing the polymeric chain motion. Hence ionic conductivity of PLT-10 decreases.

Table 4.6: Glass transition temperature (T_g) in DSC analyses for PLT-4, PLT-8 and PLT-10

Sample	**Glass transition temperature, T_g (^{o}C)**
PLT-4	83.4
PLT-8	76.2
PLT-10	83.3

4.5 TGA studies

4.5.1 First system (PVA-$LiClO_4$ based polymer electrolyte)

In this study, TGA was employed to study the thermal stability of the polymer electrolytes. Figure 4.30 illustrates the TGA thermographs of pure PVA, PL-1, PL-3, PL-4 and PL-5. The PVA film shows two major weight loss regions. There is a weight loss of 7% from 70 ℃ to 100 ℃ for the pure PVA. This is due to the evaporation of the weakly physical yet strongly chemical bound H_2O or elimination of impurities (Rajendran *et. al.*, 2007). The second weight loss occurring at around 218 ℃ is due to the decomposition of PVA film with the weight loss of 37.36 %. In addition, the weight loss of PVA also increases as the temperature increases from 250 ℃ to 300 ℃. This might be attributed to the carbonation (Ganesan *et. al.*, 2008).

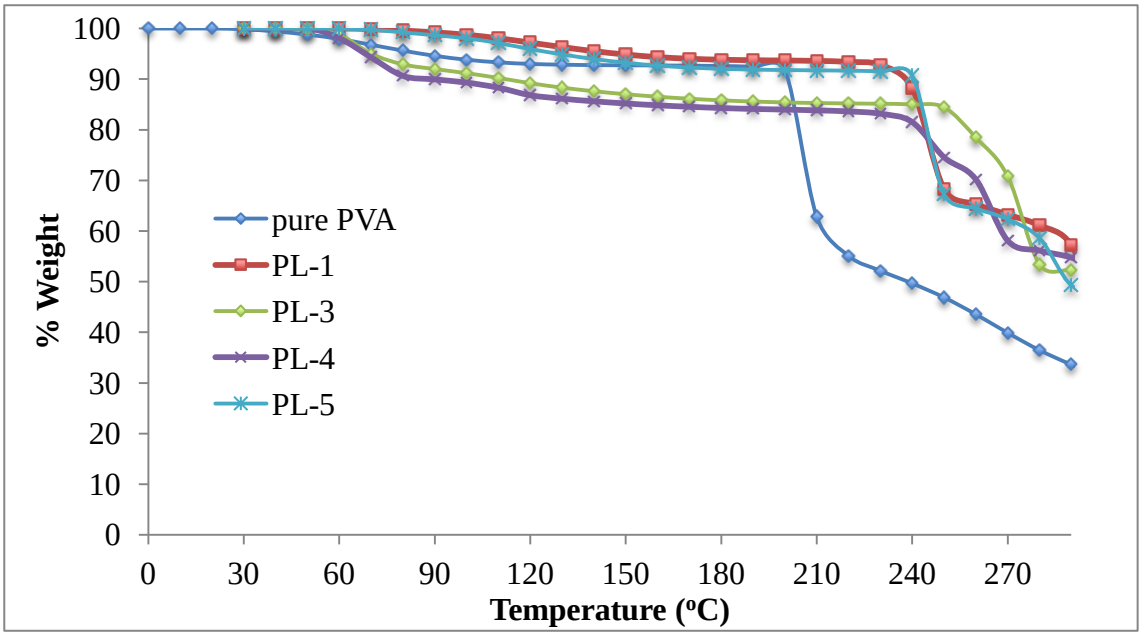

Figure 4.30: Thermogravimetric curves of pure PVA, PL-1, PL-3, PL-4 and PL-5.

PL-1, PL-3, PL-4 and PL-5 also indicate two stages of weight loss. First stage of the weight loss is ascribed to the evaporation of free and bound water. The weight loss of the polymer electrolyte for the first stage had increased compared to pure PVA. The weight loss at this stage is owing to the addition of $LiClO_4$. $LiClO_4$ is a hygroscopic substance and has the ability to absorb water from its surroundings, increasing the weight loss for PL-1, PL-3, PL-4 and PL-5 as shown in Figure 4.30.

The second weight loss for PL-1, PL-3, PL-4 and PL-5 at the temperature range of 220 ℃ to 280 ℃. The onset decomposition temperature has shifted towards higher temperature upon the addition of $LiClO_4$. The onset decomposition temperature of PL-1, PL-3, PL-4 and PL-5 is found in the range of 240 to 260 ℃. The addition of $LiClO_4$ has enhanced the thermal stability of the polymer membrane where PL-1, PL-3, PL-4 and PL-5 undergo decomposition at higher temperature.

The total percentage of weight loss from 210 ℃ to 280 ℃ for PL-1, PL-3, PL-4 and PL-5 is tabulated in table 4.7. Results show that the addition of $LiClO_4$ into the system shows the total weight loss in range of 26 % to 29 %.This infers that the thermal stability of polymer electrolytes increased upon the incorporation of $LiClO_4$.

Table 4.7: Total weight loss (%)at temperature range of 210 ℃ to 280 ℃ in TGA analyses for PL-1, PL-3, PL-4 and PL-5.

Sample	**Total weight loss at temperature range of 210 ℃-280 ℃ (%)**
PL-1	27.48
PL-3	26.70
PL-4	29.07
PL-5	26.10

4.5.2 Second system (PVA-$LiClO_4$-Sb_2O_3 based polymer electrolyte)

Figure 4.31 illustrates the TGA thermographs of PLS-2, PLS-6 and PLS-8. PLS-2, PLS-6 and PLS-8 also show two stages of weight loss. First stage of weight loss is attributed to the evaporation of free and bound water. This is attributed to the addition of $LiClO_4$ into polymer matrix as $LiClO_4$ has the capability to absorb water from its surroundings.

Figure 4.31 also shows that there is a second weight loss for PLS-2, PLS-6 and PLS-8 at the temperature range of 210 ℃ to 280 ℃. The onset decomposition temperature has shifted towards higher temperature upon the addition of Sb_2O_3. The onset decomposition temperature of PLS-2, PLS-6 and PLS-8 is approximately 250 ℃. The addition of Sb_2O_3 has enhanced the thermal stability of the polymer membrane where PLS-2, PLS-6 and PLS-8 undergo decomposition at higher temperature.

The total percentage of weight loss from 210 ℃ to 280 ℃ for PLS-2, PLS-6 and PLS-8 is tabulated in table 4.8. Results show that the addition of Sb_2O_3 into the system had reduced the percentage of weight loss. This infers that the thermal stability of polymer electrolytes increased upon the incorporation of Sb_2O_3. These composite polymer electrolytes have become more thermally stable and more resistant to heat as compared to polymer electrolytes without filler.

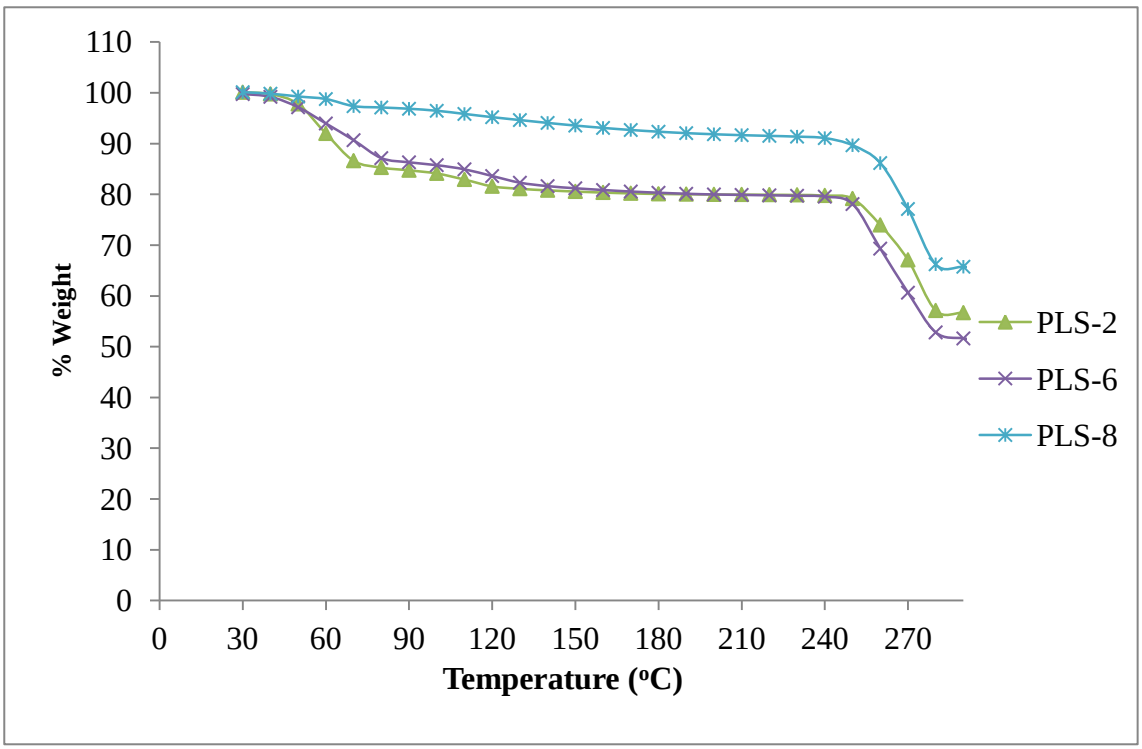

Figure 4.31: Thermogravimetric curves of PLS-2, PLS-6 and PLS-8.

Table 4.8: Total weight loss (%) at temperature range of 210 ℃ to 280 ℃ in TGA analyses for PLS-2, PLS-6 and PLS-8

Sample	Total weight loss at temperature range of 210 ℃-280 ℃ (%)
PLS-2	23.11
PLS-6	26.73
PLS-8	25.33

4.5.3 Third system (PVA-$LiClO_4$-TiO_2 based polymer electrolyte)

Figure 4.32 illustrates the TGA thermographs of PLT-4, PLT-8 and PLT-10. PLT-4, PLT-8 and PLT-10 also show two stages of weight loss. First stage of the weight loss is attributed to the evaporation of free and bound water. This weight loss is due to the hygroscopic nature of $LiClO_4$.

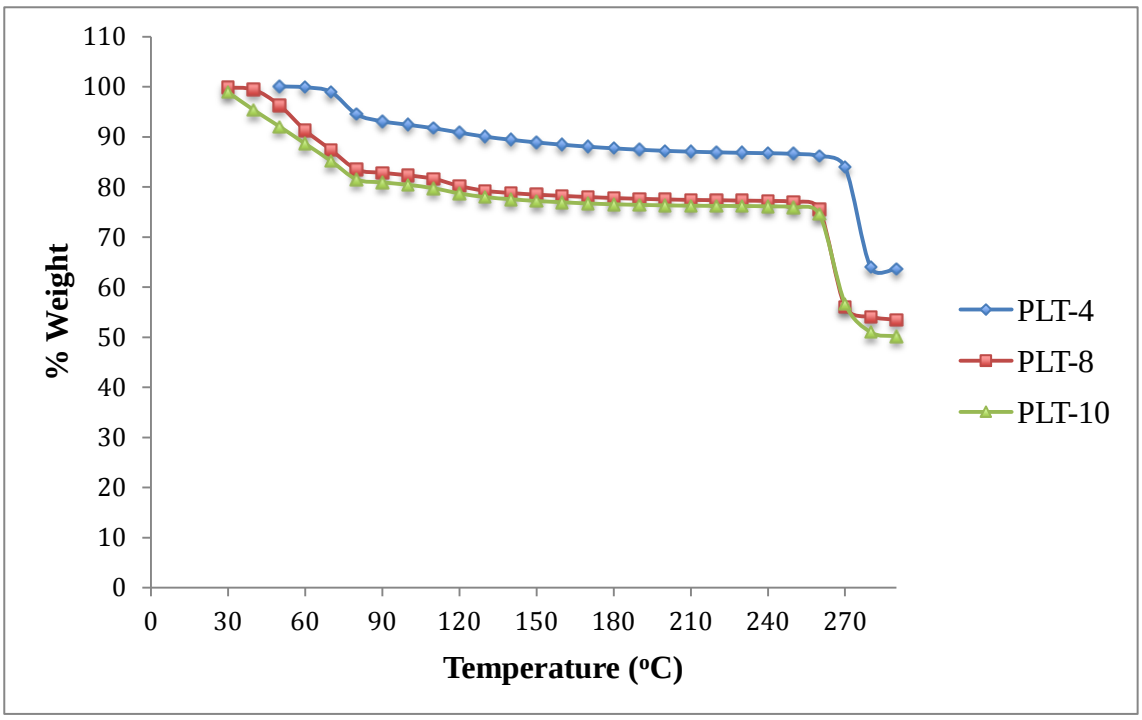

Figure 4.32: Thermogravimetric curves of PLT-4, PLT-8 and PLT-10

Figure 4.32 indicates that there is a second weight loss for PLT-4, PLT-8 and PLS-10 at the temperature range of 210 ℃ to 280 ℃. The onset decomposition temperature has shifted towards higher temperature upon the addition of TiO_2. The onset decomposition temperature of PLT-4, PLT-8 and PLT-10 is found in the temperature range of 255 ℃ to 265 ℃. The onset decomposition temperature increases extensively with the addition of TiO_2.

The total percentage of weight loss from 210 ℃ to 280 ℃ for PLT-4, PLT-8 and PLT-10 is presented in Table 4.9.Results show that the addition of TiO_2 into PVA-$LiClO_4$ system had reduced the percentage of weight loss. These polymer electrolytes with the doping of TiO_2 had become more thermally stable and more resistant to heat as compared to polymer electrolytes without filler.

Table 4.9: Total weight loss (%) at temperature range of 210 ℃ to 280 ℃ in TGA analyses for PLT-4, PLT-8 and PLT-10

Sample	Total weight lossat temperature range of 210 ℃ to 280 ℃ (%)
PLT-4	22.68
PLT-8	25.72
PLT-10	25.02

4.6 Summary

4.6.1 First system (PVA-$LiClO_4$based polymer electrolyte)

Three system of polymer electrolyte had been successfully synthesized by solution casting technique. From the first system, thin film containing 60 wt. % of PVA and 40 wt. % of $LiClO_4$, denoted as PL-4 exhibits the highest ionic conductivity value of $2.61 \cdot 10^{-5}$ S cm^{-1}. In temperature dependence ionic conductivity studies, thin films obey the Arrhenius rule as the regression values are close to unity and this indicates the hopping mechanism is favored. Beside, the ionic conductivity can be evaluated by dielectric studies due to dielectric constant is a measurement on the charge density. In this system, PL-4 shows highest dielectric constant compared to other samples and the dielectric behavior of the thin films disclose the electrode polarization effect and non-Debye properties.

XRD studies reveal the addition of $LiClO_4$ into polymer matrix had reduced the peak intensity of the relative diffraction peak at angles of $2\theta=19.8°$. The reduction in peak intensity had increased the amorphous characteristic of polymer matrix which favors the ionic conduction. In SEM studies, no phase separation is seen and it can be deduced that the complexation has occurred.

The T_g of polymer electrolytes were increased upon the addition of $LiClO_4$. This is owing to formation of transient crosslink of rotation as the number of lithium cations increased. By analyzing TGA thermograms, the second onset decomposition temperature had shifted to higher temperature upon the addition of $LiClO_4$. These results indicate that the prepared thin films possess a good thermal stability.

4.6.2 Second system (PVA-$LiClO_4$-Sb_2O_3 based polymer electrolyte)

After the analyses of first polymer electrolyte system, compatible ratio of PVA and $LiClO_4$ was used to further study. In second system, composite polymer electrolyte was prepared by solution casting technique with the inclusion of different wt. % of Sb_2O_3. Based on the analyses, PLS-6 had achieved the highest room temperature ionic conductivity value of 9.5×10^{-5} S cm^{-1}.

The filler in polymer matrix act as cross-linking center that can promote the dissociation of lithium aggregates into free ion species and eventually, more number of free lithium cation can contribute in ionic conduction as well as ionic conductivity. Temperature dependence ionic conductivity study of this system also shows that the composite polymer electrolytes obey Arrhenius rule, as there is no abrupt jump in the ionic conductivity value. The dielectric relaxation studies reveal that incorporation of Sb_2O_3 into the polymer electrolyte had increases the dielectric constant extensively and this can be ascribed to more number of ion species that contribute in electrode polarization. Beside, loss tangent studies also prove that the PLS-6 exhibits highest peak intensity compared to other sample in this system. A higher peak intensity of the

loss tangent peak will lead to higher number of free charge carrier to participate in the relaxation process.

XRD analyses divulge the measured crystallite size of polymer electrolyte at relative diffraction angle of $2\theta=19.8°$ decreases upon the addition of Sb_2O_3. PLS-6 had achieved the smallest crystallite size in this system which implies PLS-6 has the higher volume fraction of amorphous phase compared to other sample. In addition, investigation on surface morphology of composite polymer electrolyte had proven the grain size of particles become smaller upon the addition of Sb_2O_3.

DSC studies disclose the polymer electrolytes doped with Sb_2O_3 has significant effect on T_g value. PLS-6 exhibits the lowest T_g value and therefore, a flexible polymer backbone was formed that favors the ionic migration in the polymer matrix. Thermal studies reveal that the addition of Sb_2O_3 particles had reduced the total weight loss (%) at temperature range of 210 ℃-280 ℃.

4.6.3 Third system (PVA-$LiClO_4$-TiO_2 based polymer electrolyte)

In the third polymer electrolyte system, various wt. % of TiO_2 had introduced into PL-4 sample. PLT-8 (addition of 8 wt. % of TiO_2) has attained the maximum ionic conductivity value of $1.30 \cdot 10^{-4}$ S cm^{-1}. Further increment of the wt. % of TiO_2 (above 8 wt. %), shows a decline in ionic conductivity due to the TiO_2 particles having a 'blocking effect' on the conducting pathway which inhibit the ion migration. As mentioned in 4.1.3.2, the dielectric constant was increased greatly after addition of Sb_2O_3 and similar result was observed in this system. On the other hand, the ionic

conductivity of polymer electrolytes increases with increasing temperature and no phase transition is seen, as the regression values are almost unity.

From XRD analyses, the diffraction peak at angle of $2\theta=19.8°$ is shifted upon addition of TiO_2. This implies complexation had occurred between PVA, $LiClO_4$ and TiO_2. The peak intensity of diffraction peak at $2\theta=31.3°$ correspond to crystalline peak of $LiClO_4$ had reduced. Reduction in peak intensity reveals that there is more number of free cation in the matrix. Besides, the amorphous characteristic of polymer electrolyte was enhanced significantly. In this system, PLT-8 exhibits highest amorphous characteristic compared to other samples and therefore it possesses the highest ionic conductivity.

DSC studies disclose the PLT-8 has flexible polymer backbone compared to other samples as the PLT-8 shows the lowest T_g value. This implies that ionic migration in PLT-8 is more favourable compared with other samples. TGA studies had proven that the addition of TiO_2 into PL-4 had increased the thermal stability and more heat resistant as the second onset decomposition had shifted to higher temperature.

CHAPTER 5

Results and Discussion II

5.1 Comparison of PL-4 with PLS-6 on the performance of electric double layer capacitor (EDLC)

5.1.1 Linear sweep voltammetry (LSV) test

The electrochemical stability window of a given polymer electrolyte is generally determined by means of linear sweep voltammetry (Appetecchi et. al, 1997). In this section, the highest ionic conducting polymer electrolyte sample in first system and second system were used to investigate their electrochemical stability window. Before proceeding to EDLC fabrication, samples are required to be tested on operational potential for charge by LSV. An EDLC requires polymer electrolytes that possess a higher ionic conductivity and therefore, PL-4 and PLS-6 were used in fabrication of EDLC. Figures 5.1 and 5.2 depict the LSV curve for PL-4 and PLS-6, respectively. The onset of current in the anodic high-voltage range and cathodic low-voltage range are assumed to result from a decomposition process associated with the electrode (Salne, et. al., 1995). The stability window region for PL-4 is at -2.5 V to +2.5 V whereas the stability window for PLS-6 is at -2.8 V to +2.8 V. This is an indicative where no decomposition of any components in this potential range. There is a significant effect of Sb_2O_3 in polymer electrolyte on the electrochemical stability window. This is owing to high dielectric constant of Sb_2O_3 that will give a higher concentration of free charge carriers. Hence, a higher electrochemical stability window is obtained (Asmara *et. al.*, 2011).

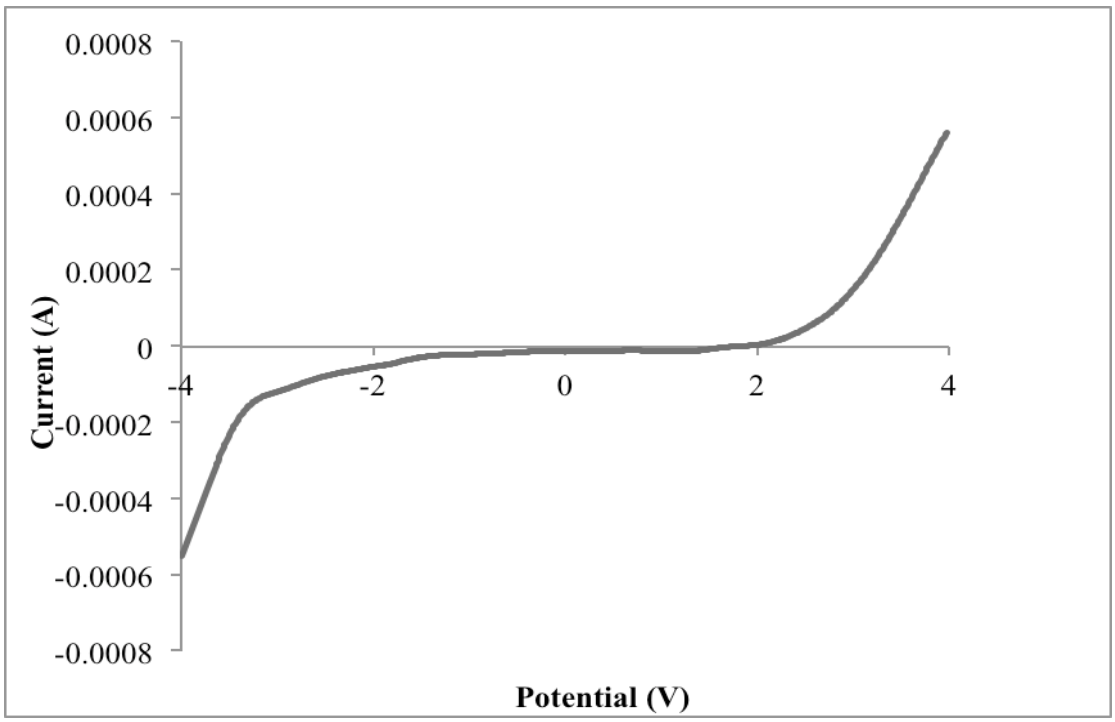

Figure 5.1: LSV curve for PL-4

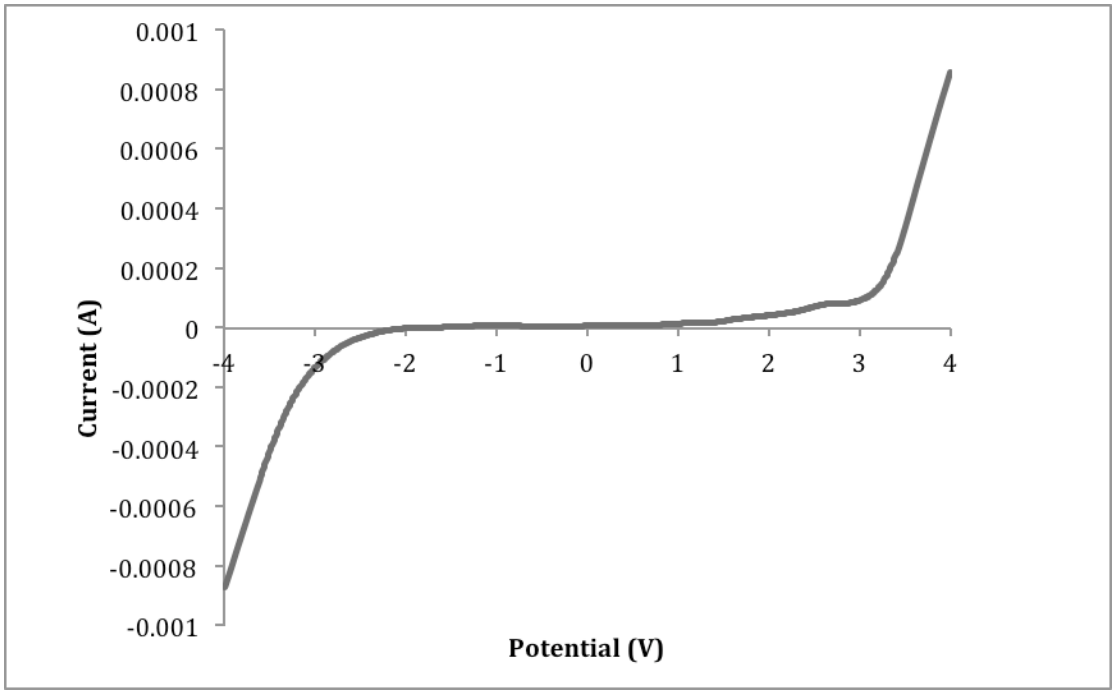

Figure 5.2: LSV curve for PLS-6

5.1.2 Cyclic voltammetry (CV) test

CV measurement was carried out to examine the capacitive behavior of electrode materials in electrochemical capacitors (Yin et. al, 2011). Figure 5.3 shows a cyclic voltammogram of PL-4 and PLS-6 taken with a potential window from 0 V to 1.0 V at a scan rate of 10 mV s^{-1}. At this sweep rate, both EDLC cells exhibit almost near rectangular shapes with slightly distorted and there is no evidence for any redox currents on both anodic and cathodic sweeps, demonstrating the typical behavior of an EDLC. In the overall performance, polymer electrolytes as separator are highly capacitive and electrochemically reversible.

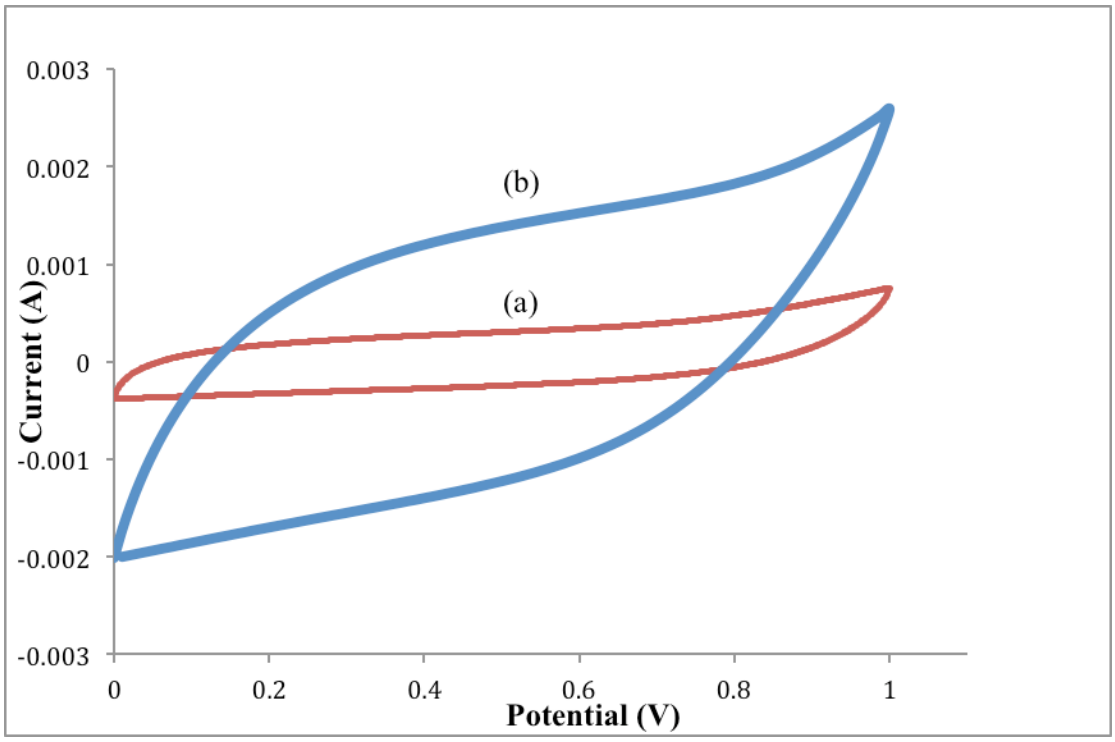

Figure 5.3: Cyclic voltammograms of (a) EDLC cell with PL-4 and (b) EDLC cell with PLS-6 at 10 mV s^{-1} scan rate.

The range of current density of EDLC cell fabricated with PLS-6 is higher than that of EDLC cell fabricated with PLS-0, which gives a higher specific

capacitance value. The specific capacitances, C_{spec} for EDLC assembled with PL-4 and PLS-6 were calculated from the CV profile using the equation:

$$C_{spec} = \frac{i}{vm} \qquad \text{(Equation 5.1)}$$

where i is the average current (A), v is the scan rate (V s^{-1}), and m is the mass of the electrode material. The calculated C_{spec} is 3.2 F g^{-1} and 13.0 F $g^{-1}$for PL-4 and PLS-6, respectively. As expected, EDLC cell with higher specific capacitance show larger rectangular shape of CV curves at constant current applied. The specific capacitance is higher in the EDLC assembled with polymer electrolyte containing Sb_2O_3. This is due to higher number of ion species to be adsorbed and desorbed in electric double layer of the EDLC. The Sb_2O_3 in the polymer system promotes the dissociation of lithium aggregates into free ions and acts as solid plasticizer. Incorporation of Sb_2O_3 will give higher number of charge carriers and an intimate contact between electrodes and electrolytes. Accordingly, the specific capacitance of the EDLC cell was enhanced.

Figure 5.4 shows the CV curves of EDLC assembled with PLS-6 at different scan rates of 10, 30, 50, 100 mV s^{-1}. As can be seen, the area of rectangular becomes larger when the scan rate increases. This implies that the voltammetric current is directly proportional to the scan rate. It can be seen that current response increases with increase in scan rate and in turn results in decrease in specific capacitance as shown in Figure 5.5. At low scan rate (10 mV s^{-1}), the ion species from PLS-6 can utilize all the vacant sites in the active electrode material, in view of the fact that the ions have enough time to diffuse into vacant site, which leads to the higher specific

capacitance. Moreover, at higher scan rate (100 mV s^{-1}), PLS-6 gave a poorer rectangular-shaped CV curve. This can be explained that the ion species from PLS-6 confront the difficulty to enter all the vacant sites in the active electrode. This is attributed to their partial rate of movement in the electrolyte (Meher *et. al.*, 2011). Consequently, specific capacitance decreases with increasing the scan rate.

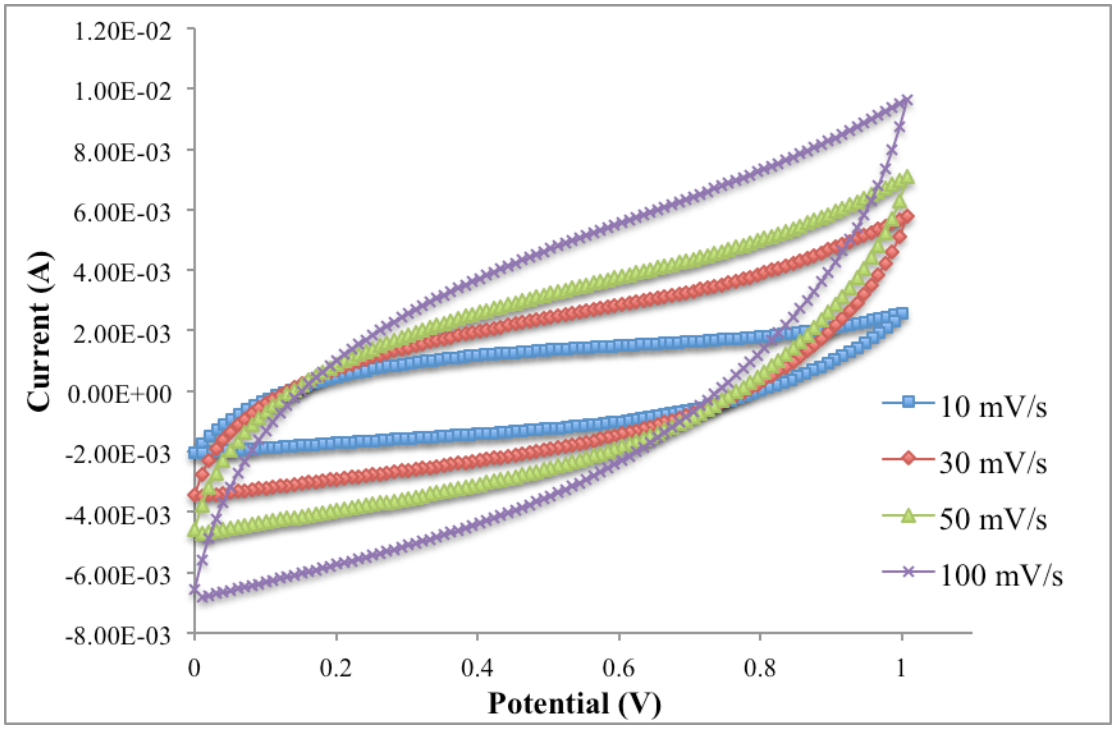

Figure 5.4: Cyclic voltammograms of EDLC cell with PLS-6 with various scan rate at 10 mV s^{-1}, 30 mV s^{-1}, 50 mV s^{-1} and 100 mV s^{-1}.

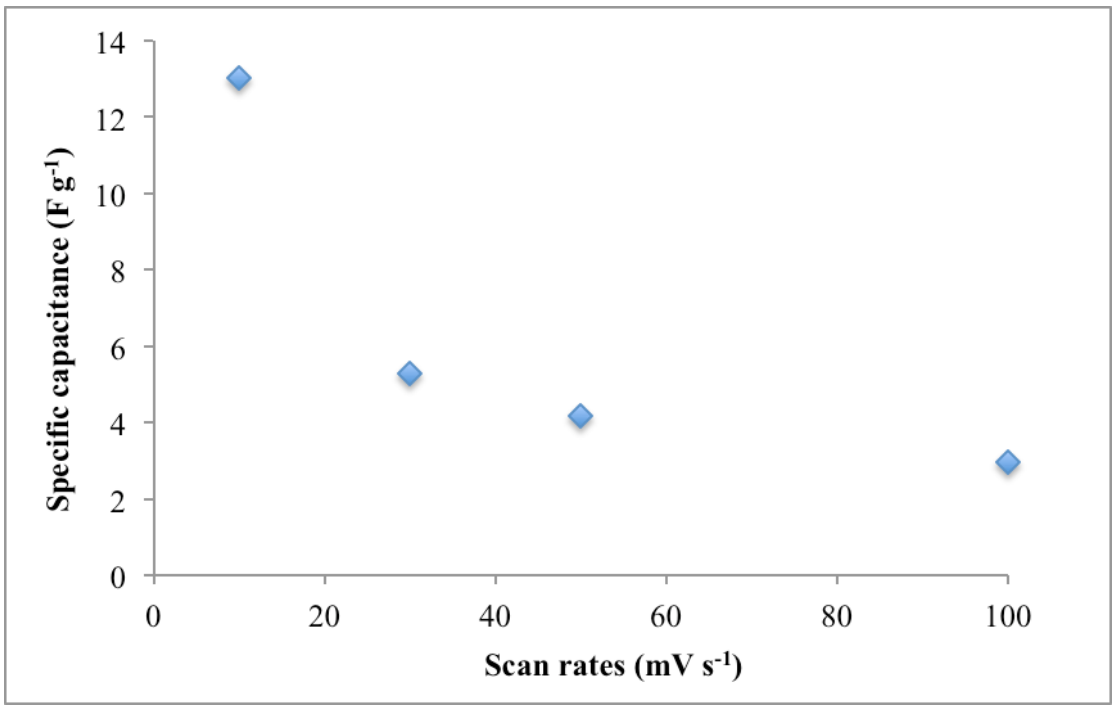

Figure 5.5: Variation of specific capacitance and scan rate for EDLC assembled with PLS-6.

5.1.3 Galvanostatic charge-discharge technique

The electrochemical storage behaviors of EDLCs were examined under constant-current charge discharge conditions. Basically, working voltage of an EDLC is largely dependent on the electrolyte breakdown voltage whereas internal resistance and capacitance rely on the electrode resistance and conductivity of electrolyte. Figure 5.6 depicts the charge discharge profile of EDLC assembled with PL-4 and PLS-6 at constant current of 1 mA. It is clearly observed that the discharging time of PLS-6 is longer than that for PL-4 because of the percentage of storage of ion species is higher in PLS-6. This result is supported by dielectric behavior studies that mentioned PLS-6 has higher charge density compared to PL-4.

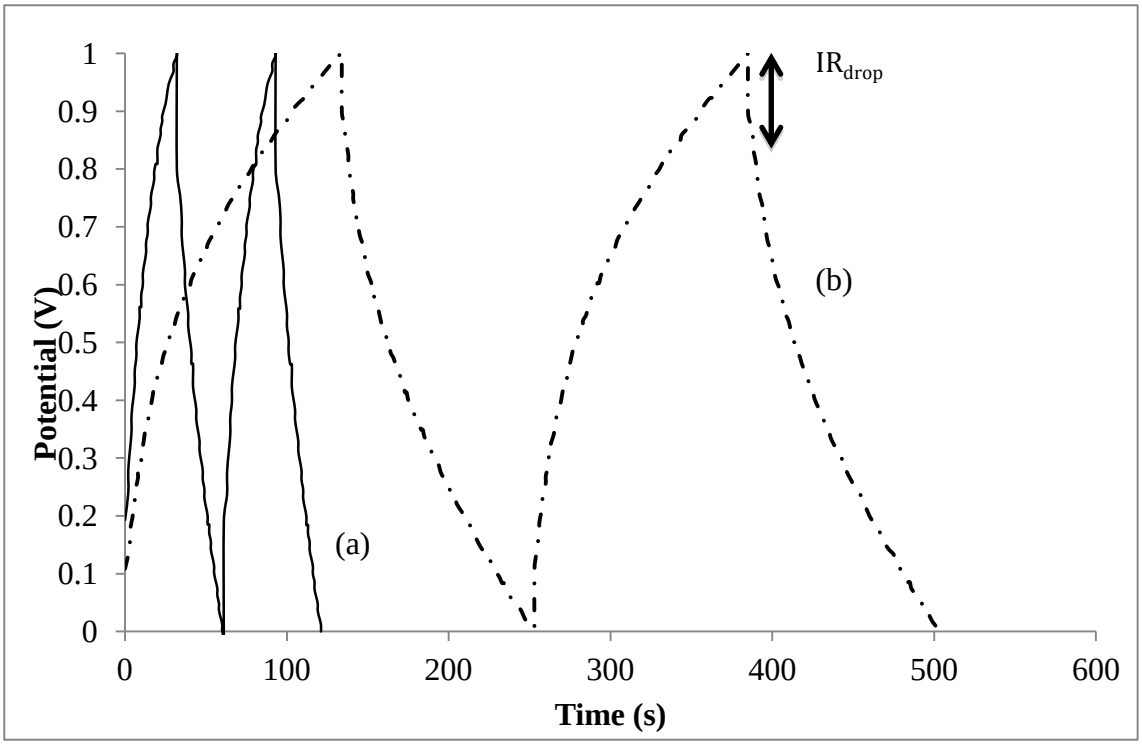

Figure 5.6: Charge-discharge pattern for (a) EDLC cell with PL-4 and (b) EDLC cell with PLS-6 at current of 1 mA.

From the charge discharge plot, an inner resistance (IR) drop of both EDLC cells was clearly spotted. The sudden jump and drop in potential during charging and discharging was ascribed to the resistance of electrolyte and the inner resistance of ion diffusion in carbon micropores. Equivalent series resistance (*ESR*) is related to ionic conductivity and this can be elucidated by concentration of ions from polymer electrolyte and electric conductivity from electrode. With the same electrode materials, the dissimilarity of *ESR* can be elucidated by the ionic conductivity of the polymer electrolytes. Lower value of ESR will exhibit higher ionic conductivity. ESR was determined by the following expression.

$$ESR = \frac{IR_{drop}}{i} \quad \text{(Equation 5.2)}$$

ESR value obtained for PL-4 and PLS-4 from the discharge profile is 199.3 Ω and 108.3 Ω, respectively. ESR value for PLS-6 had reduced compared to PL-4 and this is attributed to the incorporation of Sb_2O_3 into polymer matrix that will favors the salt dissociation leading to increment of number of free ions that can adsorbed on electric double layer of an EDLC. Lower value of *ESR* also ensures that the polymer electrolyte has an intimate contact with electrode that facilitates the transport of ions towards the pore entrance at electrode.

The specific capacitance, C_{spec} of the electrodes discharged at current of 1 mA was calculated by using the equation below:

$$C_{spec} = \frac{i \times \Delta t}{\Delta V \times m} \qquad \text{(Equation 5.3)}$$

Where i is the discharge current (A), Δt is the discharge time, ΔV is the voltage range and m is represent to mass of electrode material. The estimated C_{spec} value for EDLC with PL-4 and EDLC with PLS-6 are 3.0 and 14.5 F g^{-1}, respectively. The energy density (E) of each EDLC has been evaluated using the following expression:

$$E = \frac{1}{2} C_{spec} V^2 \text{(Equation 5.4)}$$

Where, C_{spec} is specific capacitance and V is the working voltage. The calculated energy density for PL-4 and PLS-6 is 0.36 Wh kg^{-1} and 2.01 Wh kg^{-1}. Power density was calculated by using the equation:

$$P = \frac{V^2}{4mESR} \quad \text{(Equation 5.5)}$$

Where *m* is the mass of single electrode and *ESR* is equivalent series resistance. The estimated power density for PL-4 and PLS-6 is 104.5 W kg^{-1} and 153.5 W kg^{-1}, respectively. From the data obtained, it can be concluded that, EDLC using PLS-6 (polymer electrolyte that incorporated with Sb_2O_3) gives a better performance compared to PL-4. Therefore, inorganic filler is a promising material to enhance the specific capacitance, energy density and power density of the EDLC.

For further understanding the electrochemical performances, long-term cycleability of the electrodes was also evaluated by repeating the charge/discharge test at a current of 1 mA up to 200 cycles. The specific capacitance retention ration, C_r was calculated using the following equation:

$$C_r(\%) = \frac{C_x}{C_0} \times 100 \quad \text{(Equation 5.6)}$$

Where C_x is discharge capacitance at each cycle and C_0 is discharge capacitance at the first cycle. Figure 5.7 depicts the specific capacitance retention ratio for PL-4 and PLS-6, respectively. It was observed that after both EDLC cells were charged and discharged throughout 200 cycles, the capacitance retention is about 90%. The results demonstrate that both EDLC cells maintain excellent electrochemical stability.

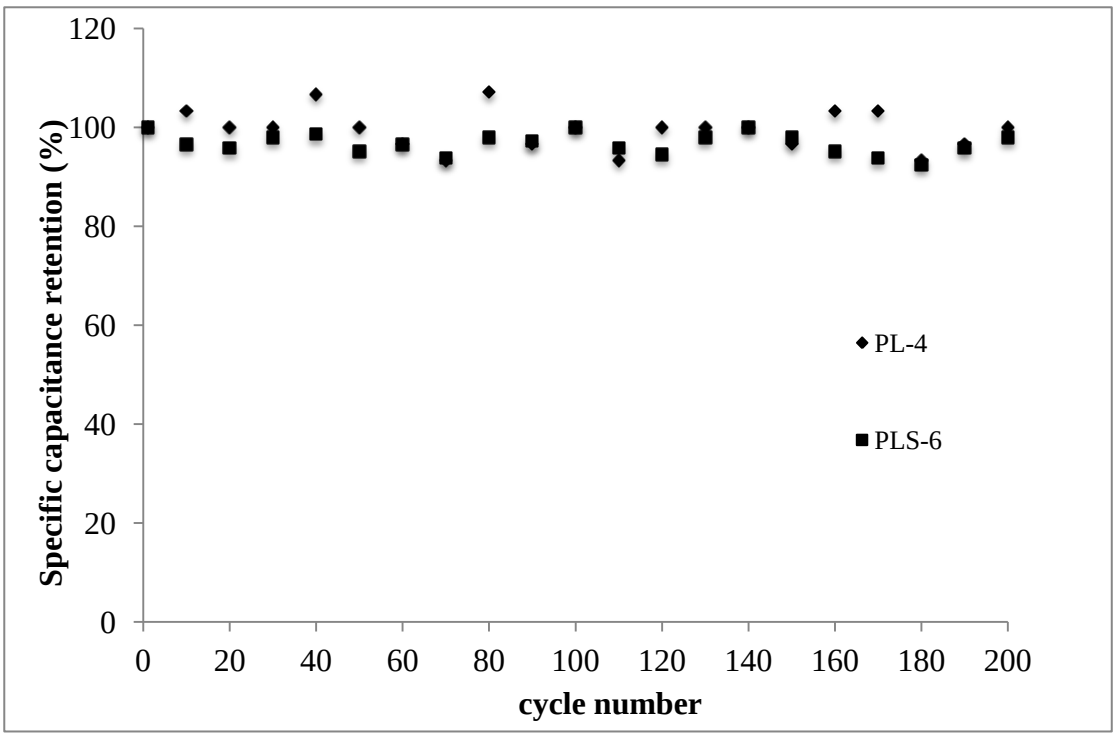

Figure 5.7: Specific capacitance retention versus cycle number for PL-4 and PLS-6 EDLC devices.

5.1.4 Impedance studies

The basis of impedance spectroscopy is to investigate the bulk and interfacial resistances of the real EDLC. Figure 5.8 shows impedance plot for the EDLC cell with PL-4 and EDLC cell with PLS-6. It is clearly shown that the typical EDLC impedance plots are observed for both samples in Figure 5.8. The observed spectra consist of a typical semicircle region at high frequency and thereafter a capacitive hike in the low frequency area. In the high frequency range, the semi-circle can be attributed to the double layer nature and charge transfer processes on the interface between the electrode and electrolyte, whereas in the low frequency range, the electrochemical process will be dominated by ion diffusion (Lee *et. al.*, 2005). Hence, the impedance plot pattern indicates the PL-4 and PLS-6 are applicable in EDLC.

As can be seen in Figure 5.8, an internal resistance (R_s) that intercept to the real axis (*x*-axis) is derived from the electroactive components and the electrical circuit of EDLC (Taberna *et. al.*, 2003) is found to be 43 Ω and 9 Ω for the EDLC cell with PL-4 and EDLC cell with PLS-6, respectively. This implies that the EDLC with PLS-6 have lower resistivity compared to EDLC with PL-4. Moreover, charge transfer resistance (R_{ct}) was determined from the diameter of semicircle of an impedance plot. Hence, the calculated R_{ct} values are 61.0 and 49.3 Ω for the EDLC cell with PL-4 and EDLC cell with PLS-6, respectively. Generally, a lower value of R_{ct} is acquired to be ideal double layer capacitive behavior. The smaller R_s value for EDLC with PLS-6 reflects an intimate contact of the PLS-6 with electrolyte that facilitates the transport of ions towards the pore entrance. This result suggests that the EDLC with PLS-6 exhibits lower ionic charge resistance compared to EDLC cell with PL-4 and this will favors fast ionic transportation. Eventually, the specific capacitance of the EDLC cells with PLS-6 increases. This can be explained in terms of flexibility of PLS-6 taking part in the penetration process into electrode from the mid to low frequency region (Arulepp *et. al.*, 2004).

The incorporation of Sb_2O_3 into polymer matrix will dissociate lithium aggregates into free charge carriers and increases the flexibility and amorphous phase of polymer chain as mentioned in previous studies. The introduction of the Sb_2O_3 into polymer electrolyte ensures the good contact between electrodes and electrolytes. Therefore more ions can penetrate into space-confined micropores. Consequently, this will cause higher output power from the EDLC with PLS-6 and C_{spec} increase (Tien *et. al.*, 2008).

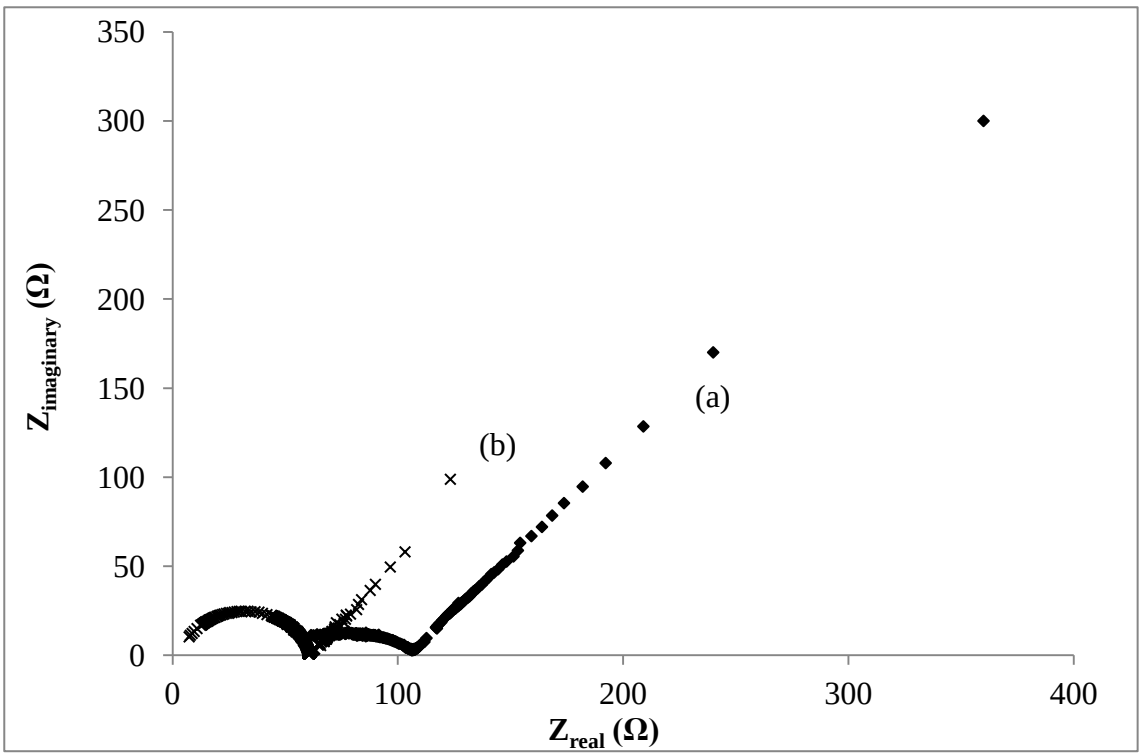

Figure 5.8: Typical impedance plot of (a) EDLC cell with PL-4 and (b) EDLC cell with PLS-6 at room temperature.

The specific capacitance-frequency dependence of EDLCs based on PL-4 and PLT-8 as the electrolyte is depicted in Figure 5.9. The C_{spec} for both EDLC cells is determined using the following equation:

$$C_{spec} = \frac{1}{2\pi f' Z_{imaginary}} \quad \text{(Equation 5.7)}$$

Where f is the applied frequency; $Z_{imaginary}$ is the imaginary part from impedance plot. The C_{spec} for EDLC with PL-4 and EDLC with PLS-6 are 2.9 F g^{-1} and 13.4 F g^{-1}, respectively. The results also show that the EDLC with PLS-6 has higher C_{spec} compared to EDLC with PL-4. Generally, the C_{spec} values of both EDLC cells measured by EIS are lower than that measured by CV and galvanostatic charge-discharge due to the fact that alternating current penetrates into the electrode bulk with more hindrance (Xing et. al., 2004).

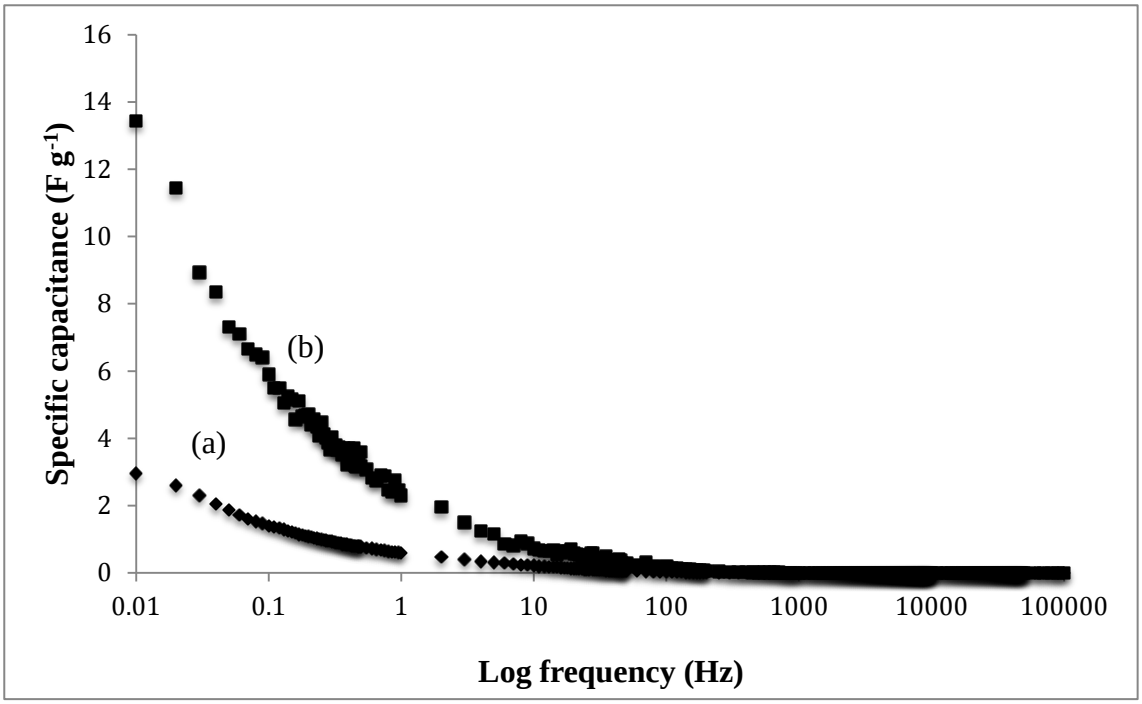

Figure 5.9: Specific capacitance versus frequency dependence of (a) EDLC with PL-4 and (b) EDLC cell with PLS-6.

5.2 Comparison of PL-4 with PLT-8 on the performance of EDLC

5.2.1 LSV test

In this section, the highest ionic conducting polymer electrolyte in third system PLT-8 was used to investigate the electrochemical stability window. Figure 5.10 depicts the LSV curve for PLT-8. The onset of current in the anodic high-voltage range and cathodic low-voltage range are assumed to result from a decomposition process associated with the electrode (Salne *et. al.*, 1995).The stability window region for PLT-8is at -2.9 V to +2.9 V. The result shows that PLT-8 does not undergo any chemical transformation within the potential region. Besides, in previous study, the electrochemical stability window for PL-4 is at -2.5 V to +2.5 V. Incorporation of TiO_2 into polymer electrolyte enlarges the operational potential to a larger region.

This is owing to high dielectric constant of TiO_2 that will give a high concentration of free charge carriers. Hence, a higher electrochemical stability window is obtained (Asmara *et. al.*, 2011).

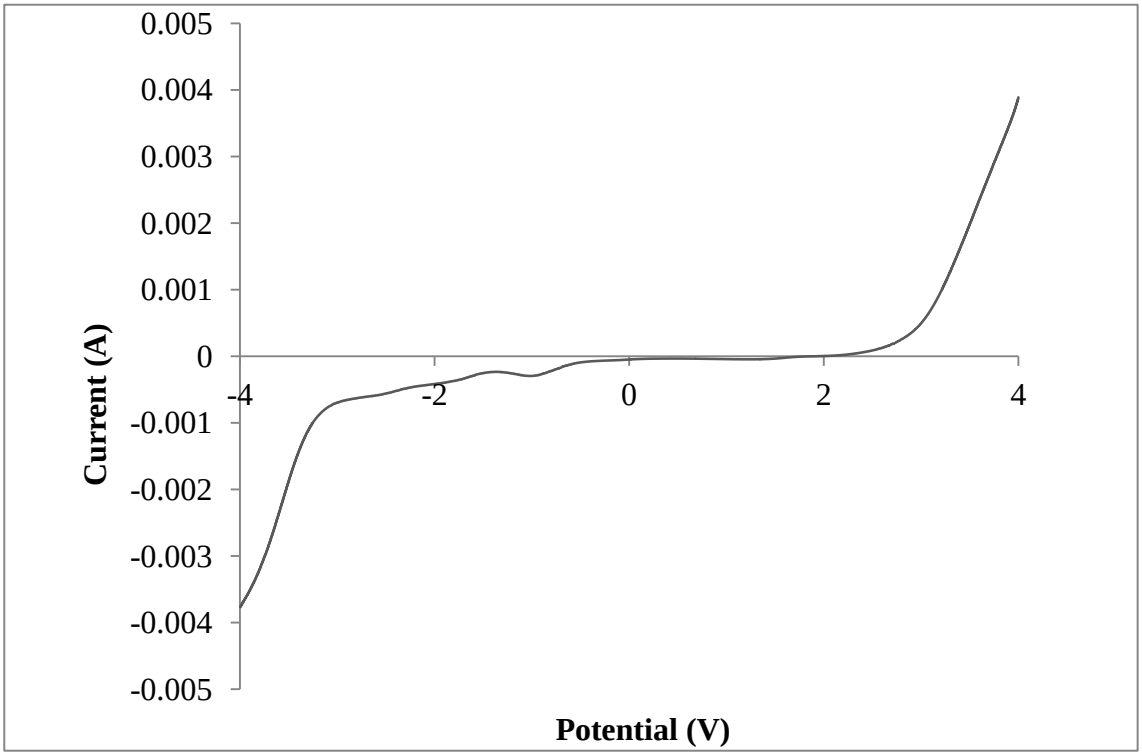

Figure 5.10: LSV curve for PLT-8

5.2.2 CV test

Cyclic voltammograms of PL-4 and PLT-8 are presented in Figure 5.11. The scanning was carried out in the voltage range between 0 to 1 V at 10 mV s^{-1} scan rate. The CV profiles of two EDLC cells were nearly rectangular shape, and there is no distinct peaks observed over the scanned potential region in both cells, which is attributable to electron-transfer processes or redox reactions. The excellent CV shape reveals a very rapid current response on voltage reversal at each end potential, and the straight rectangular sides represent a very small equivalent series resistance (ESR) of

the electrodes and also the fast diffusion of electrolyte in the films. This explains that charge and discharge occur reversibly at the electrode|electrolyte interface. This also suggests the capacitive behavior of a capacitor in both cells with a double layer formation at the interfaces. C_{spec} EDLC cell with PLT-8 as electrolyte is 10.9 F g^{-1}. The EDLC cell with PLT-8 exhibits higher specific capacitance compared to PL-4. This implies addition of TiO_2 into polymer system will increase capacitance value of EDLC.

Figure 5.12 indicates the voltammogram of EDLC cell for PLT-8 at various scan rates. It implies that the response current had increased as the scan rate increases. As can be seen, the area of rectangular becomes larger when the scan rate increases. This implies that the voltammetric current is directly proportional to the scan rate. Consequently, specific capacitance decreases with increasing the scan rate. The slight deviation from the classical rectangular shape of the CV curves is observed at higher scan rates, which is expected for a pure capacitor. The deviation also due to the finite value of the ESR in polymer electrolyte based EDLC cell (Pandey *et. al.*, 2011). As the scan rate increases, loss of energy increases and the stored charge on the electrode surface decreases leading to decrement in specific capacitance (Osaka *et. al.*, 1998).

It can be seen that current response increases with increase in scan rate and in turn results in decrease in specific capacitance as shown in Figure 5.13. At low scan rate (10 mV s^{-1}), the ion species from PLT-8 can utilize all the vacant sites in the active electrode material and therefore, ion species have high tendency to diffuse into vacant site, which leads to the higher specific capacitance. Nevertheless, at higher

scan rate (100 mV s^{-1}), PLT-8 gave a poorer rectangular-shaped CV curve. This elucidates that, it is difficult for the ion species from PLT-8 to enter all the vacant sites in the active electrode which is attributed to their partial rate of movement in the electrolyte.

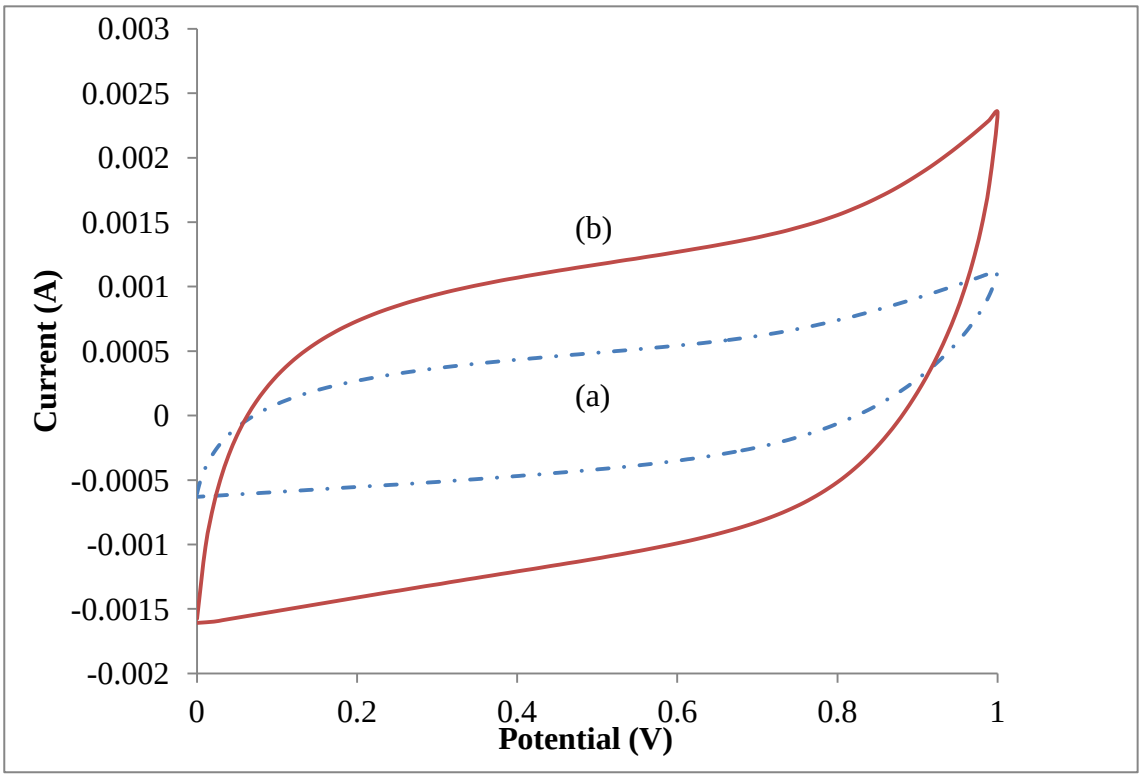

Figure 5.11: Cyclic voltammograms of (a) EDLC cell with PL-4 and (b) EDLC cell with PLT-8at 10 mV s^{-1} scan rate.

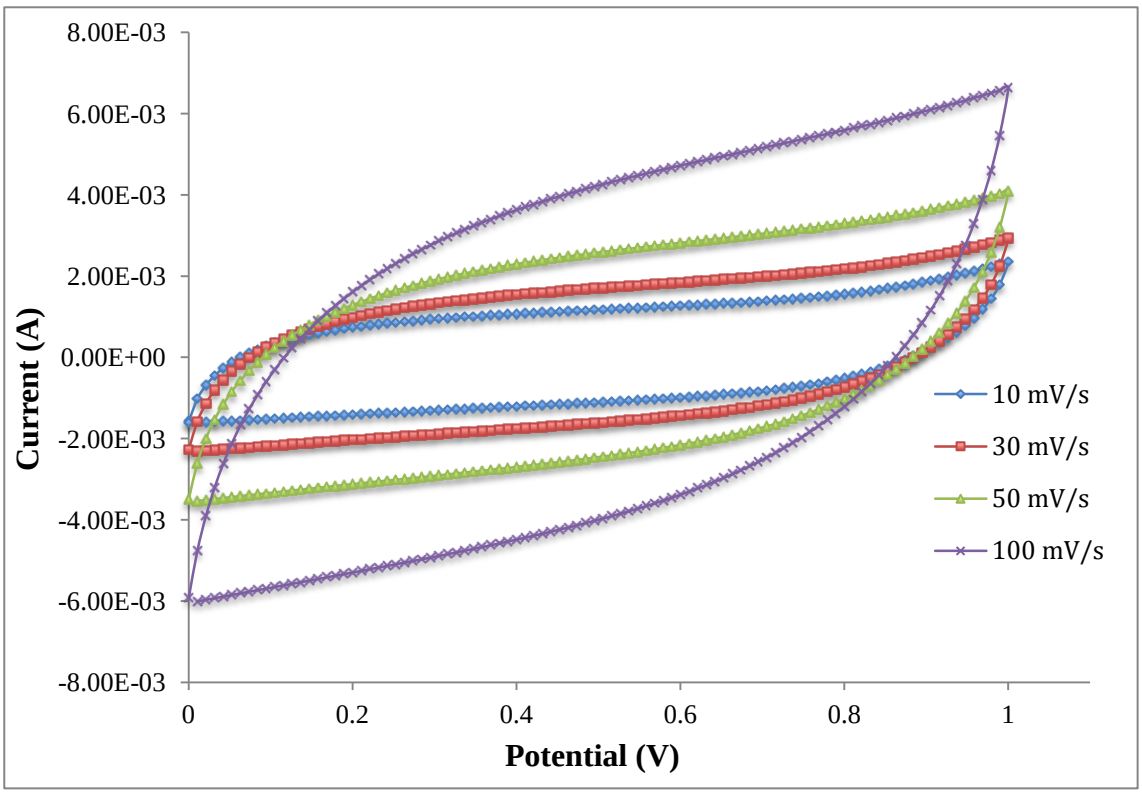

Figure 5.12: Cyclic votammograms of EDLC cell with PLT-8 with various scan rate at 10 mV s^{-1}, 30 mV s^{-1}, 50 mV s^{-1} and 100 mV s^{-1}

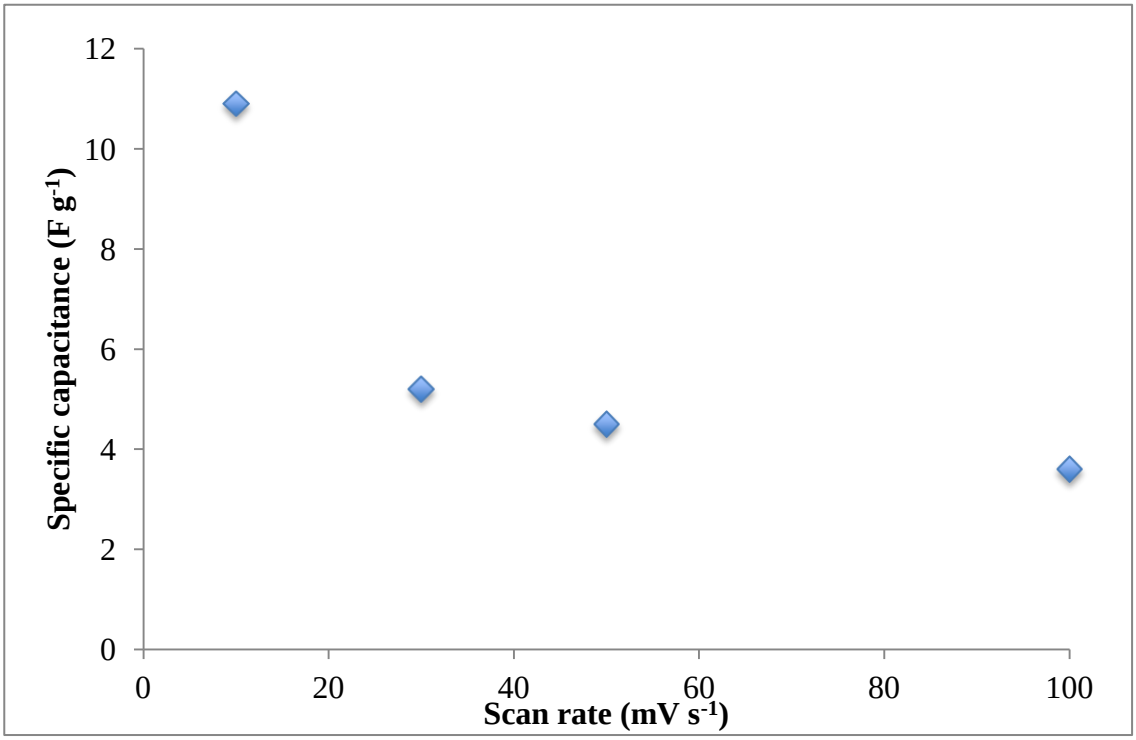

Figure 5.13: Variation of specific capacitance and scan rate for EDLC assembles with PLT-8.

5.2.3 Galvanostatic charge discharge technique

Figure 5.14 depicts the charge discharge curves for EDLC cell with PLT-8 at current of 1 mA. It shows standard capacitors behavior for the EDLC assembled with PLT-8. The time required for charge or discharge for the PLT-8 was nearly identical at low current density which reflects similar ultimate charge-storage capacities. From Figure 5.14, the initial sudden drop in the potential when discharging is ascribed to internal resistance, equivalent circuit resistance (ESR) in electrode and electrolyte and represents the resistive behavior of EDLC. The calculated ESR for EDLC cell with PLT-8 is 62.9 Ω. Lower ESR is owing to the addition of TiO_2 that promotes the salt dissociation and eventually, it increases the number of free ion species that can adsorbed on electric double layer of an EDLC. Lower value of *ESR* also ensures that the polymer electrolyte has good contact with electrode that facilitates the transport of ions towards the pore entrance at electrode. The estimated C_{spec} value for EDLC with PLT-8 is 12.5 F g^{-1}.

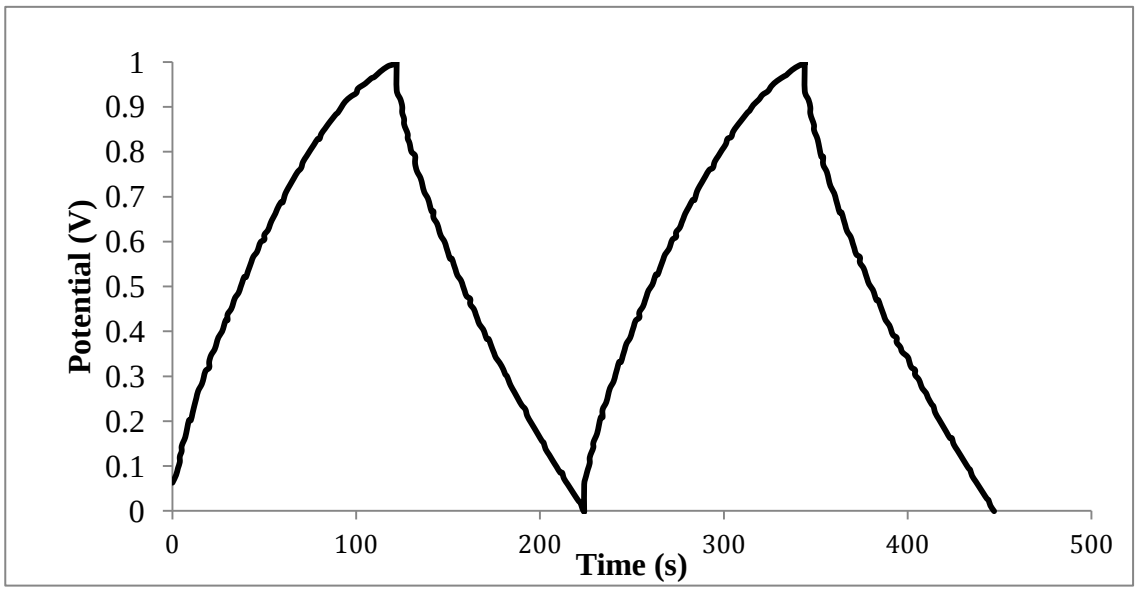

Figure 5.14: Charge-discharge pattern for EDLC cell with PLT-8 at current of 1 mA.

The calculated energy density for EDLC with PLT-8 is 1.56 Wh kg^{-1} whereas the power density for EDLC with PLT-8 is 198.7 W kg^{-1}. Results show that EDLC with PLT-8 exhibits lower ESR, higher specific capacitance and higher energy and power density compared to EDLC cell with PL-4. This implies addition of TiO_2 into polymer electrolyte enhanced the performance of EDLC cell.

The cycle stability test of EDLCs is an important parameter to evaluate the reliability of EDLC. The specific capacitance retention ratio as a function of cycle number for EDLC with PLT-8 is depicted in Figure 5.15. EDLC assembled with PLT-8 exhibits specific capacitance retention with approximately ~90% up to 200 cycles. This infered the electrode and electrolyte has intimate contact with each other. The specific capacitance retention for EDLC cell with PLT-8 is over 90 % throughout the 200 cycles. These results deduced that EDLC assembled with PLT-8 are capable to be very stable throughout the 200 cycles.

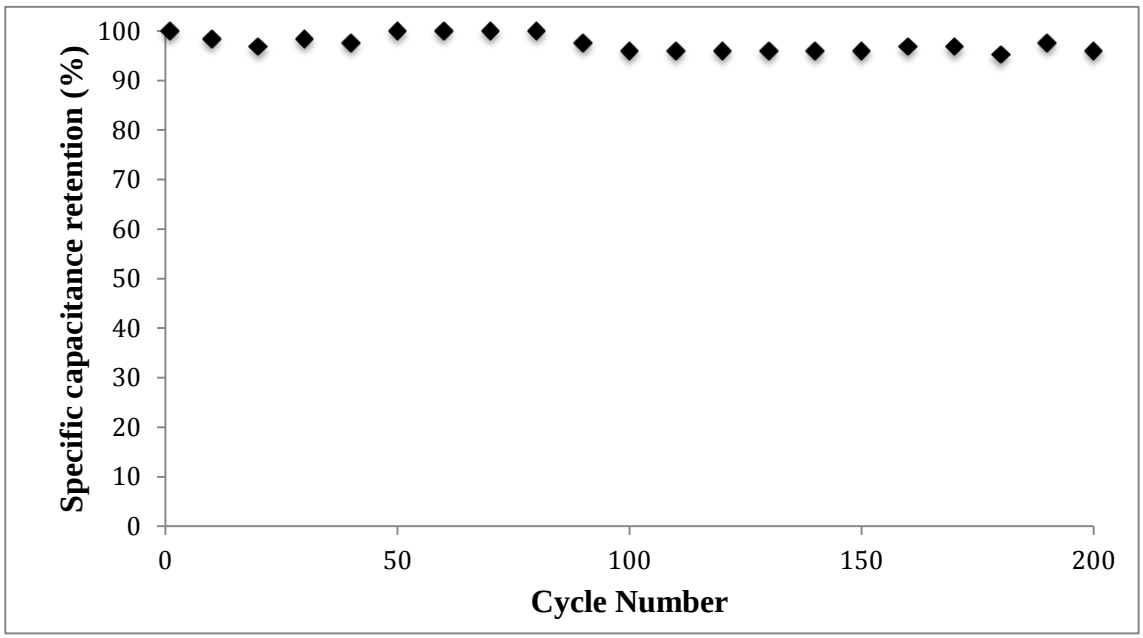

Figure 5.15: Specific capacitance retention versus cycle number for PLT-8 EDLC device.

5.2.4 Impedance studies

Figure 5.16 shows the typical EDLC impedance plot for EDLC assembled with PLT-8. The observed plot consist of a typical semicircle region at high frequency and thereafter a capacitive hike in the low frequency area. In the high frequency range, the semi-circle can be ascribed to the double layer nature and charge transfer processes on the interface between the electrode and electrolyte, whereas in the low frequency range, the electrochemical process will be dominated by ion diffusion. Hence, the impedance plot pattern indicates PLT-8is applicable to EDLC. As can be seen in Figure 5.16, an internal resistance (R_s) that intercept to the real axis (x-axis) is derived from the electroactive components and the electrical circuit of EDLC, is found to be 22 Ω for the EDLC cell with PLT-8. This implies that the EDLC with PLT-8 have lower resistivity compared to EDLC with PL-4. Moreover, charge transfer resistance (R_{ct}) was determined from the diameter of semicircle of an impedance plot. Hence, the calculated R_{ct} value is 10 Ω for the EDLC cell with PLT-8. Predominantly, a lower value of R_{ct} is required to be ideal double layer capacitive behavior.

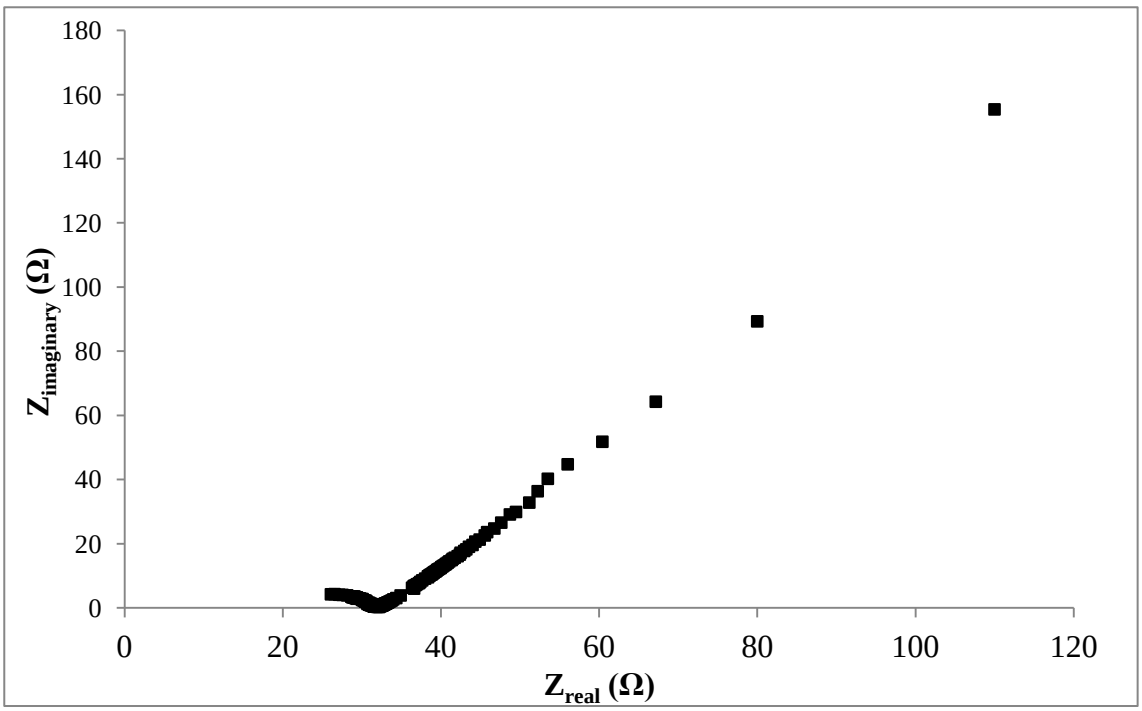

Figure 5.16: Typical impedance plot of EDLC cell with PLT-8 at room temperature.

As mentioned in section 5.1.4, smaller R_s value obtained from impedance plot reflects an intimate contact of the polymer electrolyte with electrodes will facilitates the transport of ions towards the pore entrance. Thus, results indicate EDLC cell with PLT-8 exhibits lower ionic charge resistance compared to EDLC cell with PL-4 and eventually, this favors fast ionic transportation. The phenomenon can be explained in terms of flexibility of PLT-8 taking part in the penetration process into electrode from the mid to low frequency region. Addition of TiO_2 into polymer matrix will dissociate lithium aggregates into free charge carriers and increase the flexibility and amorphous phase of polymer chain as mentioned in previous studies. The introduction of the TiO_2 into polymer electrolyte ensures the good contact between electrodes and electrolytes. Therefore, more ion species able to penetrate into space-confined

micropores. This will cause higher output power from the EDLC with PLT-8 and the C_{spec} increased.

The specific capacitance-frequency dependence of EDLCs based on PLT-8 as the electrolyte is depicted in Figure 5.17. The C_{spec} for EDLC with PLT-8 is 10.2 F g^{-1}. This result also shows that the EDLC with PLT-8 has higher C_{spec} compared to EDLC with PL-4. Again, the C_{spec} of EDLC assembled with PLT-8 measured by EIS was expected to be lower compared to CV and galvanostatic charge-discharge. This is owing to the fact that alternating current penetrates into the electrode bulk with more hindrance.

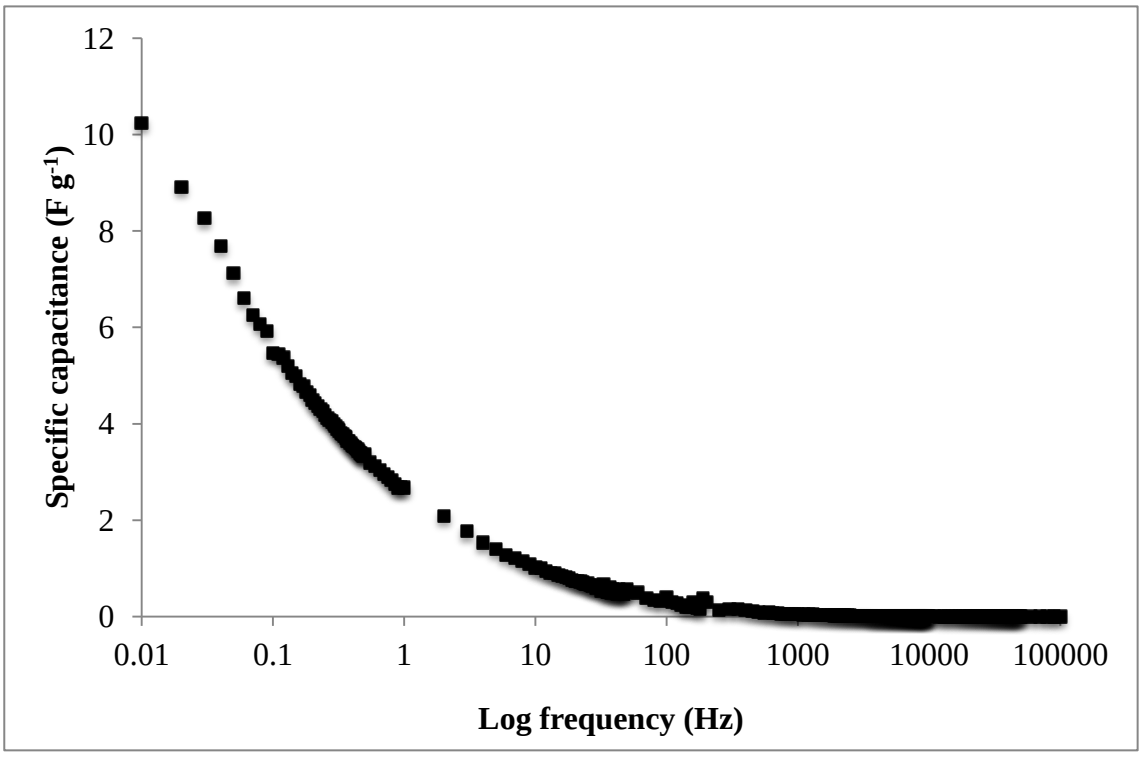

Figure 5.17: Specific capacitance versus frequency dependence of EDLC cell with PLT-8.

5.3 Summary

In this chapter, three polymer electrolyte systems had been applied on electrochemical device which is EDLC. It was found that, PL-4, PLS-6 and PLT-8 are potential candidates to be utilized as electrolytes in EDLC devices due to its high ionic conductivity. Before, the polymer films were fabricated with two electrodes; the samples were subjected to LSV test and examine the maximum operational potential during the charge-discharge. It was found that PLS-6 and PLT-8 have a bigger range in potential region compared to PL-4. This implies the addition of inorganic filler gives a remarkable outcome on the stability window analysis. CV test on EDLC devices using PL-4, PLS-6 and PLT-8 exhibit nearly rectangular shapes and there is no evidence for any redox currents on both anodic and cathodic sweeps, demonstrating the typical behavior of an EDLC.

In section 5.1, the C_{spec} for EDLC assembled with PL-4 using CV test, charge-discharge technique and impedance spectroscopy were in the range of 2.9 F g^{-1} to 3.2 F g^{-1}. Whereas the C_{spec} for EDLC assembled with PLS-6 were in the range of 13.0 F g^{-1} to 14.5 F g^{-1}. From the results obtained, it can be deduced that addition of inorganic filler into PL-4 shows a significant effect on the performance of EDLC. The increment of C_{spec} is mainly due to the increase in number of ion species that contained in polymer electrolyte. As the number of ion species being increases, more ion species able to adsorbed and desorbed in electric double layer of the EDLC. From the DSC studies, the flexibility of polymer backbone is an important parameter that alters the ion species to migrate from polymer matrix towards the electric double layer. Based on the DSC studies, PLS-6 possesses flexible polymer backbone as the

T_g value is decreases after the addition of Sb_2O_3. Therefore, ion species in PLS-6 can easily migrate towards the electric double layer. A flexible polymer backbone also provides an intimate contact between the thin films and electrodes which able to minimize the internal resistance of EDLC and this is proven in impedance analysis. On the other hand, power density and energy density calculated using charge-discharge technique also reveal EDLC with PLS-6 give a better performance compared to EDLC with PL-4.

In section 5.2, C_{spec} for EDLC assembled with PLT-8 using similar techniques as mentioned above is in the range of 10.2 F g^{-1} to 12.5 F g^{-1}. The results obtained are obviously gives better performance compared to EDLC with PL-4. TiO_2 particles can promote the dissociation of lithium aggregate to free charge carrier and enhance the power density and energy density of EDLC as well. Besides, the flexibility of polymer backbone is increased upon the addition of TiO_2. A flexible polymer backbone ensures intimate contact between thin films and electrodes, favors the ion migration and reduces the internal resistance of EDLC. As a result, the composite polymer electrolyte as separator in EDLC is a promising candidate to be used in electrochemical devices.

Chapter 6

Conclusion

In the recent century, green technology was implemented in order to lessen the environmental impact, as some of the synthetic polymers will release toxic component that is harmful on human health. Hence, PVA is choosen owing to its biodegradable nature. PVA-$LiClO_4$ based polymer electrolytes doped with Sb_2O_3 and TiO_2 were successfully prepared by solution casting technique.

PL-4 exhibits the highest ionic conductivity with a value of $2.61 \cdot 10^{-5}$ S cm^{-1} at room temperature for the first system. Maximum ionic conductivity of $9.51 \cdot 10^{-5}$ S cm^{-1} was obtained at room temperature with the addition of 6 wt. % of Sb_2O_3 (denoted as PLS-6). At dispersion of 8 wt. % of TiO_2 (denoted as PLT-8) the highest ionic conductivity value of $1.30 \cdot 10^{-4}$ S cm^{-1} was achieved. The ionic conductivity of composite polymer electrolyte obtained in the range of ~10^{-3} to ~10^{-4} S cm^{-1} had reach the satisfaction level for industry standard and able to applied on various type of electrochemical devices.

Based on the temperature dependence ionic conductivity studies, the linear relationship between log ionic conductivity and reciprocal temperature suggests that PVA based polymer electrolytes obey the Arrhenius rule. The dielectric relaxation studies had assisted to understand more on the ion mechanism of these polymer electrolyte samples. The dielectric studies also reveal the polymer electrolyte samples show Non-Debye properties.

XRD analyses have confirmed the complexation between the PVA, $LiClO_4$ and inorganic fillers. In addition, XRD studies reveal that structural modification has occurred in the all prepared polymer electrolyte systems by investigating the shifting of peak and changes of peak intensity at relative diffraction peak. The higher degree of amorphous is further verified by crystallite size at the relative diffraction peak. Surface morphology of polymer electrolytes reveal no phase separation was seen and complexation was ensured. On other hand, SEM images indicate the formation of voids and size of voids increases after inorganic filler was added which favors the ion migration.

The glass transition temperature, T_g is found to decreased upon the addition of Sb_2O_3 and TiO_2. This inferred that the polymer electrolyte doped with inorganic filler possesses a flexible backbone which favors the ion transportation. TGA studies also disclose the thermal stability of polymer electrolyte increases extensively after TiO_2 and Sb_2O_3 were incorporated. The second onset decomposition temperature had shifted to higher temperature which implies the polymer electrolytes added with inorganic filler are heat resistant. The TGA results also show that the total weight loss at the temperature range of 210 ℃-280 ℃ had decreased upon the addition of inorganic filler.

From the results obtained, PLT-8 exhibits higher ionic conductivity value compared to PLS-6. This is mainly due to the bigger size of voids that can be seen in SEM image. Eventually, more ion species can transport easily in the polymer matrix and therefore, PLT-8 indicates highest ionic conductivity value.

Electrical double layer capacitors (EDLCs) were fabricated by using PVA based polymer electrolytes. CV test, impedance analysis and charge-discharge testing divulge, the EDLC assembled with PLS-6 and PLT-8 indicates a better performance compared to EDLC assembled with PL-4. Besides, the assembled EDLC devices exhibit specific capacitance retention with approximately ~90% up to 200 cycles. These results deduce that EDLC assembled with PL-4, PLS-6 and PLT-8 are stable throughout the 200 cycles. Therefore, PVA based polymer electrolytes are promising candidates to be utilized as separators and electrolytes in EDLC.

The improvement can also be done by incorporating plasticizer such as ethylene carbonate (EC), propylene carbonte (PC), mixed salt, polymer blending and addition of ionic liquid. These materials can increase the ionic conductivity of the polymer electrolyte by increasing the amorphous region in the polymer matrix and enhance the flexbility of the polymer segments. This hence improves the performance of EDLC cells. In future work, composite polymer electrolyte also can be utilized on various type of electrochemical devices such as lithium batteries and solar owing to excellent electrical properties as it possesses a high ionic conductivity values which is suitable in electrochemical devices.

LIST OF REFERENCES

Abraham, K. M. and Alamgir, M. (1994). Room temperature polymer electrolytes and batteries based on them. *Solid State Ionics*, 70-71 (1), 20-26.

Ahmad, S., Saxena, T. K., Ahmad, S. and Agnihotry, S. A. (2006b).The effect of fumed silica on ion conduction and rheology in nanocomposite polymeric electrolytes.*Polymer*, 47, 3583-3590.

Allamgir, M. and Abraham, K. M. (1993). Li ion conductive electrolytes based on poly (vinyl chloride).*Electrochemical Society*, 140, 451 – 455.

Appetecchi G. B., Alessandrini, F., Carewska, M. Caruso, T., Prosini, P. P., Scaccia, S. and Passerini, S. (2001). Investigation on lithium-polymer electrolyte batteries.*Journal of Power Sources*, 97-98, 790-794.

Appetecchi, G. B., Croce, F. and Scrosati, B. (1997). High-performance electrolyte membranes for plastic lithium batteries.*Journal of Power Sources,* 66, 77-82.

Assender, H. E. and Windle, A. H. (1998b). Crystallinity in poly (vinyl alcohol: 2. Computer modelling of crystal structure over a range of tacticities.*Polymer*, 39, 4303-4312.

Armand, M. B. (1987).Polymer electrolytes Reviw-I. (Eds.) MacCallum, J. R. and Vincent C. A. Elsevier, London.

Armand, M. B., Chabagno, J. M. and Duclot, M. J. (1979). Preparation of a microporous polymer electrolyte based on poly (vinyl chloride)/poly (acrylonitrile-butyl acrylate) blend for Li-ion batteries. *Electrochimica Acta*, 52, 3199-3206.

Arulepp, M., Permann, L., Leis, J., Perkson, A., Rumma, K., Janes, A. and Lust, E. (2004).Influence of the solvent properties on the characteristics of a double layer capacitor.*Journal of Power Sources*, 133,320-328.

Asmara, S. N., Kufian, M. Z., Majid, S. R. and Arof, A. K. (2011). Preparation and characterization of magnesium ion gel polymer electrolytes for application in electrical double layer capacitors.*Electrochimica Acta*, 57, 91-97.

Awadhia, A., Patel, S. K. and Agrawal, S. L. (2006). Dielectric investigations in PVA based gel electrolytes. *Progress in Crystal Growth and Characterization of Materials*, 52, 61-68.

Azizi Samir, M. A. S., Alloin, F., Sanchez, J. Y., Gorecki, W. and Dufresne, A. (2004). Nanocomposite polymer electrolytes based on poly(oxyethylene and cellulose nanocrystals. *Journal of Physical Chemistry B*, 108, 10845-10852.

Barsoukov E. and Macdonald J. R. (2005). *Impedance spectroscopy: theory, experiment and applications*. (pp 2 – 4). Wiley, Interscience, Hoboken, NJ

Basak, P. and Manorama S. V. (2004). PEO-PU/PAN semi-interpenetrating polymer networks for SPEs: influence of physical properties on the electrical characteristics. *Solid State Ionics*, 167, 113-121.

Benavente, E., Santa Ana, M. A., Mendizabal, F. and Gonzalez, G. (2002) Intercalation chemistry of molybdenum disulfide.*Coordination Chemistry Reviews*. 224, 87-109.

Berthier, C., Gorecki, W., Minier, M., Armand, M. B., Chabagno, J. M. and Rigand, P. (1983). Microscopic investigation of ionic conductivity in alkali metal salts-poly (ethylene oxide) adducts. *Solid State Ionics* 11, 91-95.

Best, A. S., Ferry, A., MacFarlane, D. R. and Forsyth, M. (1999).Conductivity in amorphous polyether nanocomposite materials, *Solid State Ionics*, 126, 269-276.

Braun, D., Cherdron, H., Rehahn, M., Ritter, H. and Voit, B. (2005a). Introduction. *Polymer synthesis: Theory and Practice.* (pp. 1-37) Berlin: Springer.

Chandrasekaran, R., Soneda, Y., Yamashita, J., Kodama, M. and Hatori, H. (2008). Preparation and electrochemical performance of activated carbon thin films with polyethylene oxide-salt addition for electrochemical capacitor applications. *Journal of Solid State Electrochemistry*, 12, 1349-1355.

Chu, P. P. and Reddy, M. J. (2003). Sm_2O_3 composite PEO solid polymer electrolyte.*Journal of Power Sources*, 115, 288-294.

Chu, P. P., Reddy, M. J. and Kao, H. M. (2003). Novel composite polymer electrolyte comprising mesoporous structured SiO_2 and PEO/Li. *Solid State Ionics*, 156, 141-153.

Capiglia, C., Yang, J., Imanishi, N., Hirano, A., Takeda, Y. and Yamamoto, O. (2002). Composite polymer electrolyte: the role of filler grain size. *Solid State Ionics*, 154-155, 7-14.

Feuillade, G. and Perche, P. (1975). Ion-conductive macromolecular gels and membrane for solid lithium cells.*Journal of Applied Electrochemistry*, 5 (1), 63-69.

Ganesan, S. Muthuraaman, B., Vinod Mathew, Madhavan, J., Marumuthu, P. and Austin Suthanthiraraj, S. (2008) Performance of a new polymer electrolyte with diphenylamine in nanocrystalline dye-sensitized solar cell.*Solar Energy Materials and Solar Cells*, 92, 1718-1722.

Gray, F. M. (1997). What are polymer electrolytes? In: *Polymer Electrolytes*. (pp.1 - 26). Cambridge: The loyal Society of Chemistry.

Gray, F. M. (1991b). Aspects of Conductivity in Polymer Electrolytes.*Solid polymer electrolytes: Fundamentals of tecnological applications.* (pp. 83-91). United Kingdom: Wiely-VCH.

Guilherme, L. A., Borges, R. S., Moraes, E. Mara S., Goulart Silva, G., Pimenta, M. A., Marletta, A. and Silva R. A. (2007). Ionic conductivity in polyethylene-b-poly (ethylene oxide)/lithium perchlorate solid polymer electrolytes.*Electrochimica Acta*, 53, 1503-1511.

Gupta, P. N. and Singh, K. P. (1996). Characteriszation of H3PO4 based PVA complex system. *Solid State Ionics*, 86-88, 319-323.

Hsieh, C. –T. and Teng, H. (2002).Influence of oxygen treatment on electric double-layer capacitance of activated carbon fabrics.*Carbon*, 40, 667-674.

Ji, K. S., Moon, H. S., Kim, J. W. and Park, J. W. (2003). Role of functional nano-sized inorganic fillers in poly (ethylene oxide) based polymer electrolytes. *Journal of Power Sources*, 117, 124-130.

Kang, X. (2004). Nonaqueous Liquid Electrolytes for Lithium-Based Rechargeable Batteries.*Chemical Reviews,* 104, 4303-4417.

Kanbara, T., Inami, M. and Yamamoto, T. (1991).New solid-state electric double-layer capacitor using poly (vinyl alcohol)-based polymer solid electrolyte.*Journal of Power Sources*, 36, 87-93.

Karan, N. K., Pradhan, D. K., Thomas, R., Natesan, B. and Katiyar, R. S. (2008). Solid polymer electrolytes based on polyethylene oxide and lithium trifluoro-methane sulfonate (PEO-LiCF3SO3): Ionic conductivity and dielectric relaxation. *Solid State Ionics*, 179, 689-696.

Kim, K. M., Park, N. G. Ryu, K. S. and Chang, S. H. (2002). Characterization of poly (vinylidenefluoride-co-hexafluoropropylene)-based polymer electrolyte filled with TiO_2 nanoparticles. *Polymer*, 43, 3951-3957.

Kim, Y. T. and Smotkin, E. S. (2002). The effect of plasticizers on transport and electrochemical properties of PEO-electrolytes for lithium rechargeable batteries.*Solid State Ionics*, 149, 29-37.

Kumar, B. and Scanlon, L. G. (2001). Composite electrolytes for lithium rechargeable batteries.*Journal of Electroceramics*, 5, 127-139.

Latham, R. J., Rowladns, S. E. and Schlindwein, W. S. (2002). Supercapacitors using polymer electrolyte based on poly (urethane).*Solid State Ionics*, 147, 243-248.

Lavall, R. L., Borges, R. S., Calado, H. D. R., Welter, C., Trigueiro, J. P. C., Rieumont, J., Neves, B. R. A. and Silva, G. G. (2008). Solid State double layer capacitor based on a polyether polymer electrolyte blend and nanostructured carbon black electrode composites. *Journal of Power Sources*, 177, 652-659.

Lewandowski, A., Skorupska, K. and Malinska, J. (2000) Novel poly (vinyl alcohol)-KOH-H_2O alkaline polymer electrolyte. *Solid State Ionics*, 133, 265-271.

Lee, C. Y., Tsai, H. M., Chuang, H. J., Li, S. Y., Lin, P. and Tseng, T. Y. (2005). Charateristics and electrochemical performance of supercapacitors with manganese oxide-carbon nanotube nanocomposite electrodes.*Journal of Electrochemical Society*, 152, A716-A720.

Lindeman, M. K. (1971).*Encylopedia of Polymer Science and Technology*. (pp. 149-154) John Willey & Sons Inc. New York, Vol. 14.

Liu, S., Imanishi, N., Zhang, T., Hirano, A., Takeda, Y., Yamamoto, O. and Yang, J. (2010). Effect of nano-silica filler polymer electrolyte on Li dendrite formation in Li/poly (ethylene oxide)-Li(CF_3SO_2)2N/Li. *Journal of Power Sources*, 195, 6847-6853.

Lust, E., Janes, A. and Arulepp, M. (2004). Influence of solvent nature on the electrochemical parameters of electrical double layer capacitors. *Journal of Electroanalytical Chemistry*, 562, 33-42.

Meher, S. K., Justin, P. and Rao, G. R. (2011) Microwave-mediated synthesis for improved morphology and pseudocapacitance performance of nickel oxide. *ACS Applied Materials & Interfaces*, 3, 2063-2073.

Niu, J., Pell, W. G. and Conway, B. E. (2006). Requirements for the performance characterization of double layer supercapacitors: Applications to a high specific surface area C-cloth material. *Journal of Power Sources*, 156, 725-740.

Nookala, M., Kumar, B. and Rodrigues, S. (2002). Ionic conductivity and ambient temperature Li electrode reaction in composite polymer electrolytes containing nanosize alumina.*Journal of Power Sources*, 111,165-172.

Nogueira, A. F., Longo, C. and De Paoli, M. –A. (2004). Polymers in dye sensitized solar cells: overview and perspectives. *Coordination Chemistry Reviews*, 248, 1455-1468.

Osada, Y. and Kajiware, K. (2001). The Fundamentals. *Gel Handbook Volume 1*. (pp. 65-85. San Diego, CA: Academic Press.

Osaka, T., Liu, X. J. and Nojima, M. (1998).Acetylene black/poly (vinylidene fluoride) gel electrolyte composite electrode for an electrical double layer capacitor.*Journal of Power Sources*, 74, 122-128.

Pradhan, D. K., Choudhary, R. N. P. and Samantaray, B. K. (2009). Studies of dielectric and electrical properties of plasticized polymer nanocomposite electrolytes. *Materials Chemistry and Physics*, 115, 557-561.

Pradhan, D. K., Choudhary, R. N. P. and Samantaray, B. K. (2008). Studies of dielectric relaxation and AC conductivity behavior of plasticized polymer nanocomposite electrolytes. *International Journal of Electrochemical Science*, 3, 597-608.

Pandey, G. P., Yogesh Kumar and Hashmi, S. A. (2011). Ionic liquid incorporated PEO based polymer electrolyte for electrical double layer capacitors: A comparative study with lithium and magnesium systems. *Solid State Ionics*, 190, 93-98.

Raghavan, P., Zhao, X. H., Manuel, J., Chauhan, G. S., Ahn, J. H., Ryu, H. S., Ahn, H. J., Kim, K. W. and Nah, C. W. (2010). Electrochemical performance of electrospun poly (vinylidene fluoride-co-hexafluoropropylene)-based nanocomposite polymer electrolytes incorporating ceramic filler and room temeprature ionic liquid.*Electrochimica Acta*, 55, 1347-1354.

Rajendran, S., Ravi, S. B and Sivakumar. (2007). Effect of salt concentration in poly (vinyl chloride)/ poly (acylonitrile) based hybrid polymer electrolytes. *Journal of Power Sources*, 170, 460-464.

Ramesh, S., Yahya, A. H. and Arof, A.K. (2002).Dielectric behaviour of PVA-based polymer electrolyte.*Solid State Ionics*, 152-153, 291-294.

Ramesh, S., Yuen, T. F. and Shen C. J. (2008). Conductivity and FTIR studies on PEO-LiX [X: CF3SO3-, SO42-] polymer electrolytes. *Spectrochimica Acta Part A: Molecular Spectroscopy*, 69, 670-675.

Ramesh, S. and Arof, A. K. (2001). Structural, thermal and electrochemical cell characteristics of poly (vinyl chloride)-based polymer electrolytes.*Journal of Power Sources*, 99, 41-47.

Ramesh, S., Chiam-Wen, L. and Ramesh, K. (2011) Evaluation and investigation on the effect of ionic liquid onto PMMA-PVC gel polymer blend electrolytes. *Journal of Non-Crystalline Solids*, 357, 2132-2138.

Ramesh, S. and Arof, A. K. (2001). Structural, thermal and electrochemical cell characteristic of poly (vinyl chloride) based polymer electrolytes. *Journal of Power Sources*, 99, 41-47.

Salne, S. and Salomon, M. (1995). Composite gel electrolyte for rechargeable lithium batteries. *Journal of Power Sources*, 55, 7-10.

Saroj, A. L. and Singh, R. K. (2012). Thermal, dielectric and conductivity studies on PVA/Ionic liquid [EMIM][EtSO4] based polymer electrolytes. *Journal of Physics and Chemistry of Solids*, 73, 162-168.

Sheem, K., Lee, Y. H. and Lim, H. S. (2006). High-density positive electrodes containing carbon nanotubes to use in Li-ion cells. *Journal of Power Sources*, 158, 1425-1430.

Shin, J. H., Kim, K. W., Ahn, H. J. and Ahn, J. H. (2002). Electrochemical properties and interfacial stabilit of $(PEO)_{10}LiCF_3SO_3$-Ti_nO_{2n-1} composite polymer electrolytes for lithium/sulfure battery. *Materials Science and Engineering: B*, 95, 148-156.

Show, Y. and Imaizumi, K. (2007). Electric double layer capacitor with low series resistance fabricated by carbon nanotube addition. *Diamond & Related Materials*, 16, 1154-1158.

Singh, K. P., Singh, R. P. and Gupta, P. N. (1995). Polymer based solid state electrochromic display device using PVA complex electrolytes. *Solid State Ionics*, 78, 223-229.

Singh, K. P. and Gupta, P. N. (1998). Study of dielectric relaxation in polymer electrolytes.*European Polymer Journal*, 34, 1023-1029.

Southhall, J. P., Hubbard, H. V. St. A., Johnston, S. F., Rogers, V., Davies, G. R., Mclntyre, J. E. and Ward, I. M. (1996). Ionic conductivity and viscosity correlations in liquid electrolytes for incorporation into PVDF gel electrolytes.*Solid State Ionics*, 85, 51-60.

Souquet, J. L., Levy, M. and Ducholat, M. (1994). A single microscopic approach for ionic transport in glassy and polymer electrolytes. *Solid State Ionics*, 70-71, 337-345.

Stephen, A. M., Nahm, K. S., Kulandainathan, M. A., Ravi, G. and Wilson, J. (2006). Nanofiller incorporated poly(vinylidene flouride-hexafluoropropylene) (PVdF-HFP) composite electrolyte for lithium batteries. *Journal of Power Sources*, 159, 1316-1321.

Sun, Z. and Yuan A. (2009). Electrochemical performance of Nickel Hydroxide/ Activated Carbon Supercapacitors using a modified polyvinyl alcohol based alkaline polymer electrolyte. *Chinese Journal of Chemical Engineering*, 17, 150-155.

Taberna, P. L., Simon, P. and Fauvarque, J. F. (2003). Electrochemical characteristics and impedance spectroscopy studies of carbon-carbon supercapacitors. *Journal of Electrochemical Society*, 150, A292-A300.

Tarascon, J. M. and Guyomard, D. (1994). New electrolyte compositions stable over the 0 to 5 V voltage range and compatible with the $Li_{1+x}Mn_2O_4$/carbon Li-ion cells. *Solid State Ionics*, 69, 293-305.

Tien, C. P., Liang, W. J., Kuo, P. L. and Teng, H. S. (2008). Electric double layer capacitors with gelled polymer electrolytes based on poly (ethylene oxide) cured with poly(propylene oxide) diamines. *Electrochimica Acta*, 53, 4505-4511.

Vassal, N., Salmon, E. and Fauvarque, J. –F. (2000). Electrochemical properties of an alkaline solid polymer electrolyte based on P(ECH-co-EO). *Electrochimica Acta*, 45, 1527-1532.

Venkateswarlu, M., Narashimha Reddy, K., Rambaby, B. and Satyanarayana, N. A.c. conductivity and dielectric studies of silver-based fast ion conducting glass system. *Solid State Ionics*, 127, 177-184.

Vieira, D. F., Avellaneda, C. O. and Pawlicka, A. (2007). Conductivity study of a gelatin based polyme electrolyte. *Electrochimica Acta*, 53, 1404-1408.

Watanabe, M. and Ogata, N. (1987) in Polymer Electrolyte Reviews – I, (Eds.) MacCallum, J. R. and Vincent, C. A., Elsevier, London.

Wen, Z. Y., Itoh, T., Uno, T., Kubo, M. and Yamamoto, O. (2003).Thermal, electrical, and mechanical properties of composite polymer electrolytes based on cross-linked poly (ethylene oxide-*co*-propylene oxide) and ceramic filler.*Solid State Ionics*, 160, 141-148.

West, A. R. (1999a). *Electrical Properties. Basic Solid State Chemistry.* (pp. 321-361). West Sussex: John Wiley & Sons.

Xing, W., Qiao, S. Z., Ding, R. G., Li, F., Lu, G. Q., Yan, Z. F. and Cheng, H. M. (2006). Superior electric double layer capacitors using ordered mesoporous carbons. *Carbon*, 44, 216-224.

Yang, C. C. (2007).Synthesis and characterization of the cross-linked PVA/TiO_2 composite polymer membrane for alkaline DMFC.*Journal of membrane Science*, 288, 51-60.

Yang, C. C. (2006). Study of alkaline nanocomposite polymer electrolytes based on PVA-ZrO_2-KOH. *Material Science and Engineering B*, 131, 256-262.

Yin, J., Zheng, C., Qi, L. and Wang, H. Y. (2011) Concentration NaClO4 aqueous solutions as promising electrolytes for electric double-layer capacitors. *Journal of Power Sources*, 196, 4080-4087.

Yu, B., Zhou, F., Wang, C. and Liu, W. (2007). A novel gel polymer electrolyte based on poly ionic liquid 1-ethyl 3-(2-methacryloyloxy ethyl) imidazolium iodide. *European Polymer Journal*, 43, 2699-2707.

Zhang, L. L. and Zhao, X. S. (2009). Carbon-based materials as supercapacitor electrodes.*Chemical Society Reviews*, 38, 2520-2531.

Zhu, W., Miser, D. E., Chan, W. G. and Hajaligol M. R. (2004).HRTEM investigation of some commercially available furnace carbon blacks.*Carbon*, 42, 1841-1845.